University of Porto
Faculty of Engineering

Analytical and Experimental Study on the Evolution of Residual Stresses in Composite Materials

Jorge Borges de Almeida

Mechanical Engineer

A Thesis presented to the

Faculty of Engineering of the University of Porto

In partial fulfillment of the requirements for the Master of Science Degree in

Mechanical Engineering

Supervisor

Professor Doutor Pedro M. P. R. C. Camanho

Assessor

Professor Doutor António Torres Marques

Porto, September 20, 2005

Abstract

The main purpose of this work is to develop an analytical and experimental study regarding the origin and evolution of residual stresses in cross-ply composite laminates. The influence of environmental conditions is also addressed.

The analytical study relies on the Classical Laminate Theory. The residual stress relaxation over time will be investigated. For this purpose, CFRP specimens are manufactured and the hole drilling method is used to assess the residual stress state in symmetrical specimens. For unsymmetrical laminates, the measurement of their curvature after manufacturing and under the influence of moisture is investigated.

After the experimental determination of the stress-free-temperature, tests performed at different times after curing the material are performed to quantify the residual stress relaxation.

Numerical models using finite elements technology are used to determine the calibration coefficients for the hole drilling method and to predict the curvature of unsymmetrical laminates. Also, the behaviour of an open hole laminate subject to a thermal load is studied.

Micromechanical models were developed to assess residual stresses at the matrix level. The influence on the fibre volume fraction was studied.

Resumo

O objectivo principal deste trabalho é desenvolver um estudo analítico e experimental relacionado com a origem e evolução de tensões residuais em laminados compósitos cruzados. A influência de certas condições ambientais será estudada.

O estudo analítico baseia-se na Teoria Clássica dos Laminados. A relaxação de tensões ao longo do tempo é investigada. Para tal, provetes em carbono-epóxido são fabricados e o método do furo será usado para avaliar o estado de tensões residuais nos provetes simétricos. Para o caso dos provetes assimétricos, o estudo baseia-se na medição da respectiva curvatura após cura e sob a influência de humidade.

Após a determinação experimental da temperatura correspondente ao estado livre de tensões internas do material, são conduzidos testes em diferentes ocasiões após a cura do material para quantificar o relaxamento das tensões.

Métodos numéricos baseados na tecnologia dos elementos finitos são igualmente usados para a determinação dos coeficientes de calibração do método do furo. O comportamento de um provete de furo aberto sujeito a uma carga térmica é também estudado.

Foram desenvolvidos modelos micromecânicos para avaliar tensões residuais ao nível da matriz. A influência da fracção volúmica da fibra foi estudada.

Zusammenfassung

Der Hauptzweck dieser Arbeit ist, die Entwicklung von Eigenspannungen in gekreuzte Laminaten durch analytische und experimentelle Weisen zu studieren. Der Einfluß von Klimabedingungen wird auch adressiert.

Das CLT-Rechenverfahren wird angewendet. Die mögliche überzeitliche Entspannung der Eigenspannungen wird untersucht. Für diesen Zweck werden CFRP Laminaten hergestellt und die Bohrungmethode wird angewendet, um die Eigenspannungen in den symmetrischen Laminaten festzustellen. Nach der Herstellung von unsymmetrischen Laminaten wird die Biegung gemesst und mit numerischen Ergebnissen verglischen. Ihre Entwicklung unter den Einfluss von Feuchtigkeit wird auch erforscht.

Nach der Feststellung der spannungsfrei Temperatur des Werkstoffes, werden verschiedene Tests überzeitlich durchgeführt, um die Entspannung des Werkstoffes zu quantifizieren.

Durch die Technik der finite Elemente, werden die Biegungen der unsymmetrischen Laminaten und die Calibrationskoeffizienten für die Bohrungmethode festgestellt.

Das Verhalten einer Platte mit einem Loch unter den Einfluss einer termischen Ladung wir auch untersucht.

Micromechanische Modellen wurden entwickelt, um die Eigenspannungen am Matrixniveau festzustellen. Der Einfluß des Faseraus-

gabenbruches wurde studiert.

Resumeé

Le but principal de ce travail est développer une étude analytique et expérimentale concernant l'origine et l'évolution des efforts résiduels dans des composites stratifiés. L'influence des conditions environnementales est également adressée.

L'étude analytique se fonde sur la théorie classique des stratifiés. Le temps fini de relaxation résiduelle d'effort sera étudié. À cette fin, les spécimens de CFRP sont manufacturés et la méthode du trou incrémental est employée pour évaluer l'état résiduel d'effort dans les spécimens symétriques. Pour les stratifiés non symétriques, la mesure de leur courbure après la fabrication et sous l'influence de l'humidité est étudiée.

Après la détermination expérimentale de la température correspondant à un état libre de contraintes, les essais sont exécutés à différentes heures après avoir traité le matériel pour mesurer la relaxation résiduelle des contraintes.

Des modèles numériques employant la technologie d'éléments finis sont employées pour déterminer les coefficients de calibrage pour la méthode du trou et prévoir la courbure des stratifiés non symétriques.

En outre, le comportement d'un stratifié ouvert de trou sujet à une charge thermique est étudié.

Des modèles micromécaniques ont été développés pour évaluer des efforts résiduels au niveau de la matrice. L'influence de la fraction de

volume de fibre a été étudiée.

Contents

List of Figures

List of Tables

List of Symbols

ε_{in}	Radial strain in layer i at increment n
σ_{xx}	Normal stress along x axis
σ_{yy}	Normal stress along y axis
σ_{11}	Normal ply stress along fibre direction
σ_{22}	Normal ply stress perpendicular to fibre direction
σ_{VM}	Von Mises stress
σ_{yd}	Yielding stress
X_T^L	Unnotched laminate tensile strength
X_T	Ply longitudinal tensile strength
X_C	Ply longitudinal compressive strength
Y_T	Ply transverse tensile strength
Y_C	Ply transverse compressive strength
S_L	Tensile shear strength in the longitudinal direction
S_T	Tensile shear strength in the transverse direction
G_{Ic}	Mode I fracture toughness for transverse crack propagation
Y_T^{is}	In-situ ply transverse tensile strength
κ	Curvature
U_V	Dilatational energy density
U_{cr}	Critical dilatational energy density

θ_i	Angle between principal stress directions and global system
υ_{12}	Major Poisson's ratio
E_1	Longitudinal modulus of elasticity
E_2	Transverse modulus of elasticity
G_{12}	In-plane shear modulus
t	Thickness
E_m	Matrix modulus
E_f	Fibre modulus
t^*	Non-dimensional time
d	Hole diameter
w	Width
α_{11}	Coefficient of thermal expansion in the longitudinal direction
α_{22}	Coefficient of thermal expansion in the transversal direction
V_f	Fibre volume fraction
M	Moisture content
G	Time dependent parameter
D_x	Diffusivity

List of Abbreviations

ASTM	American Society for Testing and Materials
CLT	Classical Lamination Theory
CFRP	Carbon Fibre Reinforced Plastics
CTE	Coefficient of thermal expansion
FEM	Finite elements model
FW	Filament winding
HDM	Hole drilling method
OHT	Open-hole tensile
PMC	Polymer matrix composite
RS	Residual stress
RTM	Resin Transfer Molding
SFT	Stress free temperature
TTS	Transverse tensile strength

Acknowledgements

This work would not have been possible without the precious help of the following individuals and institutions:

Dr. Pedro Ponces Camanho, INEGI, (CEFAD)

Dr. António Torres Marques, INEGI, (CEMACOM)

Dr. João Paulo Nobre, FCTUC

Dra. Maria Teresa Restivo, FEUP

Célia Novo (MSc, INEGI, (CEMACOM)

Eng. Joaquim Fonseca, FEUP

Mr. José and Mr. Albino, FEUP

Mrs. Emilia Soares, FEUP

I would also like to thank for all support:

Cassilda Tavares (MSc, PhD student), IDMEC

Pedro Portela, Pedro Bandeira (MSc students), INEGI, (CEFAD)

Raul Campilho (MSc student)

For all software and hardware problems solutions, I am deeply thankful to:

Pedro Martins (PhD student), IDMEC

Marco Parente (PhD student)

Also, I shall not forget all of those who contribute to a healthy and charming workspace environment:

David Perez (PhD student)

Jorge Belinha (MSc student)

Paulo Neves (FCT colaborator)

Carla Roque (PhD student)

Chapter 1

Introduction

1.1 Basic Definitions

Many structural applications require the use of materials combining, simultaneously, superior strength and stiffness with low weight. Composite materials are excellent candidates for fulfilling these requirements because of their high specific properties. In this scenario, one of the most interesting aspects is the fact that the material itself is also a structure, which consists of two or more phases on a macroscopic scale, as shown in Figure 1-1[1].

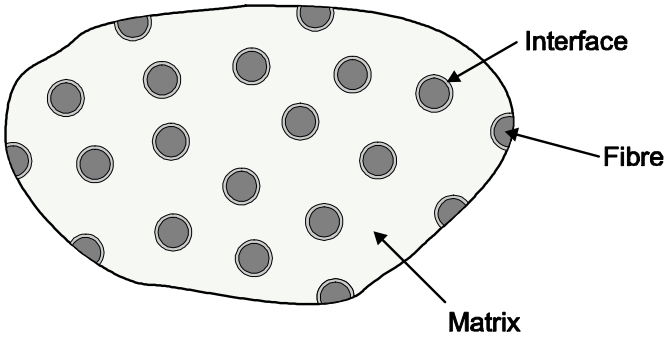

Figure 1-1: Phases of a composite system (after [1])

A structural composite is designed with the following purpose in mind: the properties and mechanical performance of the composite material are superior to those of the constituent materials when acting independently.
The matrix is the less stiff and weaker phase and is a continuous medium. The

reinforcement is usually discontinuous, stiffer and stronger. Needless to say, the properties of a composite structure depend on the properties of the constituents, geometry and phase distribution. The homogeneity of the material system depends on the more or less distribution of the reinforcement. Composite materials are, therefore, rather anisotropic in their nature. This fact implies that the material's properties, at a certain point, vary with direction or depend on the orientation of the reference axes (Figure 1-2).

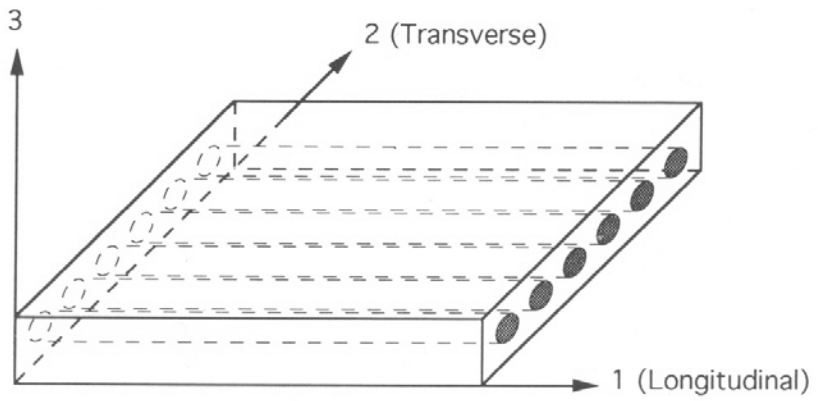

Figure 1-2: Unidirectional ply and principal coordinate axes (after [1])

A laminate is made up of several unidirectional plies stacked together with various orientations as shown in Figure 1-3 [1]. Since the principal material axes vary from ply to ply, it is desirable to analyse laminates using a common fixed system of coordinates (x,y,z). The orientation of each ply is given by the angle between the reference x-axis and the major principal material axis (fiber orientation) of the ply, measured in a counterclockwise direction on the x-y plane.

1.2 Applications of Composite Materials

Composites have unique characteristics that make them perfect material choices for several applications, such as: high strength, high stiffness, long fatigue life, low density and great adaptability to a specific function.

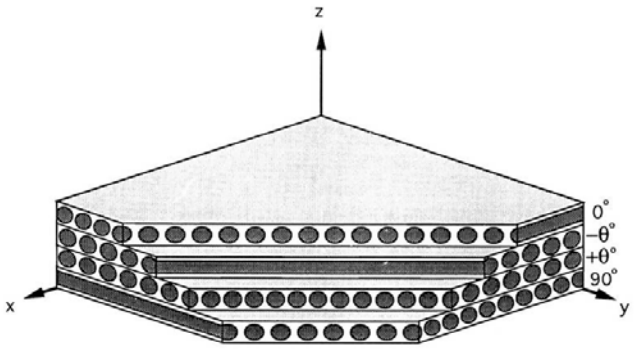

Figure 1-3: Multidirectional laminate and reference coordinate system (after [1])

The aerospace and aeronautical industries have been major users of composite technology in the last decades. From small parts to fairly large structures, weight savings while preserving high material properties has always been an issue in commercial aircrafts, such as the Boeing 777 shown in Figure 1-4 [2].

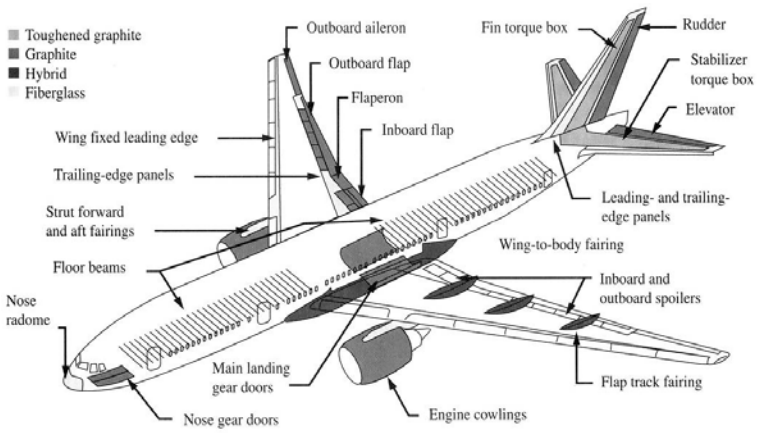

Figure 1-4: Boeing 777 commercial airliner (after [2])

Another example is a speedbrake structure of a military aircraft, the Vought A7, composed of several composite parts, Figure 1-5 [3].

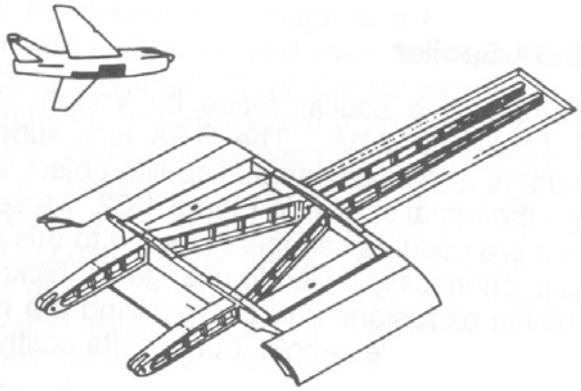

Figure 1-5: A7 speedbrake structure (after [3])

As it will be mentioned later on, manufacturing procedures induce distortions and other effects in composite materials, which may affect the component's dimensional accuracy, and even the final strength.

1.3 Environmental effects on Composite Materials

During their normal operation time, composite structures are subjected to environmental attacks, which include, among others, changes in temperature and moisture. These effects are called hygrothermal effects and can be categorized as:

- Physical and Chemical effects
- Effects on mechanical properties
- Hygrothermoelastic effects

While there is much information about these factors in the literature [1], [7], [8], a brief description will be given here.

1.3.1 Physical and Chemical effects

Moisture absorption and desorption processes in polymer matrix composites depend on the current hygrothermal state and on the environment. Basically the moisture content in the material affects the glass transition temperature of the matrix. Polymerization processes are a function of the hygrothermal properties of the constituents and the composite's current hygrothermal state. Material degradation and corrosion can also be related to hygrothermal factors.

1.3.2 Effects on mechanical properties

Time dependent properties such as the tensile modulus and shear modulus may vary with temperature and moisture concentration. Failure and strenght characteristics, specially interfacial and matrix dominated ones, may depend on temperature and humidity.

1.3.3 Hygrothermoelastic effects

The composite material undergoes reversible deformations related to thermal expansion (α) and moisture expansion (β) coefficients. Intralaminar and interlaminar stresses are developed as a result of the thermoelastic and hygroelastic inhomogeneity and anisotropy of the material.

1.4 Scope of this work

Basically, the starting point for this work is the following open question: how is the evolution of the residual thermal stresses in composites as a function of time and environmental conditions. In order to further investigate this question the discussion is organized as follows: first, a literature survey is presented. In chapter 3 the material characterization process is discussed in detail. The experimental procedures and the respective results are presented in chapter 5. Some analytical and numerical models were developed and the respective results are

discussed in chapter 6. In chapter 7, the final conclusions and suggestions for future developments are presented. In this work, symmetrical and unsymmetrical laminates will be analysed. The residual stress level after curing and the possible stress relaxation were investigated for both laminates. For the symmetrical laminates the hole drilling method (HDM) was used to determine the state of residual stress. Although the HDM has been used to quantify the level of residual stresses in composites subjected to various cooling conditions, no report regarding it's application to study the experimental evolution of residual stresses with time was available at the time of this work. The study regarding unsymmetrical laminates like the one shown in Figure 1-6 relied mostly on the measurement of their curvature. The moisture effect was also investigated. Unsymmetrical specimens

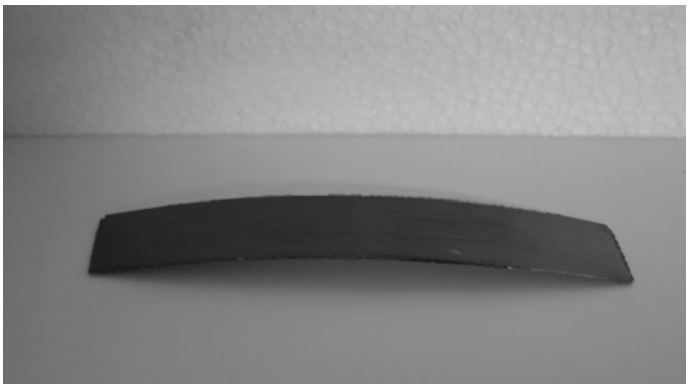

Figure 1-6: Unsymmetrical CFRP laminate

with various stacking sequences were immersed in water and the weight gain was related to their curvature change. The curvature of the laminates were also predicted using analytical and numerical tools. The results were then compared with experimental data. It is also a goal of this work to provide experimental data in all possible domains for the IM7/8552 prepreg. This material is widely used in the aeronautical and aerospace industries.

Chapter 2

Residual Stresses in Composite Materials

2.1 Development of residual stresses

One may define residual stresses in composite laminates as locked-in stresses without application of any exterior forces. This is the most basic definition that may be found in the literature.

In the case of multidirectional laminates, residual stresses are introduced during the fabrication process, and the understanding of the effects of residual stresses on the material response is needed [1], [4]. After curing and cooling the composite, the matrix is subject to a tri-axial stress state. Shrinkage during curing and the mismatch of coefficients of thermal expansion between fibre and matrix are the most important reasons for residual stresses. Since the fibre's coefficient of thermal expansion is lower compared to the matrix coefficient of thermal expansion, the resulting thermal residual stresses are of compressive nature in the fibre and tensile nature in the matrix [9]. Residual stresses may be analysed from a micromechanical or macromechanical point of view. On the micromechanical scale, residual stresses appear in unidirectional layers in and around individual fibres due to the mismatch in thermal properties of the constituents, like the difference in coefficients of thermal expansion. On a macroscopic level, laminate

residual stresses develop due to the thermal anisotropy of the respective layers. For this case, let us consider Figure 2-1. In this illustration, the development of residual stresses is shown for a simple $[0/90]_S$ laminate. If one imagines the unconstrained deformation of the individual plies and knowing the fact that $\epsilon_y^T > \epsilon_x^T$, then internal stresses will be exerted on the $0\,^\circ$ and $90\,^\circ$ plies to maintain geometrical compatibility. Other authors present different classifications of residual stress sources, like Goran et al. [10]. According to these authors, the sources of residual stresses in composite laminates can be classified as intrinsic or extrinsic. The intrinsic sources are material, lay-up and part shape related, whereas extrinsic sources are more processing and tooling related. This classification aids in explaining which sources for residual stress development are considered in the present work. For example, the mechanical interaction of the tool and the part will not be studied. Furthermore, it explains the formation of residual stresses at the fibre-matrix, lamina-laminate and structural scales. It also points out that the residual stresses at the fibre matrix level are often not considered explicitly in the design of composites, because they are taken into account in the strength properties of the material. Intrinsic sources generate residual stresses at the constituent level and the effect is integrated up through the length scales. Extrinsic sources generate stresses at the boundaries of the structure and the effect is migrated down through the length scales. Thus, intrinsic sources act from the "inside and outwards" and extrinsic sources act from the "outside and inwards". Although the authors state that intrinsic sources have the largest effect at the fibre-matrix level stresses and extrinsic sources have the largest effect at the structural level stresses, it is difficult to quantify the respective influence percentages since a lot of work is being done in the field of residual stresses development and determination procedures.

In reference [11] a good summarized and qualitative description is given for the development of residual stresses during cure:

Stage 1: The resin is in a viscous state and the curing degree is low. Therefore, the glass transition temperature, T_g, is low. At this point, no significant residual

stresses occur.

Stage 2: This stage starts at the gel point of the resin. For epoxy resins, this happens for a degree of cure of about 0.6. Degree of cure represents the extent to which curing of a thermosetting resin has progressed. From this point, the resin modulus begins to grow and the material picks up some stresses, which are quickly relieved because the temperature is relatively high comparing to T_g, being the material highly viscoelastic.

Stage 3: The start of the resin's vitrification is the point at which T_g coincides with the cure temperature. From this point on until cool down to room temperature the stresses developed contribute greatly to the total amount of residual stress of the material.

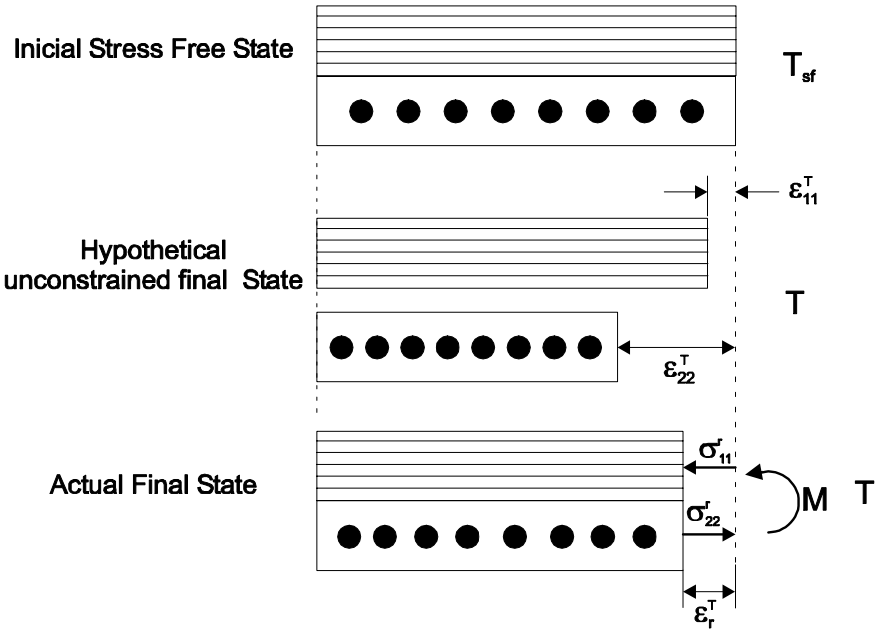

Figure 2-1: Residual stress formation after cool down (after [4])

2.2 Residual stress effects

Lu et al. [12] investigated the influence of residual stresses due mainly to fabrication conditions on the mechanical behaviour of composite laminates. The

authors used CFRP laminates that were processed from unidirectional T300/914 prepeg. A cross-ply structure was used, with the following orientation and stacking sequence: $[0_2/90_2]_S$. Three different cooling conditions were applied after the material's curing cycle, namely fast, normal and slow. The residual stress distribution along the laminate's thickness was experimentally determined using the hole drilling method, and also numerically, through the finite element method. Tensile tests were performed on the cured specimens. Lu et al. [12] concluded that the presence of a residual stress field does not influence the initial stiffness of the laminate. Differences between the ultimate tensile stresses corresponding to the three cooling conditions were observed. Stringer et al. [13] investigated the formation of residual stresses in thick polymer composites. In this case, the component was too rigid for residual stresses to be relieved by deformation ($\epsilon_{zz} = 0$). The existence of a tri-axial stress state is more favourable to the occurrence of internal damage such as delamination cracking. Stringer et al. [13] used embedded electrical resistance strain gauges and optic fibre strain sensors to monitor residual stresses during manufacturing. The processes studied were resin transfer molding (RTM) and filament winding (FW). The model developed by Stinger et al. suggested in the case of FW that a heated mandrel significantly reduces residual stresses. A lot of chemistry is involved in the online monitoring of residual stress fields. Therefore a fairly developed cure kinetics model is needed if one wishes to determine the residual stresses at any time during the cure cycle. Stringer et al. [13] pointed out an important fact related to the time at which residual stresses begin to build up: before gelation time no significant physical union exists between the matrix resin and reinforcing material, the fibres. At gelation time, the resin solidifies and it is at this point that meaningful internal residual strains begin to appear. This is important, since most residual stress predictions are determined using T_g as the maximum cure reference temperature. Residual stresses (RS) in composite laminates depend on thermoelastic properties of the material and processing temperature. The RS distribution in the various laminae depends on the stacking sequence and ply orientation. Resid-

ual stresses may have undesirable effects on the material: distortions of finished components when cooled and removed from moulds, creating dimensional instability and locked-in stresses, which may cause delamination cracking. Tensile residual stresses in the matrix are particularly important because they may represent a significant fraction of the tensile strength of the polymer and can lead to premature failure by matrix cracking. Nairn points out that the residual stress effects should be included in every composite fracture model because they may contribute to the energy release rate [14].

2.3 Experimental Methods for assessing residual stresses in composite materials

Many experimental techniques are described in the literature for the determination of residual stresses in composite materials. It is important to mention the main advantages and disadvantages of each one. A brief description of each technique will be given in the following subsections. One thing to remind is that residual stresses cannot be measured directly: the residual strains must be first determined and then proceed to calculate the stresses.

2.3.1 Embedded Strain Gauges

The use of embedded strain gauges in composite laminates to directly measure process induced strains is quite expensive because it requires special strain gauges capable of supporting high curing temperatures and pressures [15]. Also, it is not very practical, since a precise alignment of the strain gauges is needed and it may be quite difficult to achieve. Further, it creates a localised delamination in the composite material, whose effect on the measured strains is unknown.

2.3.2 X-Ray Diffraction

In reference [16] a X-Ray diffraction method for determining thermal residual stresses in unidirectional laminates is proposed. The authors use embedded aluminum and silver inclusions placed between certain plies of a laminate. The experimental results are then compared with numerical results. The main advantage of this method is that it allows to obtain the complete stress tensor. In the specimens investigated in this work [16], a triaxial state of stress exists, which would not be detected if another process relying on plane stress state was used. On the other hand, this method has some drawbacks, which are related to the fact that particle shape has a strong influence on the measured X-Ray stresses. Also, for the method to be more accurate, the particles' distribution in the laminate needs to be strictly controlled. This method is clearly not suitable for measuring residual stresses in previously manufactured structures.

2.3.3 Successive Grooving Technique

Yu et al. [5] describe a technique involving the cut of a progressively deepening thin slit through the thickness of a composite part promoting stress relaxation. For strain measuring, a strain gauge must be placed on the face of the part opposite to the groove, as shown in Figure 2-2. Cutting the groove modifies the overall stress field within the part, and its geometry changes until another self-equilibrating state of stress is attained. The internal through the thickness residual stresses may then be determined. Although the authors mention the key advantage of this method being the low quantity of removed material, the precise alignment of the cutting element and the strain gauge is difficult to achieve. Also, the location of the strain sensing device may not be achievable for larger parts or structures.

2.3.4 First Ply Failure Method

The residual stress level in a symmetrical laminate may be estimated from the difference in transverse tensile strength of a $[90]_n$ lay-up and the in situ transverse tensile strength (TTS) of a cross-ply laminate [17]. But this method does not provide any information regarding the through the thickness distribution of residual stresses. Also, the in situ TTS of a 90° ply in a cross-ply laminate will be influenced not only by residual stress effects but also by the constraining effect of the adjacent plies, which increases the in-situ TTS. The effect of adjacent plies is thoroughly explained in reference [18].

2.3.5 The Hole Drilling Method

Initially developed for isotropic materials, specially metals, the hole drilling method (HDM) has been adapted to other material such as polymers and composites [19], [20]. In the case of metals it has even been standardized [6]. However, this standard is not suitable for composite materials [21]. In reference [21] the standard was applied and inconclusive results regarding the values of the residual stresses were obtained. Some suggestions for future analysis are given and studied in the present work, such as the assessment of the drilled hole's quality and the usage of a modified HDM which takes into account the layered nature and orthotropy of the material. Sicot et al. [22] described the application of the

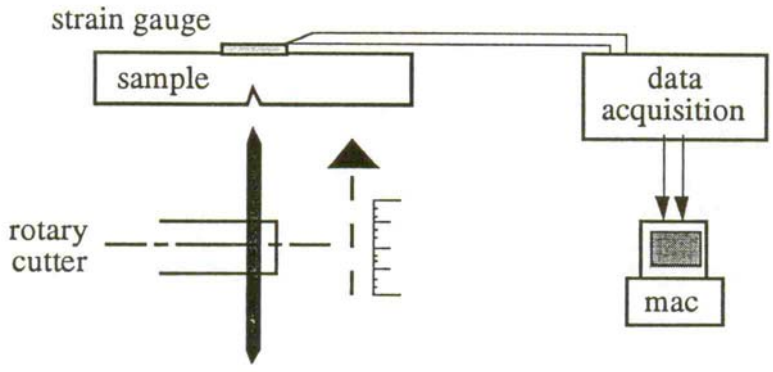

Figure 2-2: Grooving experimental setup (after [5])

incremental hole drilling technique to composite laminates. A very small hole is drilled and the resulting relaxation strains are measured with a proper strain gauge. But in this case, the alignment of the drilling device with the strain gauge, which is a crucial step, is accomplished by using an optical device prior to the drilling process, ensuring a perfect alignment. Also, this method is more practical in terms of drilling equipment than the method described in 2.3.3. Figure 2-3 [6] shows the main components of the drilling device mostly used to perform the residual stress experimental measurements.

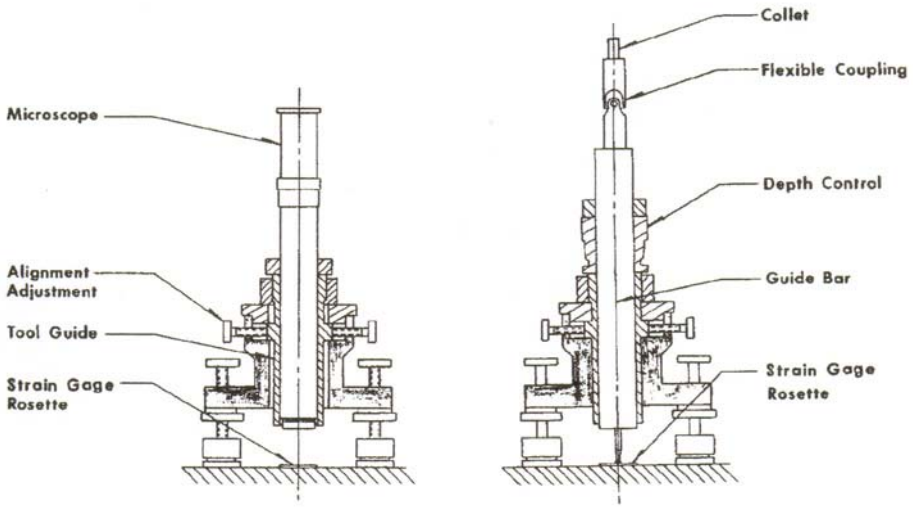

Figure 2-3: Main components of a typical drilling equipment for residual stress analysis (after [6])

Chapter 3

Material Characterization

3.1 Introduction

The determination of the mechanical properties relevant to this work is of crucial importance. The mechanical properties are inputs for the numerical and analytical procedures. Mechanical as well as thermomechanical properties were determined following standard procedures. Although some of the properties are available from the material's manufacturer, it is always advisable to conduct experiments to determine the material's properties, since deviations may occur. In this Chapter a brief description of all test procedures is given.

3.2 Material Description

For the manufacture of all specimens a Hexcel's IM7/8552 carbon epoxy unidirectional pre-preg was chosen. It is a high performance composite material used mostly in the aeronautical and aerospace industries. The material was properly conditioned, according to the manufacturer's instructions.

3.2.1 Curing cycle and Residual Stress Development

In the production of composite parts the pertinent processing parameters are time, temperature and pressure. Slight deviations from the recommended pro-

cessing conditions can result in unacceptable quality. One of the most significant problems in the processing of composites is residual stresses, as processing-induced residual stresses can be high enough to cause cracking within the matrix even before mechanical loading. This microcracking of the matrix can expose the fibers to degradation by chemical attack. Strength is adversely affected by residual stresses since a pre-loading has been introduced. White et al. [23] describe a model which predicts the residual stress history during cure. Since this work is focused only on the final stress state after curing, the models will be considered linear elastic, i.e. the analysis is restricted to the cooldown phase of the cure cycle. Nevertheless, a detailed description of the curing cycle will be given to allow for a better understanding of the formation of residual stresses. The standard process cycle for polymer matrix composites (PMCs) is a two step cure cycle. In such cycles the temperature of the material is increased from room temperature to the first dwell temperature and this temperature is held constant for about one hour. Afterwards, the temperature is increased again to the second dwell temperature and held constant for two to eigth hours. Then, the part is cooled down to room temperature at a constant rate. The purpose of the first dwell is to allow gases (entrapped air, water or volatiles) to escape the matrix material and to allow the matrix to flow, thus facilitating compaction of the part. This means the viscosity must be low during the first dwell. The purpose of the second dwell is to allow crosslinking of the polymer to take place. It is in this phase that the strength and related mechanical properties of the composite are developed. The issue of residual stresses becomes more important when high-temperature resins are involved, because they are processed at higher temperatures. Chemically, the reinforcing fibres are affected very little during the process cycle. The polymer matrix on the other hand will contract during crosslinking by as much as 6% in thermosets. Regarding thermally-induced deformations, these occur because the polymer matrix has a higher CTE than the fibre, typically an order of magnitude or more. After processing, the composite must be well-bonded and continuous, so these deformations are balanced internally within the composite and resid-

ual stresses are induced. The effects of residual stresses are obviously noted in unsymmetric laminates. With symmetric lay-ups, the resulting laminate will remain flat after production, since the in-plane strains are compensated through the thickness. With unsymmetric layups the laminate will experience out of plane deformations, due to the variation of strains across the thickness. The respective curvature is directly related to the magnitude of the induced residual stresses. A proper residual stress model should incorporate viscoelastic material behaviour, chemical and thermal shrinkage effects and also mechanical property development during cure [23].

3.2.2 Curing Procedure

Figure 3-1 shows the cure cycle recommended by Hexcel for monolithic parts. It is important to mention that the curing times may be slightly higher for thicker components. In this case, the use of thermocouples for temperature monitoring is essential. After all plies were properly cut the production of several plates, from

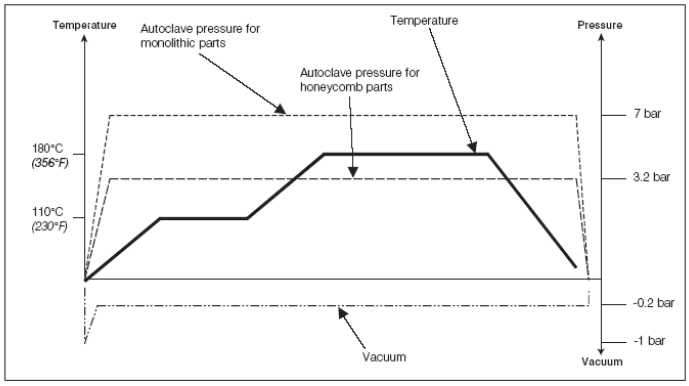

Figure 3-1: Cure cycle for honeycomb and monolithic components

which the specimens were machined, was performed in a Satim 40 ton hydraulic hot press, model PML 1 (Figure 3-2), with temperature stages of 110 °C during 1 hour, followed by 180 °C for 2 hours. The pressure of 7 bar was applied during the entire cycle. The heating and cooling rates were 3 °C/min.

Figure 3-2: Satim hydraulic hot press

3.3 Experimental Tests

3.3.1 Selection of Strain Gauges

The strain gauges used for the characterization of the pre-preg material are of the following type: "HBM 1, 5/350LY11", "HBM 3/350LY11", "HBM 6/350LY11", "HBM 3/350LC11" and "HBM 6/350LC11". These strain gauges were chosen due to the following reasons:

- Their 350 Ω resistance, associated with a high voltage supply, promotes a better hysteresis effect and the zero load stability.
- The strain gauges already incorporate electrical wiring allowing the remaining electrical cables to be welded without damaging the composite material.
- The grid size is approximately ten times bigger than the fibre diameter, allowing the characterization of the composite material.
- The strain gauges are compensated for steel. Taking into account that the tests will be performed at constant temperature, the effect of small

temperature variations will be neglected.

- The strain gauges from series "C" are specially suited for the tests at temperature extremes.
- The purchase cost was also a factor in their selection process.

The strain gauges were connected to the data acquisition system in quarter-bridge using the three wires technique. This technique allows the system to be calibrated so that temperature variations do not affect the measured data.

3.3.2 Surface preparation

Surface preparation is of crucial importance in strain gauging, because it influences the quality of the adhesion between the test specimen and the strain gauge. The surface preparation will be performed as follows:

- Surface degreasing using "HBM - RMS1" cleaning solution, which is basically a mixture of acetone and isopropanol.
- Manually abrasion of the specimen surface with sandpaper n ^{o} 400.
- Cleaning with ethanol to remove the dust originated by the abrasion process.
- Degreasing using "HBM - RMS1" to assure a total removal of all the possible dust and grease that may remain on the specimen surface.

3.4 Strain gauge bonding

After the cleaning process, and to complete the strain gauging process, it is necessary to execute the steps described beneath:

- Orientation guidelines are drawn upon the specimen surface to aid the correct alignment of the strain gauge.

- The strain gauge is finally glued using "HBM Z70", which is an acrylic based adhesive.

The specimen is ready to be soldered to the data acquisition system wires. After this process, the specimens were stored in an environmental chamber at 23 °C and 50% of relative humidity.

3.4.1 Ply Properties

Longitudinal Tensile Test

The purpose of the tensile tests is to measure the mechanical properties of the ply under tensile loading. The tests were performed according to the ASTM [24] test standard.The longitudinal tensile test measures the modulus of elasticity E_1 and the major Poisson's ratio ν_{12}. Information regarding the lay-up and test parameters are given in Table 3.1. Figure 3-3 shows the stress strain curves

Table 3.1: Longitudinal tensile test matrix

Test Type	Lay-up	number of specimens	Control type	Speed
Tensile	$(0)_8$	5	Displacement	2 mm/min

obtained.

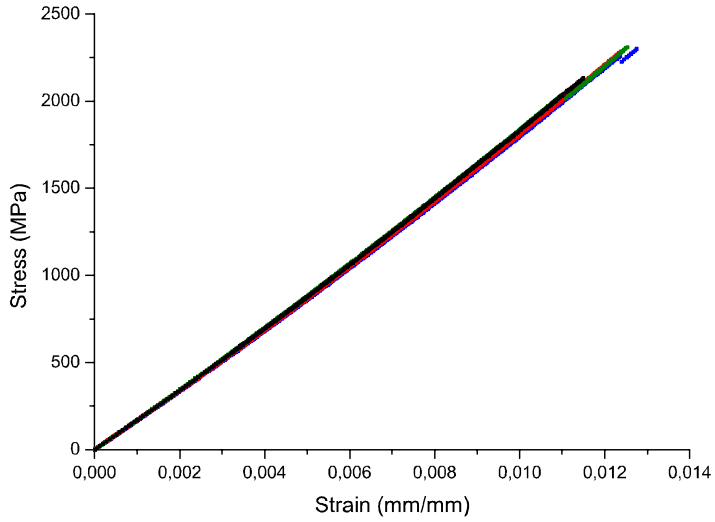

Figure 3-3: Stress-strain relation for the 0 ° specimens loaded in tension

Table 3.2 shows the experimentally obtained values for E_1, ν_{12} and X_T.

Table 3.2: Results of the longitudinal tensile test- specimens with tapered end tabs.

Spec. Ref.	w (mm)	t (mm)	E_1 (GPa)	υ_{12}	X_T (MPa)
PT01C	15.01	0.98	138.84	0.31	2426.95
PT02C	15.00	0.98	169.83	0.33	2298.23
PT03C	15.00	0.98	170.57	0.29	2283.27
PT04C	15.00	0.99	174.17	0.34	2308.42
PT05C	15.00	0.99	173.68	0.31	2131.18
Average	15.00	0.98	171.42	0.32	2289.61
STDV	-	-	2.38	0.02	105.39
COR	-	-	1.39	6.18	4.60
IC (%)	-	-	± 2.95	± 0.02	± 130.84

Transversal Tensile Test

This test was also performed according to the same ASTM test standard mentioned above. The transversal tensile test measures the modulus of elasticity E_2 and the minor Poisson's ratio ν_{21}. Information regarding the lay-up and test parameters are given in Table 3.3. Figure 3-4 shows the stress strain curves

Table 3.3: Transversal tensile test matrix

Test Type	Lay-up	number of specimens	Control type	Speed
Tensile	$(90)_{16}$	5	Displacement	1 mm/min

obtained. Table 3.4 shows the results obtained in the 90^o tensile tests.

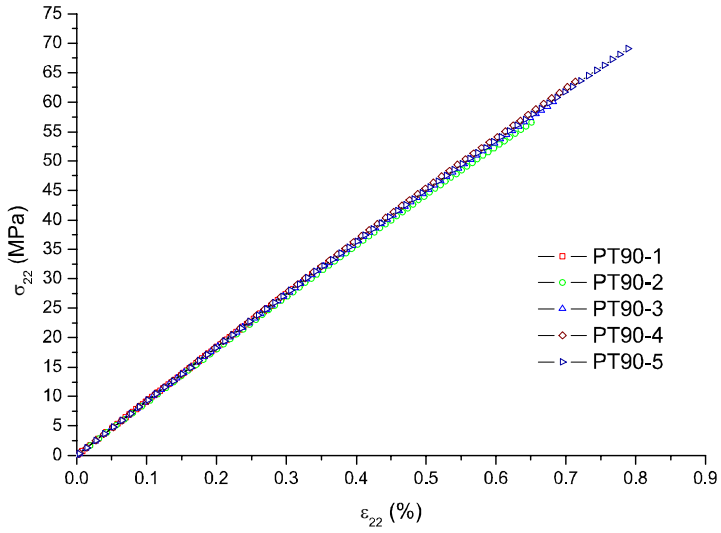

Figure 3-4: Stress-strain relation for the 90 ° specimens loaded in tension

Shear Test

The shear tests were performed according to ASTM [25] to obtain the in-plane shear modulus G_{12} and the in-plane shear strength S_L. Information regarding the lay-up and test parameters are given in Table 3.5. The results of the tests performed are shown in Figure 3-5. Table 3.6 shows the results obtained in the shear tests. Table 3.7 summarizes the ply properties of the material, considering a transversely isotropic behaviour.

Table 3.4: Results of the transverse tensile test.

Spec. Ref.	w (mm)	t (mm)	E_2 (GPa)	Y_T (MPa)
PT90-1	24.72	1.99	9.02	-
PT90-2	24.57	1.99	8.98	56.61
PT90-3	24.67	1.99	9.04	60.05
PT90-4	24.74	1.99	9.21	63.45
PT90-5	24.75	1.98	9.13	69.03
Average	24.69	1.99	9.08	62.29
STDV	-	-	0.09	5.29
COR	-	-	1.03	8.50
IC (%)	-	-	±0.12	±8.42

Table 3.5: Shear test matrix

Test Type	Lay-up	number of specimens	Control type	Speed
Shear	$(45/-45)_{4S}$	5	Displacement	1 mm/min

Coefficients of thermal expansion

The experimental characterization of the composite's CTEs, α_{11} and α_{22}, was performed according to the dilatometer's manufacturer's instructions. Specimens with a section of 10x10mm^2 were cut with a water jet machine from a unidirectional plate as shown in Figure 3-6. The plate consisted of 76 unidirectional plies which were carefully layed-up by hand and then hotpressed using the equipment shown in Figure 3-2. As mentioned earlier, thicker laminates should be monitored during cure and therefore two thermocouples were used for checking temperature evolution. Before testing using the equipment shown in Figure 3-7, the specimens were conditioned in an oven at 70 °C for two hours, to remove absorved moisture and reduce the level of residual stresses, as proposed in [26], [27]. The heat rates are shown in Figure 3-8. Before the tests each specimen must be measured. The respective lengths are shown in Table 3.8.

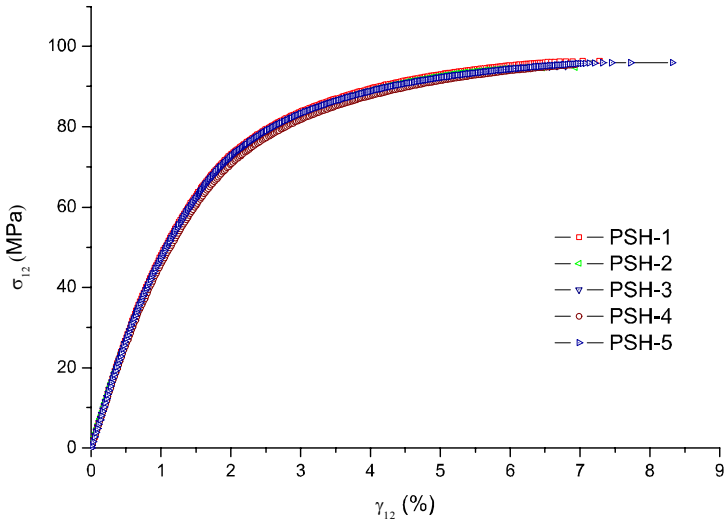

Figure 3-5: Stress-strain relation for the shear specimens loaded in tension

Table 3.6: Results of the shear tests.

Spec. Ref.	w (mm)	t (mm)	S_L (MPa)	G_{12} (GPa)
PSH-1	24.75	1.99	93.07	5.42
PSH-2	24.81	1.99	92.81	5.20
PSH-3	24.63	2.00	92.00	5.30
PSH-4	24.75	1.99	91.53	5.11
PSH-5	24.81	1.99	92.28	5.40
Average	24.75	1.99	92.34	5.29
STDV	-	-	0.62	0.13
COR	-	-	0.67	2.53
IC (%)	-	-	±0.77	±0.17

Table 3.7: Ply properties (transversely isotropic)

E_1(GPa)	E_2(GPa)	E_3(GPa)	υ_{12}	υ_{13}	υ_{23}	G_{12}(GPa)	G_{13}(GPa)	G_{23}(GPa)
171.42	9.08	9.08	0.32	0.32	0.32	5.29	5.29	3.44

Table 3.8: Measured parameters

Spec. Ref.	L (mm)	d (mm)
CTEH-1	44.94	10.35
CTEH-2	45.05	10.38
CTEH-3	45.06	10.35
CTEH-4	44.99	10.35
CTEH-5	44.86	10.35
CTET-1	45.08	10.35
CTET-2	44.92	10.36
CTET-3	45.12	10.37
CTET-4	44.85	10.37
CTET-5	45.10	10.39

Table 3.9 shows the results for the coefficient of thermal expansion in the fibres' direction. The results of the tests are shown in Figures 3-9 and 3-10 Table 3.10 shows the results for the coefficient of thermal expansion transversal

Table 3.9: Results of the dilatomeric tests α_{11}

Spec. Ref.	w (mm)	t (mm)	Heat. Vel.	α_{11} ($10^{-6}/^{o}$C)
CTEL-1	10.00	10.00	1.00	-5.84
CTEL-2	10.00	10.00	1.00	-4.67
CTEL-3	10.00	10.00	1.00	-5.06
CTEL-4	10.00	10.00	1.00	-6.35
Average	-	-	-	-5.48
STDV	-	-	-	0.76
COR	-	-	-	-13.81
IC (%)	-	-	-	1.05

to the fibres' direction.

Hysteresis is observed after cool down of the specimens. It is generally thought to be a result of the adhesive between the gauge and specimen being affected by the heat. It is also possible that viscoelastic effects may influence the material response of the composite at higher temperatures. Higher rates of temperature change appear to produce more hysteresis, indicating that the material is not in thermal equilibrium. However, at lower temperatures, the heating and the

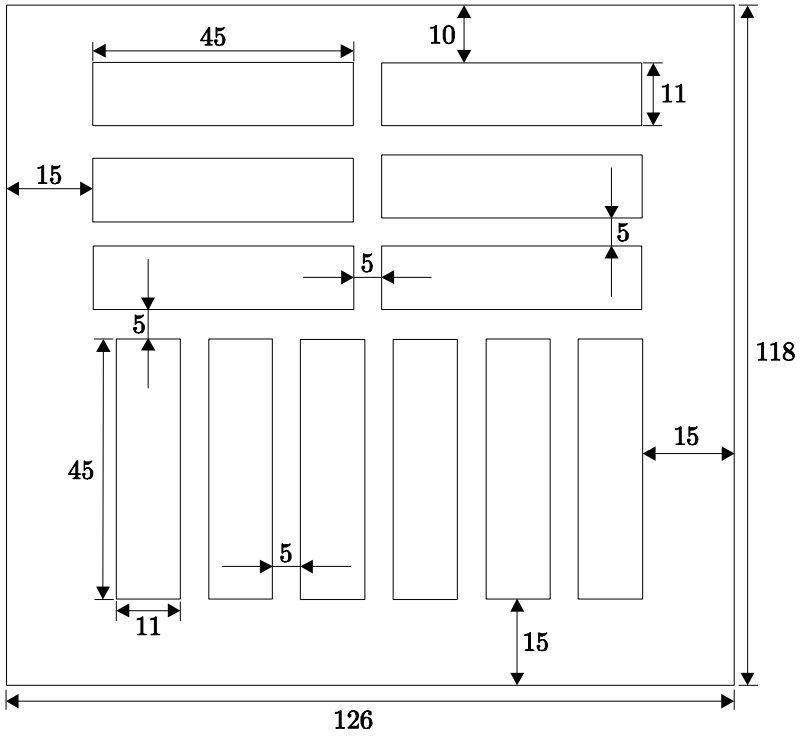

Figure 3-6: Plate and specimens' dimensions (mm)

cooling data are consistent and the coefficients well defined.

Determination of the stress free temperature

The stress free temperature (SFT) is needed to calculate the thermal loads in the analytical as well in the numerical models. For this purpose unsymmetric laminates with the following stacking sequence [0/90] were used. The following experimental method was used to determine the SFT: the laminates were conditioned in a temperature chamber at a constant moisture environment, while the temperature was sequentially increased. At each temperature increment a high resolution photograph was taken. Then the height h (Figure 3-11) was determined by using an image treatment software.

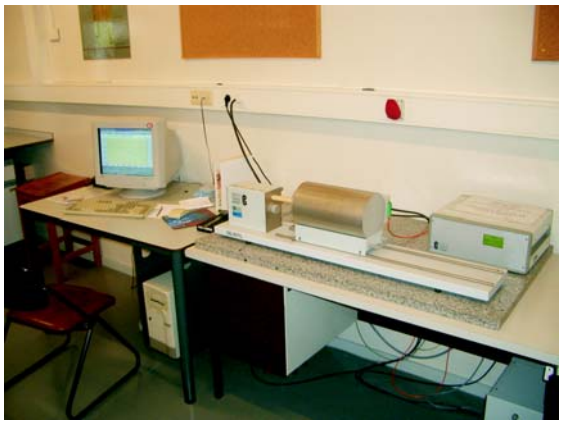

Figure 3-7: Dilatometer

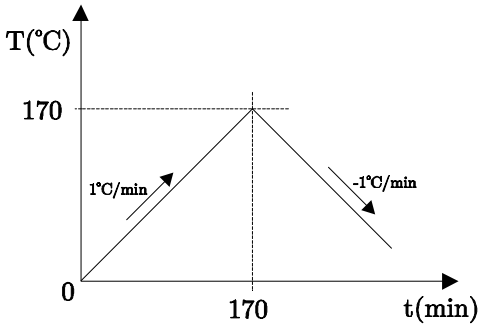

Figure 3-8: Heating and cooling rates

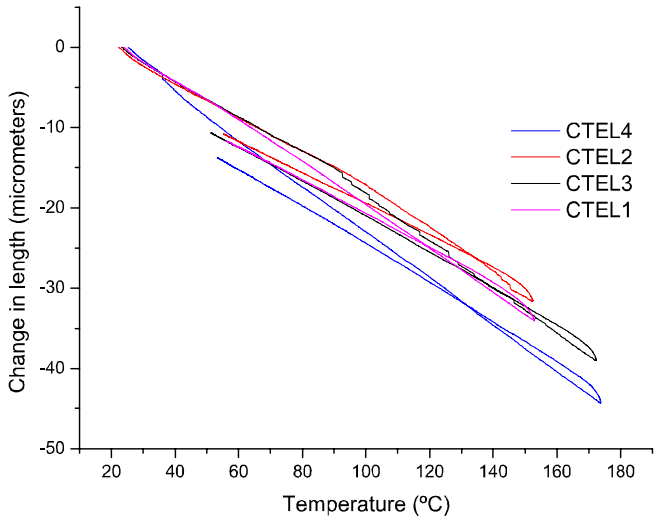

Figure 3-9: Results of the dilatometer test in the longitudinal direction

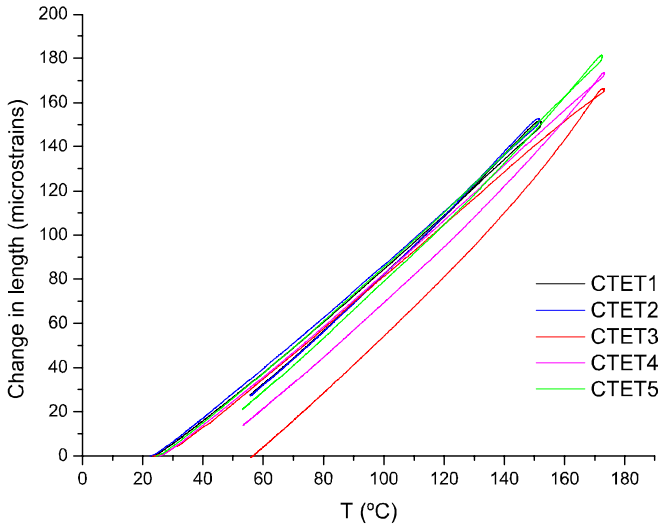

Figure 3-10: Results of the dilatometer test in the transverse direction

Table 3.10: Results of the dilatomeric tests α_{22}.

Spec. Ref.	w (mm)	t (mm)	Heat. Vel.	α_{22} ($10^{-6}/^{o}$C)
CTET-1	10.00	10.00	1.00	25.70
CTET-2	10.00	10.00	1.00	25.90
CTET-3	10.00	10.00	1.00	25.56
CTET-4	10.00	10.00	1.00	25.79
CTET-5	10.00	10.00	1.00	26.25
Average	-	-	-	25.84
STDV	-	-	-	0.26
COR	-	-	-	1.01
IC (%)	-	-	-	0.32

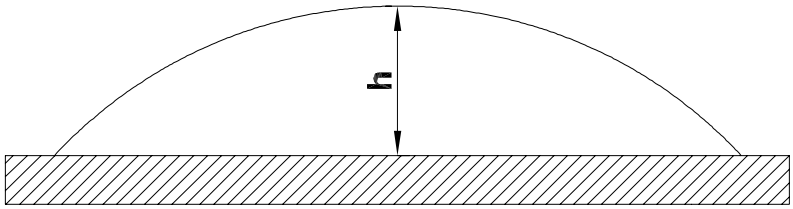

Figure 3-11: Measured height

Then a plot is made, as illustraded in Figure 3-12 to extrapolate the value of the stress free temperature. To facilitate this extrapolation, a simple proce-

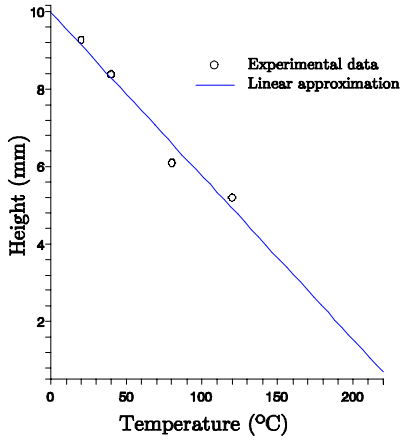

Figure 3-12: Determination of the stress free temperature

dure was implemented using Maple, following the flowchart of Figure 3-13. The respective code is shown in the appendix.

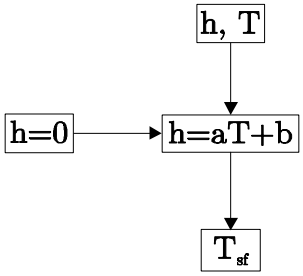

Figure 3-13: Flowchart for the stress free temperature

The stress free temperature obtained using this method is approximately 236^{o}C, which is much higher than the curing temperature of 180^{o}C. A similar

experiment conducted by Flaggs et al. [28] gives a stress free temperature approximately 10^{o}C higher than the curing temperature. This is due to the chemical shrinkage of the resin which is never recovered. The reason for the results disparity of the procedure carried out in this work relies, certainly, on the measuring method used: although the pictures taken were of great quality, there was some difficulty in finding the reference points needed. Therefore all further calculations, numerical and analytical, used the curing temperature of 180^{o}C when needed.

Image processing Method for determining Fibre Volume Fraction

The measurement of the fibre volume fraction, V_f, is an useful technique to assess the quality of the manufacturing process. It was initially attempted to measure the fibre volume fraction by burning the epoxy resin according to the ASTM standard D3171. However, the technique was not successful because part of the fibres also burned during the test. Therefore, the fibre volume fraction was measured using image processing techniques. Sixteen digital micrographs of the cross-section of the specimens were taken using a digital camera linked to an optical microscope. The images were afterwards modified to pure black and white using MatLab [29], and the fibre volume fraction was calculated using MatLab toolboxes as the ratio between the area in white, corresponding to the fibres, and the total area of the image, as shown in Figure3-14. The average

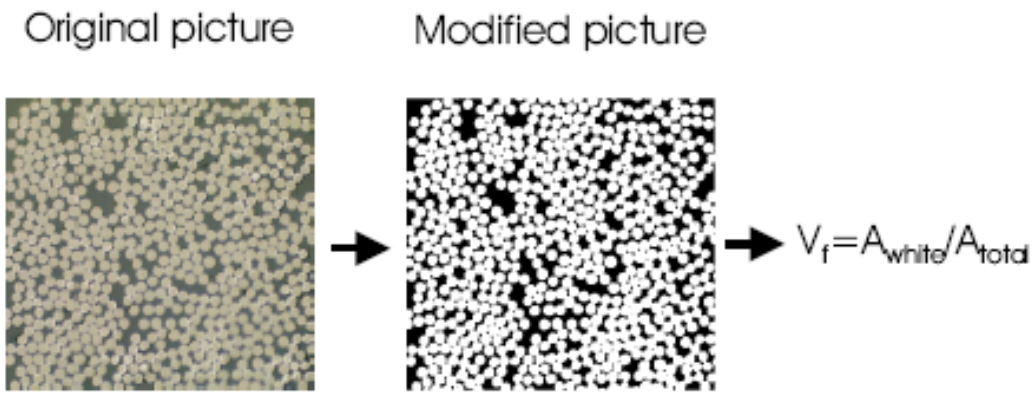

Figure 3-14: Laminate micrograph

fibre volume fraction using the procedure mentioned above was 59.1 percent. Using this information, the microscopic properties of the constituents, fibre and matrix, may be obtained by applying the rule of mixtures. They will be needed for the numerical simulations regarding a micro/mezoscale based model for residual stress determination.

3.4.2 Micromechanical properties

In this section the moduli of the fibre and matrix were determined and compared with the manufacturer's values. The microscopic properties were needed for the development of micromechanical models in Chapter 6. The following assumptions are made: The fibers are:

- Homogeneous
- Linearly elastic
- Orthotropic
- Regularly spaced
- Perfectly aligned
- Perfectly bonded

The matrix is:

- Homogeneous
- Linearly elastic
- Isotropic
- Void-free

Equation (3.1) shows the rule of mixtures, which represents a linear behaviour of the apparent Young's modulus, E_1, from E_m to E_f as V_f varies from 0 to 1.

$$E_1 = E_f \times V_f + E_m \times V_m \tag{3.1}$$

where V_f and V_m are the fiber and matrix volume fractions, respectively. Obviously, they are related to each other by Equation (3.2).

$$V_f = 1 - V_m \tag{3.2}$$

Regarding the Young's modulus in the transverse direction, E_2, it is defined as follows:

$$\frac{1}{E_2} = \frac{V_f}{E_f} + \frac{V_m}{E_m} \tag{3.3}$$

Solving Equations 3.1 and 3.3 for E_m and E_f, one gets the results shown in Table 3.11. The coefficients of thermal expansion in the longitudinal and perpendicular

Table 3.11: Fibre and matrix moduli

$E_f\,(GPa)$	$E_f\,(GPa)\,(Hexcel)$	$E_m\,(GPa)$	$E_m\,(GPa)\,(Hexcel)$
287.43	276.00	3.78	3.32

directions of the fibre are shown in Table 3.12. This method based on the simple

Table 3.12: Coefficients of thermal expansion

$\alpha_m\,(10^{-6}/°\mathrm{C})$	$\alpha_{f1}\,(10^{-6}/°\mathrm{C})$	$\alpha_{f2}\,(10^{-6}/°\mathrm{C})$
43.35	-0.90	7.20

rule of mixtures allows to obtain a rather good approximation of the constituents moduli. However, for the coeficients of thermal expansion of the matrix and fiber it does not work very well, because the fiber is not isotropic and a third equation would be needed to solve for α_{1f} and α_{2f}. The values presented in Table 3.12 are from the manufacturer. For the purpose of facilitating the determination of the constituents' moduli from the macroscopic properties, a simple Maple code was developed, whoose flowchart is shown in Figure 3-15. The respective code is presented in the appendix.

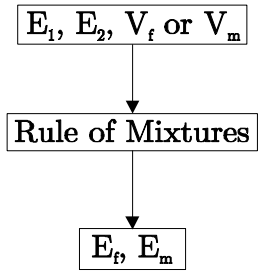

Figure 3-15: Flowchart for the determination of microscopic properties

3.5 Manufacture of specimens for hole drilling and hygrothermal tests

In this section the manufacturing process of the specimens for the hole drilling method and the water absorption tests is described. After an unsuccessfull attempt to produce the rather thin specimens using the hot press, it was decided to use an autoclave instead. For specimens with few layers it would be necessary to use a very thin steel sheet to control the thickness of the specimens and to avoid excessive resin flow. Also, the use of an autoclave allows for simultaneous production of specimens with different stacking sequences, thus increasing productivity.

3.5.1 Specimens' specifications and manufacture

Table 3.13 shows all the specifications regarding the specimens used in the hole drilling method.

Table 3.13: Specimen characterisitcs for the hole drilling experiments

Spec. Ref.	Lay-up	Specimens Qty.	Thickness (mm)
HDM0	$[0_2/90_2]_s$	1	1.048
HDM1	$[0_2/90_2]_s$	1	1.048
HDM2	$[0_2/90_2]_s$	1	1.048

Figure 3-16 shows the designation for each layer, which is used later in Chapter 5 to demonstrate the development of the residual stress in each ply with time.

$0^{\circ}(1)$
$0^{\circ}(2)$
$90^{\circ}(1)$
$90^{\circ}(2)$
$90^{\circ}(3)$
$90^{\circ}(4)$
$0^{\circ}(3)$
$0^{\circ}(4)$

Figure 3-16: Ply designation

Table 3.14 shows all the specifications regarding the specimens used in the hygrothermal experiments. Unlike the specimens used to determine basic material properties, an autoclave is used to produce the test specimens. The curing cycle is the same, as shown in Figure 3-1. Autoclave processing is used for the manufacture of superior quality structural components containing high fibre volume and low void contents. The autoclave is a pressure vessel which provides the curing conditions for the composite where the application of vacuum, pressure, heat up rate and cure temperature are controlled. Also, productivity is drastically increased, allowing a large amount of specimens with different sizes to be simultaneously manufactured, while maintaining the same quality.

Table 3.14: Specimen characterisitcs for the moisture absorption experiments

Spec. Ref.	Lay-up	Specimens Qty.	Thickness (mm)
MST1	$[0/90]$	5	0.262
MST2	$[0/90_2]$	5	0.393
MST3	$[0/90_4]$	5	0.655
MST4	$[90/0/90_3]$	5	0.655

Figure 3-17: Autoclave equipment used

Chapter 4

Analytical Determination of Residual Stresses

Residual stresses may be predicted by the classical laminate theory at the macroscopic level. However, when large displacements are involved, such as out-of-plane displacements in unsymmetric laminates, classical laminate theory alone is unable to correctly predict such shapes. The algorithm implemented here was used to determine the residual stress state according to the CLT at the ply level immediately after manufacture of the cross-ply specimens.

4.1 Stress-Srain relations of an individual ply within a laminate

The plane stress constitutive relation of ply k is established as:

$$\begin{bmatrix} \sigma_x \\ \sigma_y \\ \tau_s \end{bmatrix}_k = \begin{bmatrix} Q_{xx} & Q_{xy} & Q_{xs} \\ Q_{yx} & Q_{yy} & Q_{ys} \\ Q_{sx} & Q_{sy} & Q_{ss} \end{bmatrix}_k \begin{bmatrix} \epsilon_x \\ \epsilon_y \\ \gamma_s \end{bmatrix}_k \tag{4.1}$$

The total strains at any point may be related to the laminate's reference plane and curvatures as follows:

$$\begin{bmatrix} \epsilon_x \\ \epsilon_y \\ \gamma_s \end{bmatrix} = \begin{bmatrix} \epsilon_x^o \\ \epsilon_y^o \\ \gamma_s^o \end{bmatrix} + z \begin{bmatrix} \kappa_x \\ \kappa_y \\ \kappa_s \end{bmatrix} \tag{4.2}$$

Substituting Equation 4.2 in 4.1 we obtain:

$$\begin{bmatrix} \sigma_x \\ \sigma_y \\ \tau_s \end{bmatrix}_k = \begin{bmatrix} Q_{xx} & Q_{xy} & Q_{xs} \\ Q_{yx} & Q_{yy} & Q_{ys} \\ Q_{sx} & Q_{sy} & Q_{ss} \end{bmatrix}_k \left\{ \begin{bmatrix} \epsilon_x^o \\ \epsilon_y^o \\ \gamma_s^o \end{bmatrix} + z \begin{bmatrix} \kappa_x \\ \kappa_y \\ \kappa_s \end{bmatrix} \right\}_k \tag{4.3}$$

Equation 4.3 states that the stress components at any point within a laminate

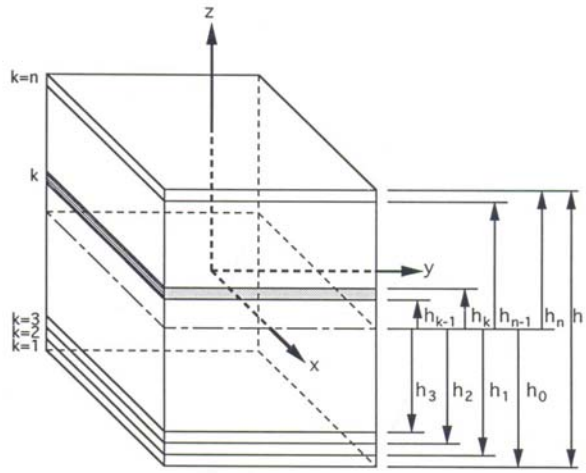

Figure 4-1: Reference plane and ply coordinates (after [1])

are obtained by knowing the strains of a point from the reference plane and the curvature of the layer containing the point of interest. However, this Equation does not take into account the free strains of the layer when it is subjected to a hygrothermal loading. Inverting Equation (4.1) and considering the principle of

strain superposition within a laminate:

$$\begin{bmatrix} \epsilon_x \\ \epsilon_y \\ \gamma_s \end{bmatrix}_k = \begin{bmatrix} S_{xx} & S_{xy} & S_{xs} \\ S_{yx} & S_{yy} & S_{ys} \\ S_{sx} & S_{sy} & S_{ss} \end{bmatrix}_k \begin{bmatrix} \sigma_x \\ \sigma_y \\ \tau_s \end{bmatrix}_k + \begin{bmatrix} \varepsilon_x \\ \varepsilon_y \\ \varepsilon_s \end{bmatrix}_k \tag{4.4}$$

In layer k the total strains $[\epsilon]^k_{x,y}$ equalize the sum of the strains produced by the existing stresses in the layer, $[\sigma]^k_{x,y}$, and the free unconstrained strains $[\varepsilon]^k_{x,y}$. Inverting Equation (4.4) gives the stresses in any layer k as follows:

$$\begin{bmatrix} \sigma_x \\ \sigma_y \\ \tau_s \end{bmatrix}_k = \begin{bmatrix} Q_{xx} & Q_{xy} & Q_{xs} \\ Q_{yx} & Q_{yy} & Q_{ys} \\ Q_{sx} & Q_{sy} & Q_{ss} \end{bmatrix}_k \begin{bmatrix} \epsilon_x - \varepsilon_x \\ \epsilon_y - \varepsilon_y \\ \gamma_s - \varepsilon_s \end{bmatrix}_k \tag{4.5}$$

Taking Equation (4.2) into account, one obtains the following more generalized equation:

$$\begin{bmatrix} \sigma_x \\ \sigma_y \\ \tau_s \end{bmatrix}_k = \begin{bmatrix} Q_{xx} & Q_{xy} & Q_{xs} \\ Q_{yx} & Q_{yy} & Q_{ys} \\ Q_{sx} & Q_{sy} & Q_{ss} \end{bmatrix}_k \begin{bmatrix} \epsilon^o_x + z\kappa_x - \varepsilon_x \\ \epsilon^o_y + z\kappa_y - \varepsilon_y \\ \gamma^o_s + z\kappa_s - \varepsilon_s \end{bmatrix}_k \tag{4.6}$$

In the following section the procedure for the determination of residual stresses owing to thermal effects only is thoroughly explained. It was implemented using the software Maple 9.5 [30].

4.1.1 Analytical Procedure for RTS Determination

The strains due to the thermal difference ΔT are first determined using Equation 4.7.

$$\begin{bmatrix} \varepsilon_x \\ \varepsilon_y \\ \varepsilon_s \end{bmatrix}_k = \begin{bmatrix} \alpha_x \\ \alpha_y \\ \alpha_s \end{bmatrix}_k \Delta T \tag{4.7}$$

The thermal loads are calculated for the laminate as follows:

$$\begin{bmatrix} N_x^{HT} \\ N_y^{HT} \\ N_s^{HT} \end{bmatrix} = \sum_{k=1}^{n} \begin{bmatrix} Q_{xx} & Q_{xy} & Q_{xs} \\ Q_{yx} & Q_{yy} & Q_{ys} \\ Q_{sx} & Q_{sy} & Q_{ss} \end{bmatrix}_k \begin{bmatrix} \varepsilon_x \\ \varepsilon_y \\ \varepsilon_s \end{bmatrix}_k t_k \tag{4.8}$$

For the thermal moments:

$$\begin{bmatrix} M_x^{HT} \\ M_y^{HT} \\ M_s^{HT} \end{bmatrix} = \sum_{k=1}^{n} \begin{bmatrix} Q_{xx} & Q_{xy} & Q_{xs} \\ Q_{yx} & Q_{yy} & Q_{ys} \\ Q_{sx} & Q_{sy} & Q_{ss} \end{bmatrix}_k \begin{bmatrix} \varepsilon_x \\ \varepsilon_y \\ \varepsilon_s \end{bmatrix}_k z_k t_k \tag{4.9}$$

where t_k and z_k are the layer's thickness and distance to the reference plane. The results of Equations (4.8) and (4.9) are used to calculate the reference plane strains and the laminate's curvatures, as shown in Equations (4.10) and (4.11).

$$\begin{bmatrix} \epsilon_x^o \\ \epsilon_y^o \\ \gamma_s^o \end{bmatrix}_k = \begin{bmatrix} a_{xx} & a_{xy} & a_{xs} \\ a_{yx} & a_{yy} & a_{ys} \\ a_{sx} & a_{sy} & a_{ss} \end{bmatrix}_k \begin{bmatrix} N_x^{HT} \\ N_y^{HT} \\ N_s^{HT} \end{bmatrix} + \begin{bmatrix} b_{xx} & b_{xy} & b_{xs} \\ b_{yx} & b_{yy} & b_{ys} \\ b_{sx} & b_{sy} & b_{ss} \end{bmatrix}_k \begin{bmatrix} M_x^{HT} \\ M_y^{HT} \\ M_s^{HT} \end{bmatrix} \tag{4.10}$$

$$\begin{bmatrix} \kappa_x \\ \kappa_y \\ \kappa_s \end{bmatrix}_k = \begin{bmatrix} c_{xx} & c_{xy} & c_{xs} \\ c_{yx} & c_{yy} & c_{ys} \\ c_{sx} & c_{sy} & c_{ss} \end{bmatrix}_k \begin{bmatrix} N_x^{HT} \\ N_y^{HT} \\ N_s^{HT} \end{bmatrix} + \begin{bmatrix} d_{xx} & d_{xy} & d_{xs} \\ d_{yx} & d_{yy} & d_{ys} \\ d_{sx} & d_{sy} & d_{ss} \end{bmatrix}_k \begin{bmatrix} M_x^{HT} \\ M_y^{HT} \\ M_s^{HT} \end{bmatrix} \tag{4.11}$$

The total strains are determined using Equation (4.2). The residual stresses are then calculated by means of Equation (4.5).

4.1.2 Maple code for the CLT implementation

The Maple code used is explained in the appendix. Although there are other well developed programmes based on the CLT [31], the procedures illustrated below were used and may serve as a basis for future development of analytical tools using mathematical computation programmes like Maple. Figure 4-2 shows the flowchart including all the data inputs needed by the algorithm. Although

only the orientation of the plies is read from a file, all the information regarding number of plies and their properties could also be in an input file. First, the

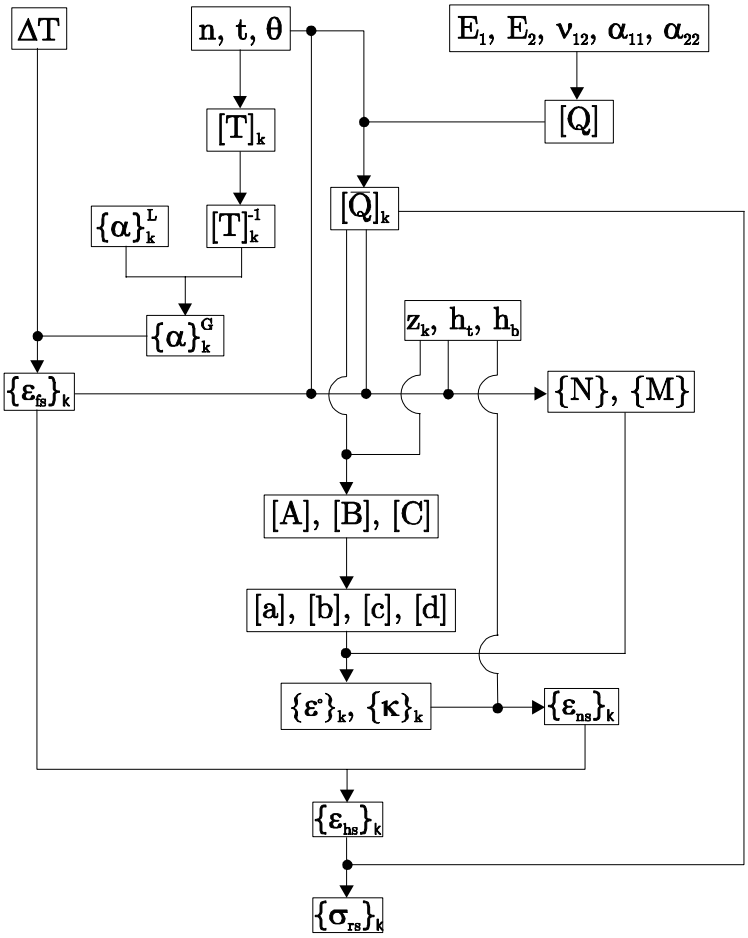

Figure 4-2: Classical Laminate Theory flowchart

ply stiffness and the transformation matrices $[Q]$ and $[T]_k$, respectively, are determined. Using ΔT and the vector $\{\alpha\}_k^G$ containing the coefficients of thermal expansion in the local coordinate system the free strains $\{\varepsilon_{fs}\}_k$ are calculated. The laminate loads and moments, $\{N\}$, $\{M\}$, respectively, are then calculated. Using the reduced transformation matrix $\left[\overline{Q}\right]_k$ and the ply coordinates, the laminate stiffness matrices $[A]$, $[B]$ and $[D]$ are determined. The laminate compliance matrices $[a]$, $[b]$, $[c]$ and $[d]$ follow. These are used together with $\{N\}$ and $\{M\}$ to obtain the laminate midplane strains and curvatures $\{\varepsilon^o\}_k$ and $\{\kappa\}_k$, respectively. The difference between the free strains, $\{\varepsilon_{fs}\}_k$ and the net strains, $\{\varepsilon_{ns}\}_k$, are the hygrothermal strains $\{\varepsilon_{hs}\}_k$, which are multiplied by $\left[\overline{Q}\right]_k$ to obtain the

residual stresses vector $\{\sigma_{rs}\}_k$ for each ply.

Chapter 5

Experimental Procedures

The hole drilling method applied to orthotropic materials as described in reference [22] is used for the determination of residual stresses in symmetric laminates. A detailed description of the method is presented in this Chapter.

5.1 Theoretical formulation

The model used to determine the residual stress distribution is based on the assumptions indicated bellow:

- the material is elastic and orthotropic
- the stress component (σ_{zz}) perpendicular to the surface is very small

Sicot [22] adapted a previous work developed by Soete [32] and Lake [33] to the case of orthotropic materials and also the incremental character of the hole drilling method and the consequent redistribution of the stresses after each increment.

The change in strain at any location, for a fixed radial distance from the centre of the hole, can be described by the following equation:

$$\varepsilon_{in}(\theta_i) = A_{in}(\sigma_{1hi} + \sigma_{2hi}) + (\sigma_{1hi} - \sigma_{2hi})(B_{in}\cos(2\theta_i) + C_{in}\sin(2\theta_i)) \qquad (5.1)$$

where ε_{in} is the strain contribution of layer i for the total strain measured at the nth increment, σ_{1hi} and σ_{2hi} are the main residual stresses in layer i (the depth of the layer is h_i), θ_i is the angle between the reference gauge and the first main direction of residual stress and A_{in}, B_{in} and C_{in} are the calibration coefficients for the nth increment and loading on the ith layer.

The strain measurements in three directions are used to determine the three unknown factors σ_{1hi}, σ_{2hi} and θ_i for each drilling increment. For example, when the first increment is drilled (h_i=h_1), the strain is obtained for the three directions corresponding to the orientations of the strain gauges:

$$\begin{cases} \varepsilon_{11}^{1}(\theta_1) = A_{11}(\sigma_{1h1}+\sigma_{2h1}) + (\sigma_{1h1}-\sigma_{2h1})(B_{11}\cos(2\theta_1) + C_{11}\sin(2\theta_1)) \\ \varepsilon_{11}^{2}(\theta_1) = A_{11}(\sigma_{1h1}+\sigma_{2h1}) + (\sigma_{1h1}-\sigma_{2h1})(B_{11}\cos(2(\theta_1+\alpha)) + C_{11}\sin(2(\theta_1+\alpha))) \\ \varepsilon_{11}^{3}(\theta_1) = A_{11}(\sigma_{1h1}+\sigma_{2h1}) + (\sigma_{1h1}-\sigma_{2h1})(B_{11}\cos(2(\theta_1+\beta)) + C_{11}\sin(2(\theta_1+\beta))) \end{cases} \tag{5.2}$$

where ε_{11}^{j} is the contribution in the jth direction and α and β are the angles of the $2nd$ and $3rd$ direction of measurement.

After the nth increment the total depth becomes hn and the equations become:

$$\begin{cases} \varepsilon_{nn}^{1}(\theta_n) = A_{nn}(\sigma_{1hn}+\sigma_{2hn}) + (\sigma_{1hn}-\sigma_{2hn})(B_{nn}\cos(2\theta_n) + C_{nn}\sin(2\theta_n)) \\ \varepsilon_{nn}^{2}(\theta_n) = A_{nn}(\sigma_{1hn}+\sigma_{2hn}) + (\sigma_{1hn}-\sigma_{2hn})(B_{nn}\cos(2(\theta_n+\alpha)) + C_{nn}\sin(2(\theta_n+\alpha))) \\ \varepsilon_{nn}^{3}(\theta_n) = A_{nn}(\sigma_{1hn}+\sigma_{2hn}) + (\sigma_{1hn}-\sigma_{2hn})(B_{nn}\cos(2(\theta_n+\beta)) + C_{nn}\sin(2(\theta_n+\beta))) \end{cases} \tag{5.3}$$

However, after the first increment, the change in the hole geometry must also be taken into account. Each previously removed layer affects the total strain measured on the surface. So the strain measured on the surface due to the removed layer only is expressed as follows (to simplify $\varepsilon_{nn}^{j} = \varepsilon_{n}^{j}$):

$$\varepsilon_{n}^{1} = \varepsilon_{mn}^{1} - \sum_{i=1}^{n-1} \varepsilon_{in}^{1} \tag{5.4}$$

$$\varepsilon_n^2 = \varepsilon_{mn}^2 - \sum_{i=1}^{n-1} \varepsilon_{in}^2 \tag{5.5}$$

$$\varepsilon_n^3 = \varepsilon_{mn}^3 - \sum_{i=1}^{n-1} \varepsilon_{in}^3 \tag{5.6}$$

where ε_{in}^j is the contribution of the i layer in j direction in the case of the nth increment and ε_{mn}^j is the total strain measured on the surface by the strain gauges in the j direction.

For example, after three increments the resulting expression is:

$$\varepsilon_3^1 = \varepsilon_{m3}^1 - \sum_{i=1}^{2} \varepsilon_{i3}^1 = \varepsilon_{m3}^1 - \left(\varepsilon_{13}^1 + \varepsilon_{23}^1\right) \tag{5.7}$$

After substituting in Equation (5.1):

$$\varepsilon_3^1 = \varepsilon_{m3}^1 - \begin{array}{l}[(A_{13}\left(\sigma_{1h1} + \sigma_{2h1}\right) + \left(\sigma_{1h1} - \sigma_{2h1}\right)\left(B_{13}\cos(2\theta_1) + C_{13}\sin(2\theta_1)\right)) + \\ +(A_{23}\left(\sigma_{1h2} + \sigma_{2h2}\right) + \left(\sigma_{1h2} - \sigma_{2h2}\right)\left(B_{23}\cos(2\theta_2) + C_{23}\sin(2\theta_2)\right))]\end{array} \tag{5.8}$$

With this method Sicot [22] considers that for each increment the total strain measured on the surface can be divided into two parts:

- the first is due to the residual stress on the removed layer
- the second is the contribution of the residual stress redistribution caused by the change in geometry.

For a strain gauge similar to the one shown in Figure 5-2, three equations are obtained for each drilling increment by reversing the system as follows:

$$\sigma_{1hn} = \frac{\varepsilon_n^1\left(A_{nn} - B_{nn}\sin 2\theta_n + C_{nn}\cos 2\theta_n\right) - \varepsilon_n^2\left(A_{nn} - B_{nn}\cos 2\theta_n - C_{nn}\cos 2\theta_n\right)}{2A_{nn}B_{nn}\left(-\sin 2\theta_n + \cos 2\theta_n\right) + 2A_{nn}C_{nn}\left(\sin 2\theta_n + \cos 2\theta_n\right)} \tag{5.9}$$

$$\sigma_{2hn} = \frac{-\varepsilon_n^1\left(A_{nn} + B_{nn}\sin 2\theta_n - C_{nn}\cos 2\theta_n\right) + \varepsilon_n^2\left(A_{nn} + B_{nn}\cos 2\theta_n + C_{nn}\cos 2\theta_n\right)}{2A_{nn}B_{nn}\left(-\sin 2\theta_n + \cos 2\theta_n\right) + 2A_{nn}C_{nn}\left(\sin 2\theta_n + \cos 2\theta_n\right)} \tag{5.10}$$

$$\theta_n = \frac{1}{2}\tan^{-1}\left[\frac{C_{nn}\left(\varepsilon_n^3 - \varepsilon_n^1\right) - B_{nn}\left(2\varepsilon_n^2 - \varepsilon_n^1 - \varepsilon_n^3\right)}{C_{nn}\left(2\varepsilon_n^2 - \varepsilon_n^1 - \varepsilon_n^3\right) - B_{nn}\left(\varepsilon_n^3 - \varepsilon_n^1\right)}\right] \tag{5.11}$$

The determination of the calibration coefficients which are needed for Equations (5.9) to (5.11) is explained in the next section.

5.2 Specimens

The hole drilling method was applied on specimens with the dimensions shown in Figure 5-1. The stacking sequence and number of test specimens is shown in Table 5.1.

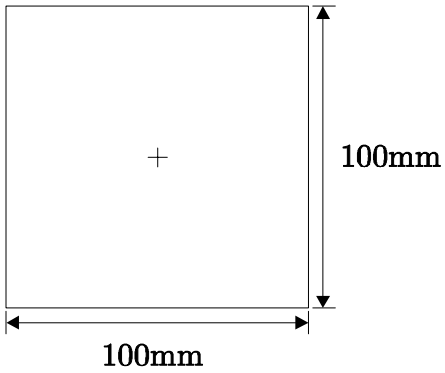

Figure 5-1: Dimensions of the specimen used with the HDM

Table 5.1: Test plan for the hole drilling method

Spec. Ref.	Time after cure (months)	Lay-up	Specimens Qty.
HDM1	0	$[0_2/90_2]_S$	1
HDM2	1	$[0_2/90_2]_S$	1
HDM3	2	$[0_2/90_2]_S$	1

5.3 Strain Gauging

The strain gauge used is of the type "HBM RY61". Figure 5-2 shows the main parameters of the strain gauge to be considered. The values of r_i and r_o corre-

spond to the distances from the centre to the beginning and ending of the strain gauges.

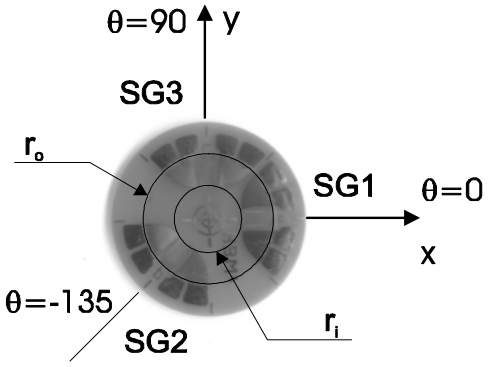

Figure 5-2: Parameters of the rosette strain gauge

Table 5.2: Strain gauge caracteristics

SG type	Hole radius (mm)	r_o (mm)	r_i (mm)	Nominal resitance (Ω)
HBM RY61	1.5	3.05	1.5	120

The rosette strain gauge has a nominal resistance of 120Ω. The instrumentation procedures are the same as those mentioned in Chapter 3 with the only difference being the fact that the surface of the specimen is not abraded, it is only degreased with the "HBM-RMS1" cleaning solution. This is because the residual stress state of the specimen may be changed if manual abrasion is carried out. Although no literature reference was found regarding this fact, experiments carried out in the past by HBM using a cast polyester specimen led to this affirmation.

5.4 Hole Quality

To assess the quality of the drilled hole, a specimen was cut and polished to search for possible drilling damage in the vicinity of the hole's surface, as shown in Figure 5-3.

The samples were obtained by cutting sections of the specimens using a silicon carbide saw and by casting it into acrylic resin. The cure of the resin took place

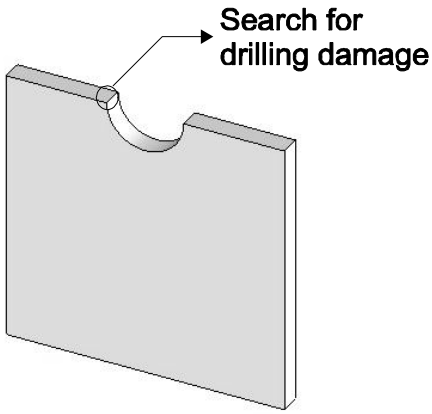

Figure 5-3: Specimen used for microscopic inspection

at room temperature. The surface to be analysed was previously marked in the specimen and to avoid any interference of the cutting process the sample was cut in a plane parallel to this surface. The surface of the resin parallel to the composite surface was ground on a rotary grinder until reaching the composite surface to be analysed. The cast specimen's height was measured in between to assure the location of the surface to be micrographed.The polishing procedure began with 80 grit paper, then 160, 320 and 800. After these steps the specimen was polished with a diamond sprayed cloth, first 3 μm and then 1 μm. An optical microscope was used for damage detection.

Delamination is the main concern regarding the drilling procedures of composite laminates [34], [35]. It reduces the structural integrity of the laminate and may influence drastically the measured relieved strains. Basically, damage may occur at the entrance and at the exit of the drilling tool. To avoid delamination when the drill is approaching the last plies of the laminate, this must be properly backed up.

In Figure 5-4 the hole was drilled using the parameters specified in Table 5.4. The surface of the hole is quite straight, which is a necessary condition for the correct applicability of the hole drilling method.

Figure 5-5 shows a quasi-isotropic laminate which was drilled at 100.000 RPM.

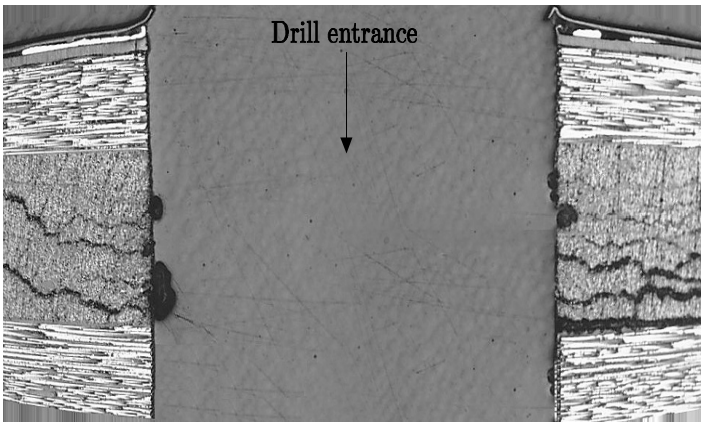

Figure 5-4: Cross ply laminate micrograph

The drill advance was done manually. It may be seen that the surface of the hole is rather irregular. The $+45^o$ and -45^o plies are noticed to be particularly damaged. Although this laminate was not used for residual stress experiments in this work, it demonstrates the effect of a specific drilling procedure on the surface of the hole. The drill was the same as in Figure 5-4.

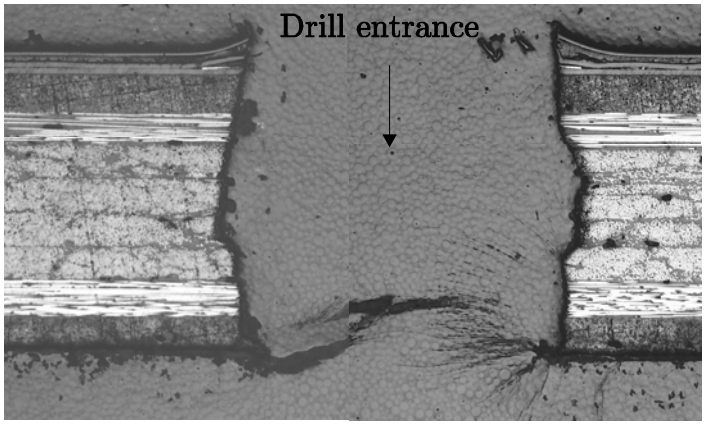

Figure 5-5: Quasi isotropic laminate micrograph

5.5 Determination of the calibration coefficients

The determination of the constants A_{in}, B_{in} and C_{in} is of crucial importance for the successful calculation of the residual stress values in the composite specimen. It was decided to determine these coefficients numerically because it is very difficult, or even impossible, to apply a known residual stress field for calibration

purposes in a 1.5mm diameter hole. Also, the orthotropic properties of the material are known and therefore reliable finite element models can be developed to determine the calibration constants. The calibration coeficients depend on the geometry of the hole, the strain gauge rosette and the relative position of layer i. The finite element simulations use 3D orthotropic brick elements of the C3D8R type. All simulations are done using the ABAQUS Standard software [36].

The coefficient A_{in} can be determined by applying an equibiaxial residual stress field, equivalent to a uniform pressure P acting on the inside surface of the hole, as shown in Figure 5-6.

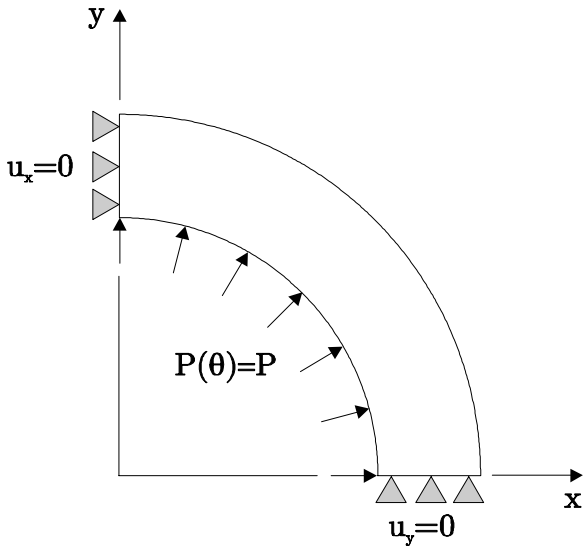

Figure 5-6: Applied load to determine A_{in}

Using the FEM model, the radial displacements corresponding to the strain gauges boundaries are obtained. Using Equation 5.12 A_{in} is determined.

$$A_{in} = \frac{U_{in}(r2,0) - U_{in}(r1,0)}{2\sigma L} \tag{5.12}$$

where $L = r_2 - r_1$ corresponds to the gauge length, $U_{in}(r1,0)$ and $U_{in}(r2,0)$ are the displacements corresponding to the strain gauge borders as shown in Figure 5-7. Note that this and the following calibration coefficients have the unit MPa^{-1}.

The coefficients B_{in} and C_{in} can be determined by applying a shear stress

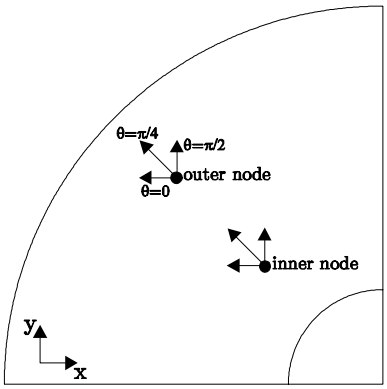

Figure 5-7: Nodes where the displacements are determined

field on the inside surface of the hole, as shown in Figure 5-8.

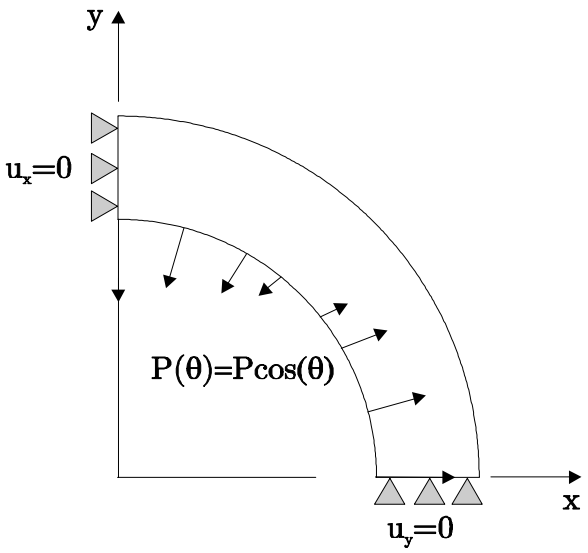

Figure 5-8: Applied load to determine B_{in} and C_{in}

To simulate this stress distribution in the finite element programme Abaqus [36], a small Fortran [37] subroutine was implemented. The respective code is shown in Figure 5-9.

The coefficients B_{in} and C_{in} are calculated by means of Equations (5.13) and (5.14), respectively.

$$B_{in} = \frac{U_{in}(r2, 0) - U_{in}(r1, 0)}{2\sigma L} \tag{5.13}$$

```
SUBROUTINE DLOAD (F,KSTEP,KINC,TIME,NOEL,NPT,LAYER,KSPT,COORDS,
&JLTYP,SNAME)
INCLUDE 'ABA_PARAM.INC'
DIMENSION COORDS(3)
CHARACTER*80 SNAME
PI=2.*ASIN(1.D0)
THETA=PI*COORDS(3)/180.D0
P=1.
JLTYP=21
F=P*COS(2*THETA)
RETURN
END
```

Figure 5-9: Fortran subroutine DLOAD

$$C_{in} = \frac{U_{in}(r2, \pi/4) - U_{in}(r1, \pi/4)}{2\sigma L} \tag{5.14}$$

For example, Figure 5-10 presents the case where for each ply four drilling increments are used. The coefficients A_{14}, A_{24}, A_{34} and A_{44} may be determined.

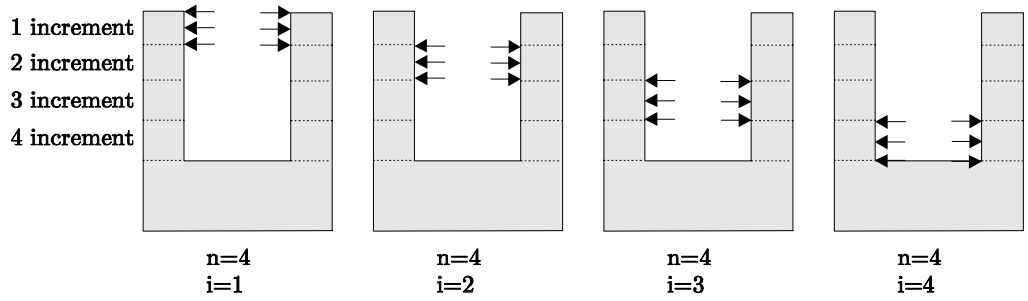

Figure 5-10: Fourth drilling stage

Figures 5-11 to 5-18 show the finite element results of the spacial displacement U_1, which is needed for the determination of the calibration coefficients. The picture on the left corresponds to the load case represented in Figure 5-6, the one on the right is related to the load case shown in Figure 5-8.

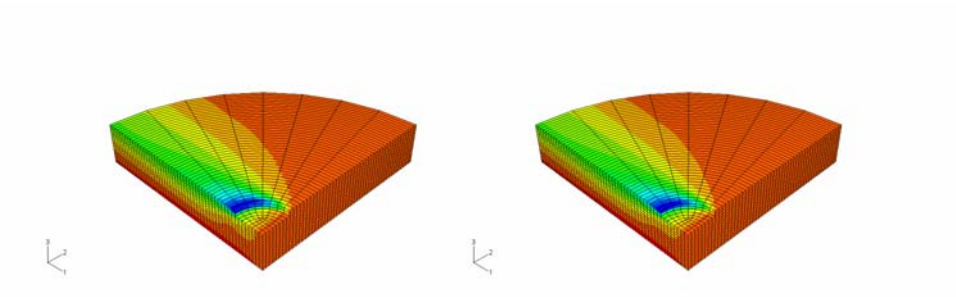

Figure 5-11: First increment

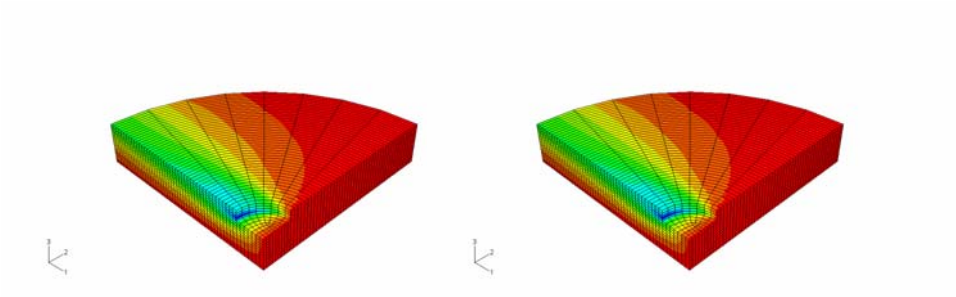

Figure 5-12: Second increment

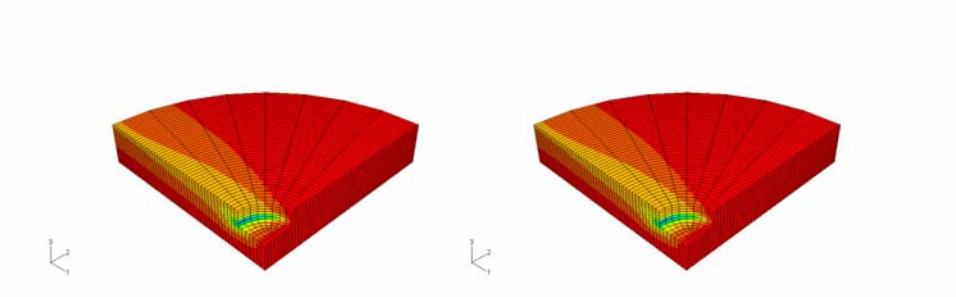

Figure 5-13: Third increment

Although the applied loads are different in Figures 5-11 to 5-18, the distribution of the displacement fields are rather similar.

Figures 5-19 to 5-21 show the displacements obtained at the surface of the FEM model for the needed directions $\theta_n = 0$, $\theta_n = \frac{\pi}{2}$ and $\theta_n = \frac{\pi}{4}$.

The calibration coefficients are indicated in Table 5.3.

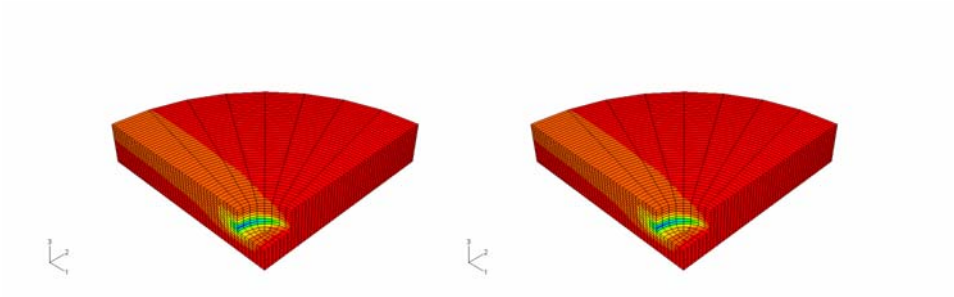

Figure 5-14: Fourth increment

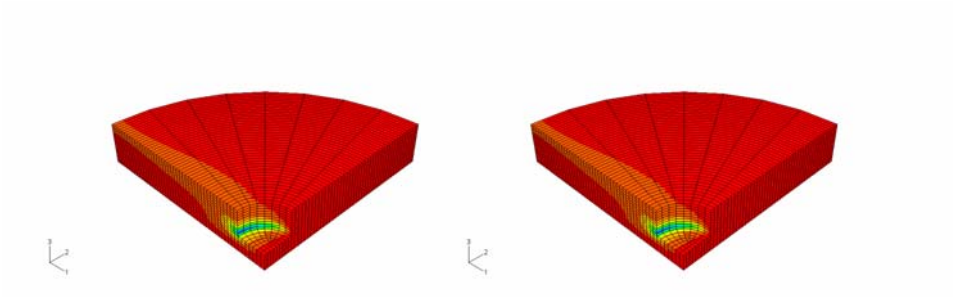

Figure 5-15: Fifth increment

5.5.1 Measurement of residual strains

For the experimental measurement of the residual strains, specimens with the caracteristics shown in Figure 5-1 were used. A hard metal cutting tool with a tip diameter of 1.5 mm was used to make an incremental hole in the composite specimen. In this work, the depth of each increment coincides with the cured layer thickness i.e. one drill increment per ply was chosen. According to Sicot [38] the number of increments used has little influence on the calculated residual strains. Table 5.4 shows the drilling parameters used.

The specimens were drilled in a CNC machine, as shown in Figure 5-22.

Drilling test after the curing cycle

Figure 5-23 shows the strains measured the day after curing of the specimen. Between each drilling increment the strains were allowed to relax for two minutes. This timing was found to be adequate for strain stabilization between drilling increments based on previous experiments.

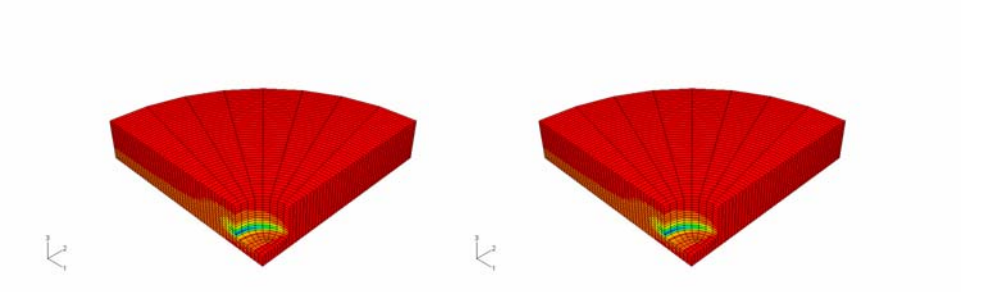

Figure 5-16: Sixth increment

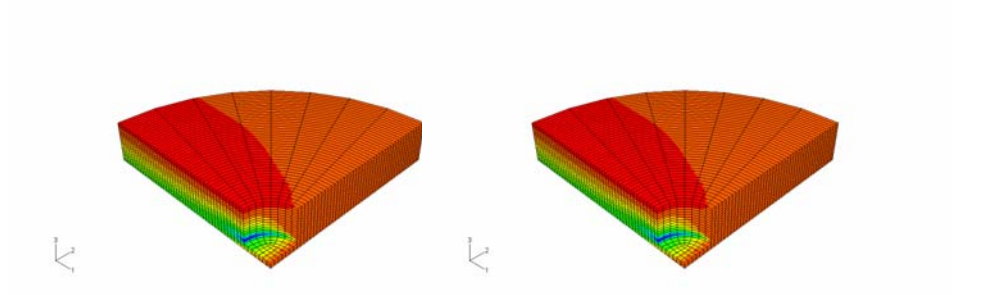

Figure 5-17: Seventh increment

Figures 5-24 and 5-25 show the residual stresses through the thickness of the specimen in material coordinates. The principal residual stresses were first determined using equations (5.9) to (5.11). Using a properly defined transformation matrix they were transformed in local material stresses.

Drilling test after one month of the curing cycle

Figure 5-26 shows the measured strains after one month passed since the curing of the specimen.

Drilling test after two months of the curing cycle

Figure 5-27 and 5-28 show the residual stresses through the thickness of the specimen in material coordinates. The principal residual stresses were first determined using equations (5.9) to (5.11). Using a properly defined transformation matrix they were transformed in local material stresses.

Figure 5-29 shows the measured strains after two months passed since the curing of the specimen.

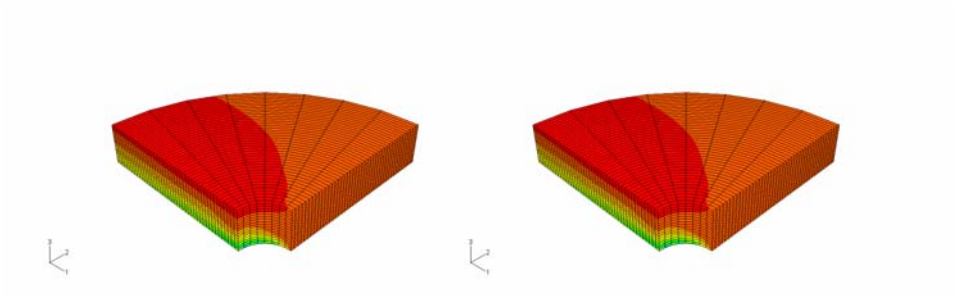

Figure 5-18: Eighth increment

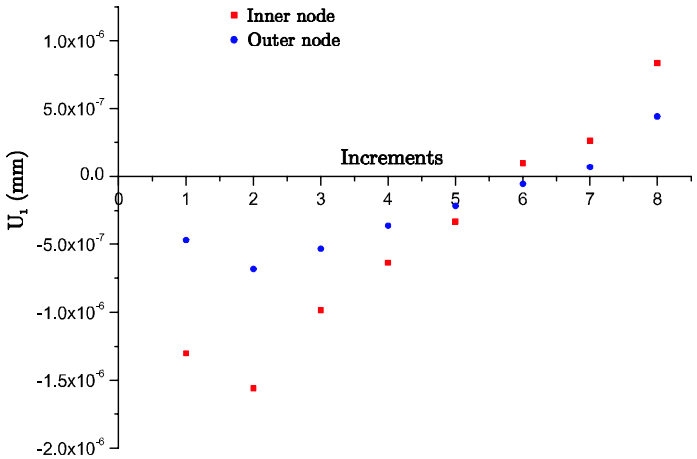

Figure 5-19: Displacements U1 ($\theta_n = 0$)

Figure 5-30 and 5-31 show the residual stresses through the thickness of the specimen in material coordinates. The principal residual stresses were first determined using equations (5.9) to (5.11). Using a properly defined transformation matrix they were transformed in local material stresses.

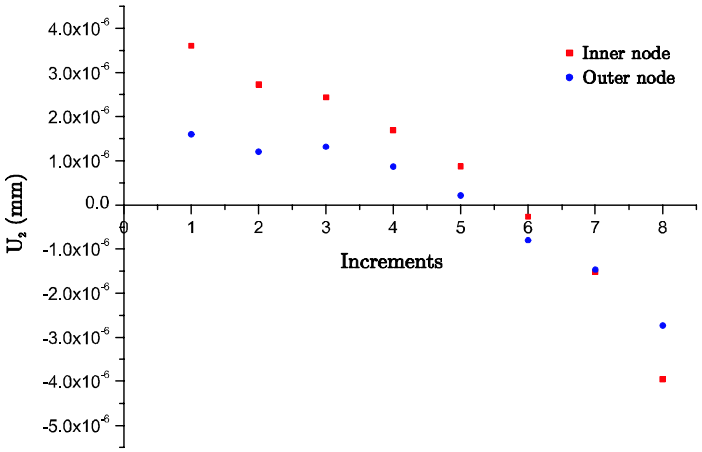

Figure 5-20: Displacements U1 ($\theta_n = \frac{\pi}{2}$)

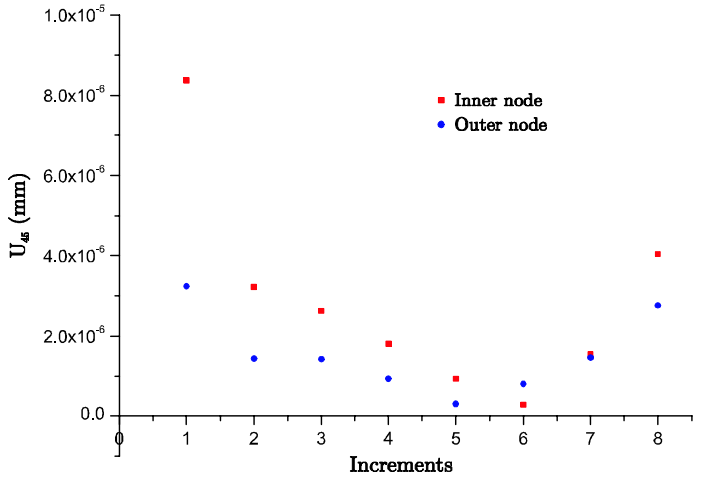

Figure 5-21: Displacements U1 ($\theta_n = \frac{\pi}{4}$)

Table 5.3: Calibration coefficients

Layer	A_{in} (MPa^{-1})	B_{in} (MPa^{-1})	C_{in} (MPa^{-1})
1	1.68E-6	3.55E-6	-1.70E-6
2	1.27E-6	1.30E-6	-5.70E-7
3	1.21E-6	1.21E-6	-3.90E-7
4	8.27E-7	8.27E-7	-2.80E-7
5	3.53E-7	3.53E-7	-2.00E-7
6	-3.40E-7	-3.40E-7	1.68E-7
7	-9.60E-7	-9.60E-7	-2.60E-8
8	-2.20E-6	-2.20E-6	-4.10E-7

Table 5.4: Hole drilling parameters

RPM	Feed rate (mm/min)	Increment depth (mm)	n^o of increments
3000	1	0.131	8

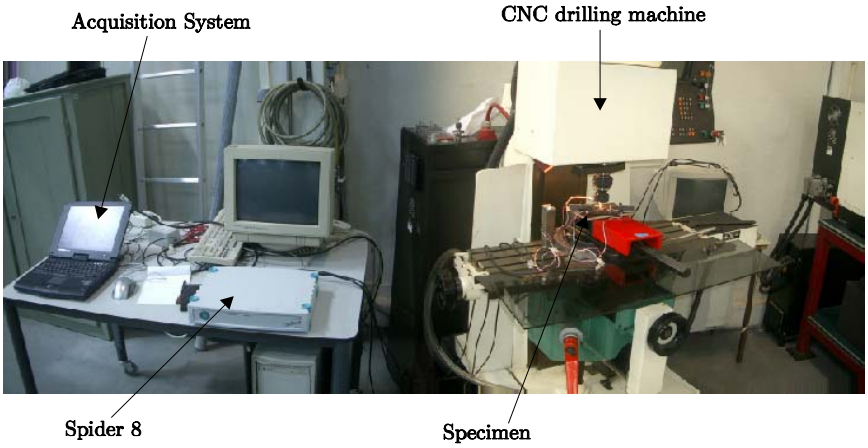

Figure 5-22: Experimental setup used for the drilling procedure

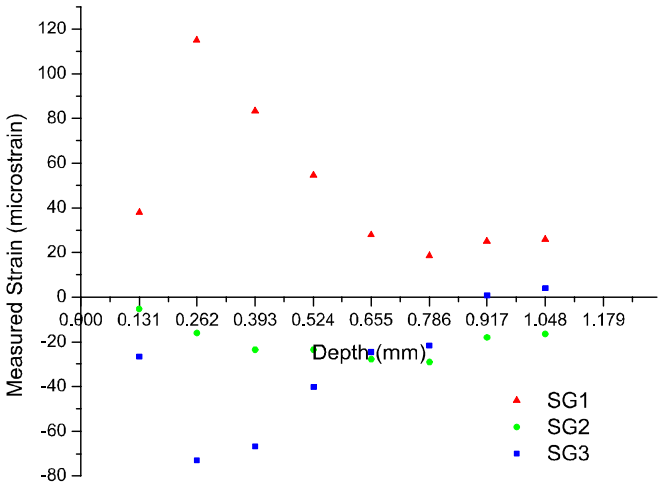

Figure 5-23: Measured strains

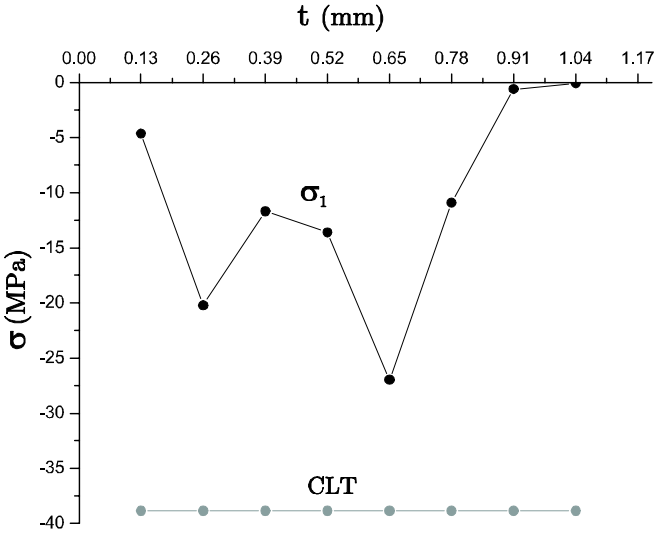

Figure 5-24: Longitudinal residual stresses after curing

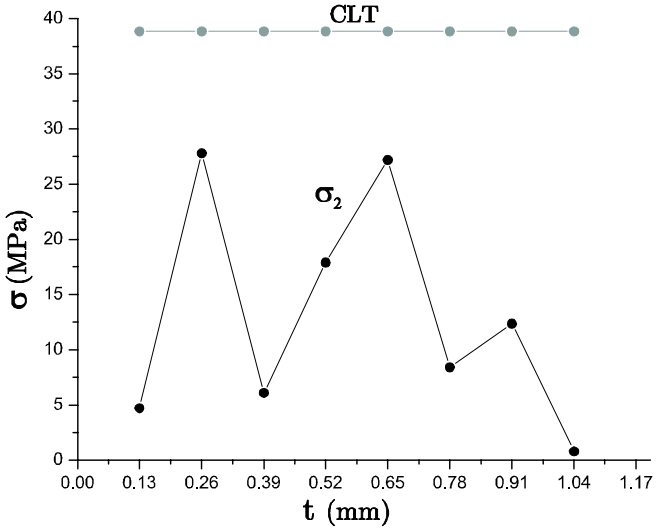

Figure 5-25: Transversal residual stresses after curing

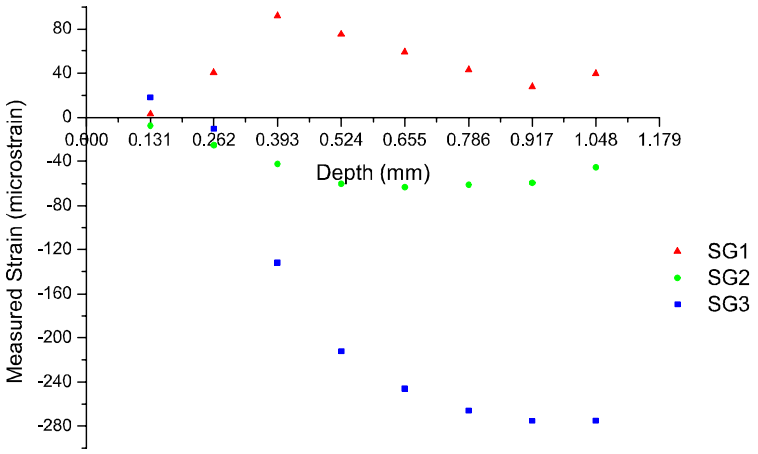

Figure 5-26: Measured strains

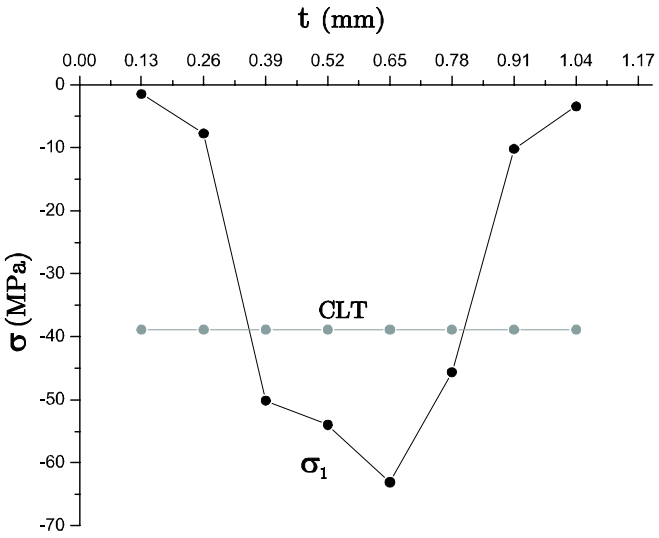

Figure 5-27: Longitudinal residual stresses one month after curing

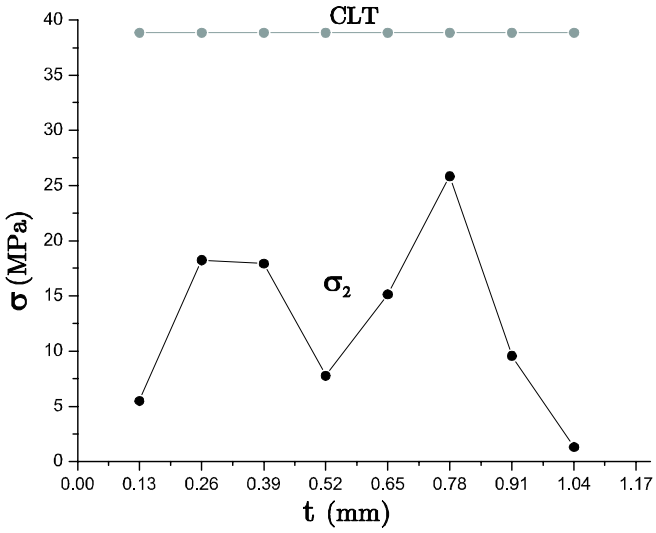

Figure 5-28: Transversal residual stresses one month after curing

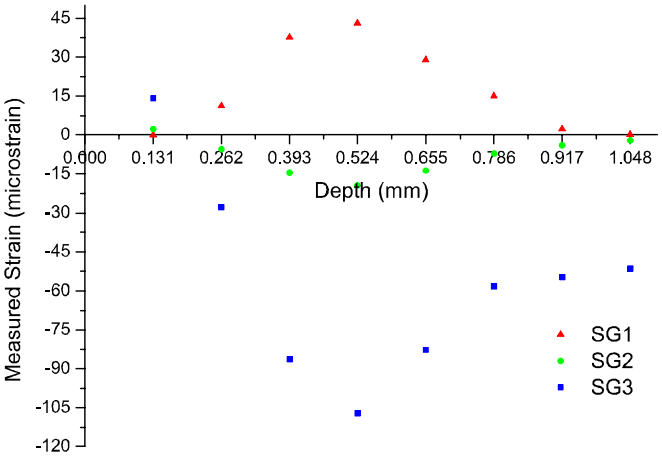

Figure 5-29: Measured strains

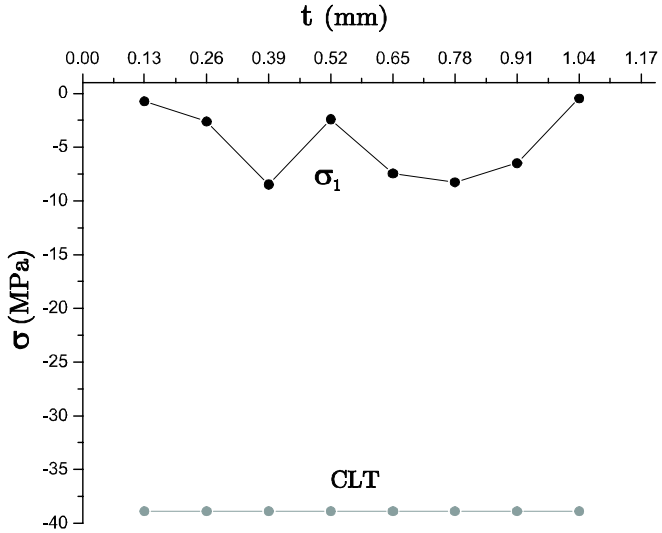

Figure 5-30: Longitudinal residual stresses two months after curing

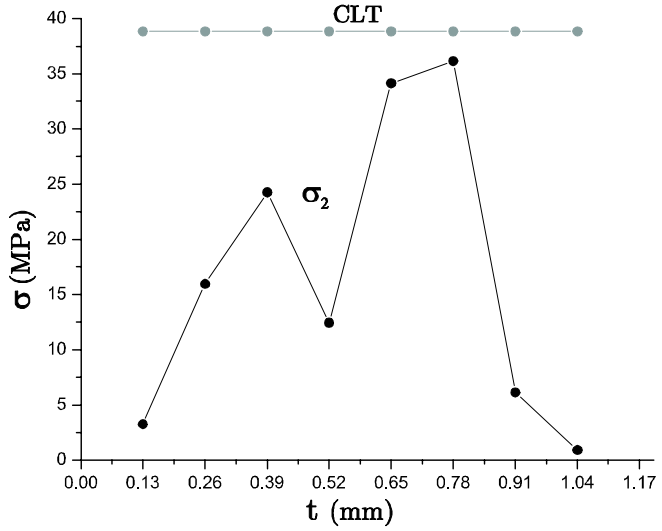

Figure 5-31: Transversal residual stresses two months after curing

Evolution of residual stresses with time

For a better understanding of the evolution of the residual stresses in the laminate, each ply group, 0^o and 90^o, respectively, was analysed separately, as shown in Figures 5-32 to 5-35.

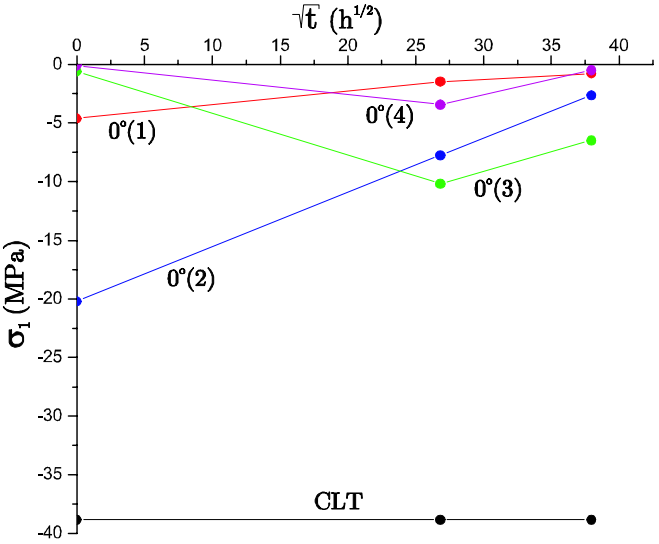

Figure 5-32: Evolution of residual stresses (σ_1) for the 0^o plies

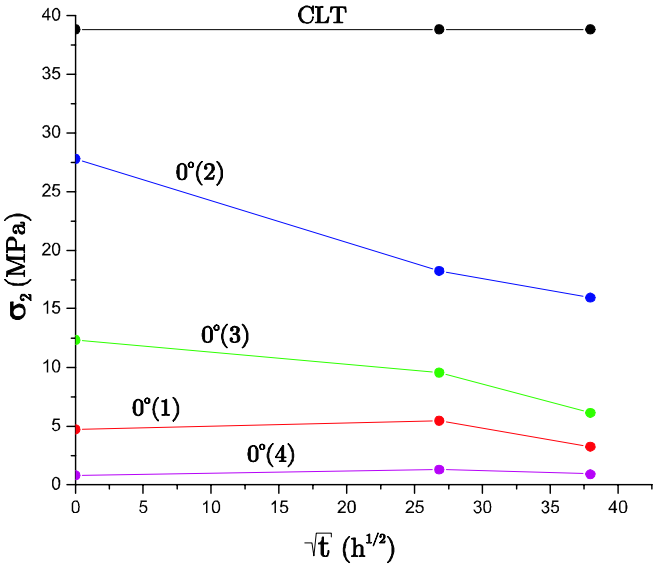

Figure 5-33: Evolution of residual stresses (σ_2) for the 0^o plies

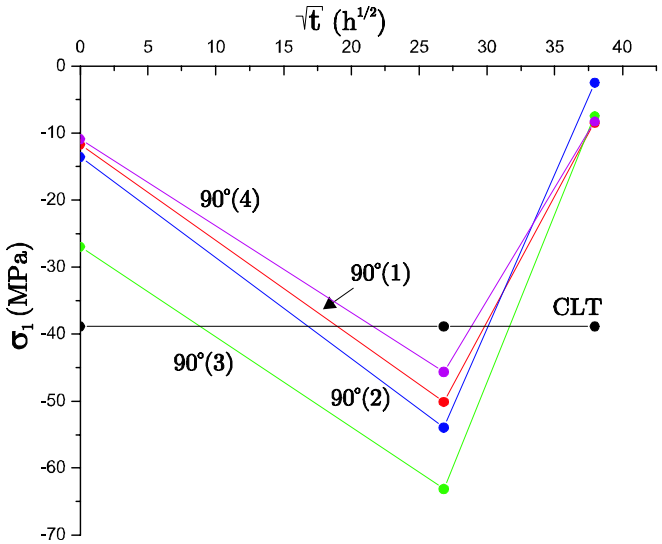

Figure 5-34: Evolution of residual stresses (σ_1) for the 90^o plies

Interpretation of the hole drilling tests

The strains measured by the gauges vary significantly from test to test. Their behaviour is unpredictable, although a decrease in the measured strains was expected with time. It happened for SG1, but not for the remaining strain gauges. The hole drilling method was used to determine residual stresses in $[0_2/90_2]_s$ laminates. The goal was to determine the stress level at different periods of time after manufacturing and check for possible stress relaxation.

The classical laminate theory predicts a value of -38.85 MPa for σ_1 and 38.85 MPa for σ_2. It is clear that the residual stresses obtained by the hole drilling method are not constant through the thickness of the specimens. σ_1 is negative in the 0^o layers. σ_2 is positive in the 90^o. The values of σ_1 for the 0^o plies seem generally to relax with time, particularly in the $0^o(1)$ and $0^o(2)$ plies. However, in the third and fourth plies the stresses determined after one month of fabrication are actually lower, than those calculated immediately after curing, but increase thereafter.

At the 90^o group there is a decrease in σ_1 for all plies, but after two months σ_1 increases again.

In the transversal direction, some stress relaxation is noticed in the 0^o plies,

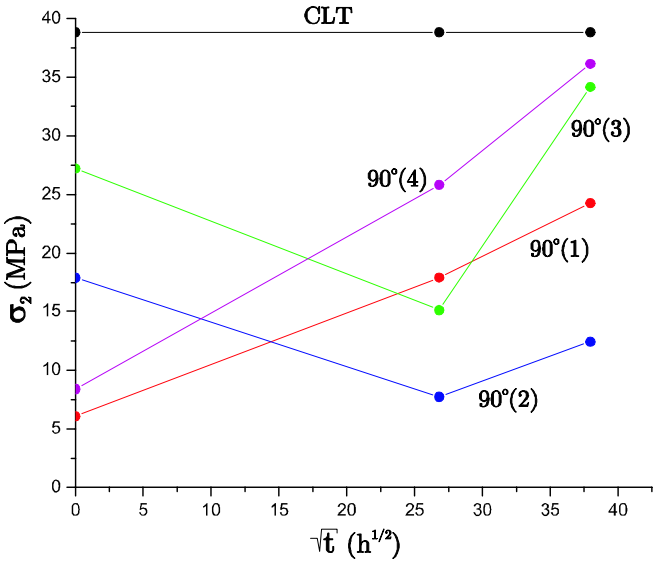

Figure 5-35: Evolution of residual stresses (σ_2) for the 90^o plies

particularly in the second and third plies. In the 90^o plies there seems to be a decrease in the stress level for the second and third plies, but an increase takes place after the second drilling test.

It is interesting to compare the values of σ_{22}^{rs} with the in-situ transversal strenght Y_{is}^T of the 90^o plies. The in-situ transversal strength is calculated according to Equation 5.15, considering a thick embedded ply. The distinction between thin and thick plies for in-situ transversal strength determination is given elsewhere [18].

$$Y_{is}^T = 1.12\sqrt{2}Y_{ud}^T \tag{5.15}$$

where Y_{ud}^T is the transversal tensile strength of a unidirectional ply. Substituting Y_{ud}^T for the value obtained experimentally in Chapter 3 Table 3.4, the in-situ transversal strength equals 98.66MPa. Note that in Figure 5-35 one of the plies reaches a value of about 36MPa, which is 37% of the in-situ transversal strenght of the ply. However, it is unlikely that the cracks observed in Figure 5-4 were caused by the thermal load alone. It is more likely that they were caused by the drilling procedure. These cracks obviously influence the measured strains, and, consequently, the determined residual stresses, because a change in local proper-

ties occurs. How to quantify this influence is certainly an interesting challenge, but it will remain for further investigation.

5.6 Moisture effect on composite laminates

In this section the effects of moisture in CFRP laminates are studied. The sorption processes of solvents in polymeric composites and their effects on material performance are highly complex issues. These subjects were studied extensively during the several past decades with the majority of investigations focusing on sorption processes and reporting weight-gain data. Fewer researchers attempted to correlate deformation, strenght and durability with fluid exposure. The difficulty in conducting a comprehensive study of this subject stems from three major drawbacks:

- there is a large variety of composite materials
- the even larger diversity of fluids and exposure conditions, such as levels of relative humidity, acidity, external stress and temperature
- the excessively long times required for specimen conditioning

Figure 5-36 exhibits typical weight-gain data versus the square-root of non-dimensional time, $\sqrt{t^*}$, the line LF corresponds to a linear Fickean behavior, while data along lines B and A correspond to the so-called a two-stage diffusion, and the absence of an equilibrium weight-gain level, respectively. In this work, similar graphs of this kind will be produced as well as others relating time and weight gain with curvature.

5.6.1 Unsymmetrical laminates

For the purpose of verifying the dimensional change in the curvature of unsymmetrical laminates, the specimens were immersed in water to guarantee 100% humidity. They were kept in small containers in a temperature chamber at 25^{o}C.

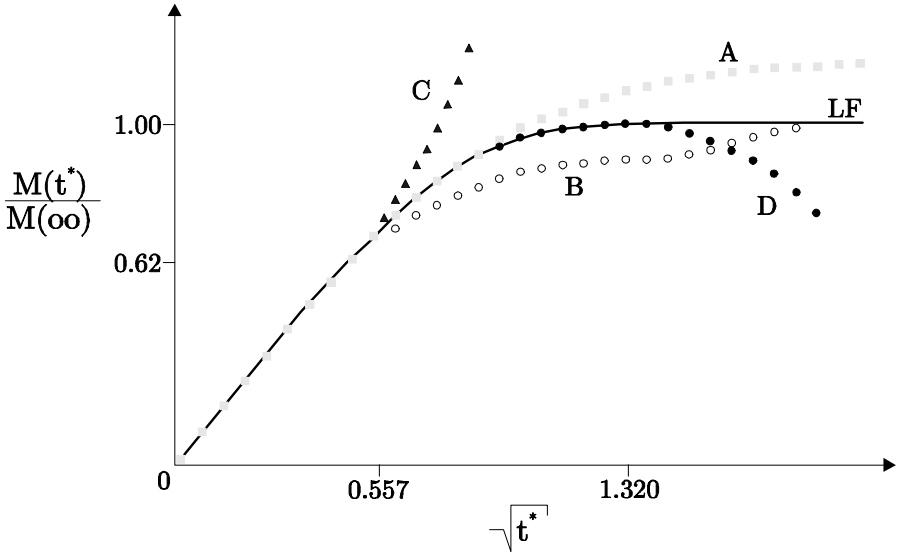

Figure 5-36: Schematic curves representing linear and non-linear absorption processes

Table 5.5 shows the stacking sequences of the specimens. Their geometry is shown in Figure 5-37. Particularly, the number of 90^o plies effect on the saturation time and curvature performance was studied. Since the weight gain of typical poly-

Table 5.5: Test plan for the moisture absorption experiments

Spec. Ref.	Lay-up	Specimens Qty.	Temperature (^{o}C)	Humidity (%)
MST1	$[0/90]$	5	25	100
MST2	$[0/90_2]$	5	25	100
MST3	$[0/90_4]$	5	25	100
MST4	$[90/0/90_3]$	5	25	100

meric composites is relatively small (on the order of 1%) mass measurement equipment must be selected accordingly. For coupons weighing more than 50 g, a balance accurate to 0.001 g is generally adequate. For smaller coupons with mass down to 5 g, a precision analytical balance capable of reading to 0.0001 g is required [39]. Figure 5-38 shows the equipment used for the weighing process, which satisfies the last requirement.

The moisture content in the specimens in function of time may be predicted. In this work the experimental data is compared with an anlytical model based

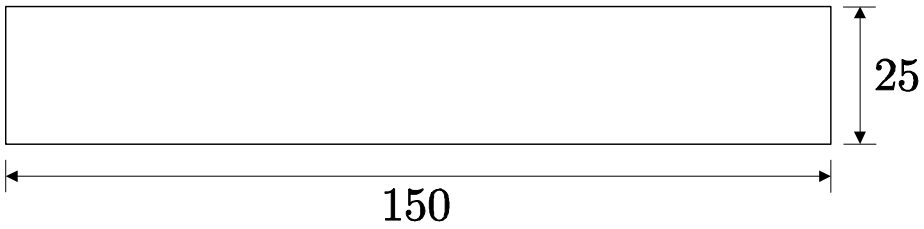

Figure 5-37: Geometry of specimens used for absorption experiments

Figure 5-38: Weighing device for the determination of absorbed moisture

on Fick's diffusion equation. It is considered that [7]:

- The material is exposed to the environment on one or two sides with both sides being parallel (one dimensional problem)
- The initial temperature and moisture distributions are uniform inside the material
- The moisture content of the material during adsorption and desorption is:

$$M = G\,(M_m - M_i) + M_i \tag{5.16}$$

where M_i is the initial moisture content of the material, M_m is the maximum moisture content which can be attained under the given environmental conditions, and G is a time dependent parameter, given by Equation (5.17).

$$G = 1 - \exp\left[-7.3\left(\frac{D_x t}{s^2}\right)^{0.75}\right] \tag{5.17}$$

For a material exposed on two sides to the same environment s (Figure 5-39) is equal to the thickness (s=h) of the laminate, as is the case in this work.

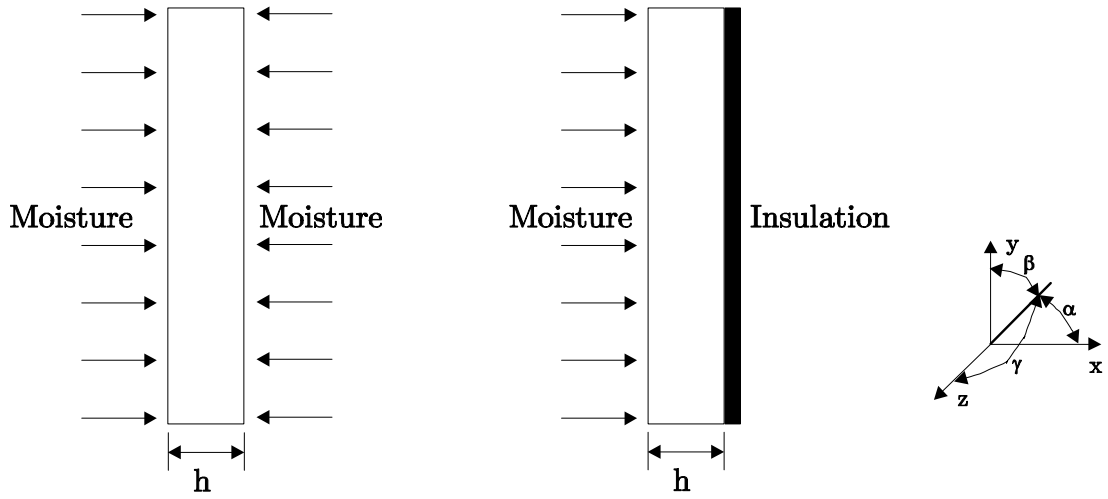

Figure 5-39: Moisture absorption possibilities

For a material insulated on one side (thermal insulation, impermeable to moisture) s is twice the thickness (s=2h). D_x is the diffusivity of the material in the direction normal to the surface. For fiber reinforced composites in which the orientations of all the fibers with respect to the x, y, and z axes are α, β and γ, D_x is defined as:

$$D_x = D_{11}\cos^2\alpha + D_{22}\sin^2\alpha \tag{5.18}$$

where D_{11} and D_{22} are the diffusivities in the directions parallel and normal to the fibers (longitudinal and transversal directions) and α is the orientation of the fibre in relation to the x direction, as shown in Figure 5-39. If D_x is not known it may be estimated from the diffusivity of the matrix D_r and the volume fraction of the fibers V_f using Equation (5.19):

$$D_x = D_r\left[(1 - V_f)\cos^2\alpha + \left(1 - 2\sqrt{\frac{V_f}{\pi}}\right)\sin^2\alpha\right] \tag{5.19}$$

This equation may be applied to unidirectional and laminated composites. In the latter case in each laminate:

- D_r must be the same
- V_f must be the same
- The fibers must be in a plane parallel to the surface ($\alpha = 90^o$). The orientations of the fibers relative to the y and z directions may vary from laminate to laminate.

Experimental evidence indicates that the maximum moisture content is insensitive to the temperature but depends on the moisture content of the environment. For a material immersed in liquid, as is the case in this work, M_m is a constant. For a material exposed to humid air M_m depends on the relative humidity ϕ according to Equation (5.20):

$$M_m = a\phi^b \tag{5.20}$$

where a and b are parameters to be determined experimentally. For this study, a and b were not determined because the specimens were always immersed in water.

Since the information regarding D_r was not available for this work, D_x had to be measured directly using experimental data and Equation (5.21).

$$D_x = \pi \left(\frac{h}{4M_m} \right)^2 \left(\frac{M_2 - M_1}{\sqrt{t_2} - \sqrt{t_1}} \right)^2 \tag{5.21}$$

The parameters M_1, M_2, M_m, $\sqrt{t_1}$ and $\sqrt{t_2}$ are shown in Figure 5-40. Edge effects were neglected.

Absorption Results

Figures 5-41 to 5-44 show the evolution of moisture in the specimens with time. Analytical and experimental values are presented.

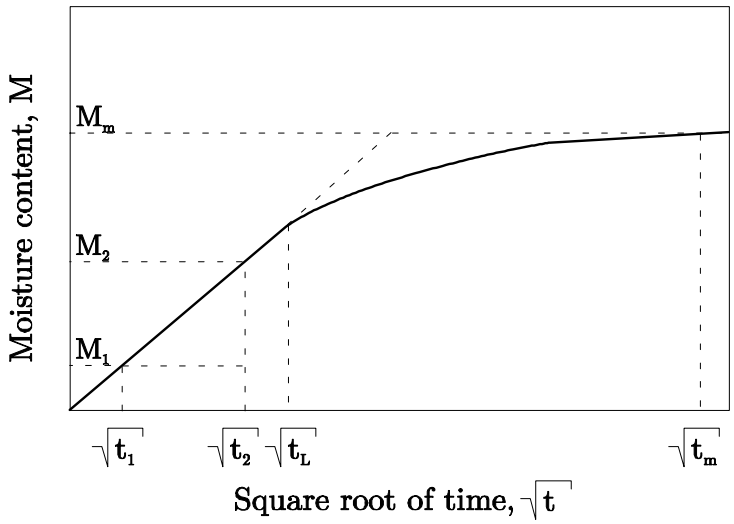

Figure 5-40: Illustration of the change of moisture content with the square root of time. For $t<t_L$ the slope is constant

The analytical prediction works quite well for the [0/90] laminates. But as the number of 90^o plies increases, the experimental values move away from the analytical prediction. The effect of moisture on the curvatures of the laminates is shown in Figure 5-45.

After the absorption processes, all specimens were dried in an oven for 48 hours at 70^oC. Their weight was registered and it may be seen that all specimens recovered their initial state, with very little weight change, as shown in Table 5.6.

Table 5.6: Weight comparison after drying

Specimen	Weight before absorption (g)	Weight after drying (g)	Difference (%)
[0/90]	1.4426	1.4430	0.028
$[0/90_2]$	2.1494	2.1499	0.022
$[0/90_4]$	3.6764	3.6739	-0.069
$[90/0/90_3]$	3.7408	3.7418	0.028

Two and even three stages diffusion processes may be observed in the case of the $[0/90_2]$, $[0/90_4]$ and $[90/0/90_3]$ laminates, respectively. Although no explanation for these phenomenons was found, they are related to reversible effects, according to reference [8]. These types of behaviour are in perfect agreement

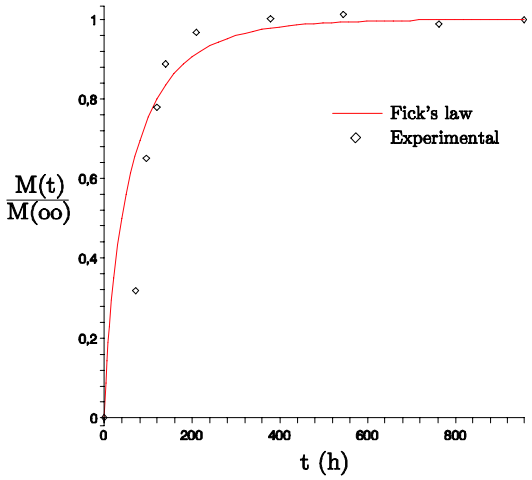

Figure 5-41: Moisture absorption for the [0/90] laminates

with curves A and B of Figure 5-39. According to Weitsman [8], weight-gains along the curves LF, A and B of Figure 5-39 are potentially associated with reversible or almost reversible effects of fluids on polymeric composites, while curves C and D are indicative of irreversible fluid-induced damage (interfacial fiber/matrix debondings and leaching of material into the ambient, respectively) that may cause permanent degradations in material properties. However, the behaviour of the curves depends on the fluid exposing conditions, i.e. the curves A and B may switch to harmful processes if, for example, the fluid temperature is increased. The curvature behaviour of the $[0/90_4]$ and $[90/0/90_3]$ laminates is quite similar, because of the same number of plies, but it is also evident that the different position of the 0° ply influences the initial curvature and hence the subsequent development. It is clear that the increase in the number of plies also increases the time needed to reach saturation, as shown in Figure 5-46.

The moisture effect on the laminates is rather similar to the temperature effect: increasing the moisture content decreases the curvature. At this point, an apparent relaxation of strains was observed but no quantitative information was obtained.

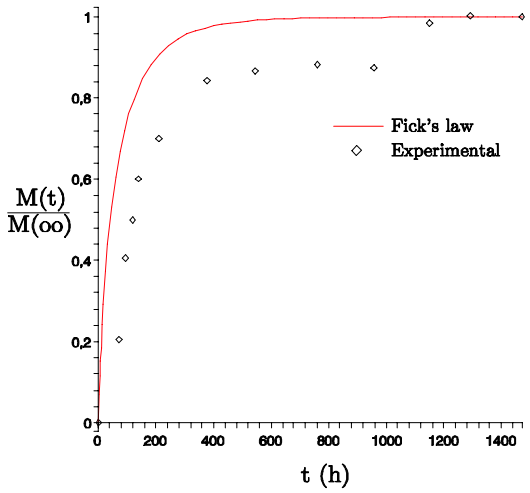

Figure 5-42: Moisture absorption for the $[0/90_2]$ laminates

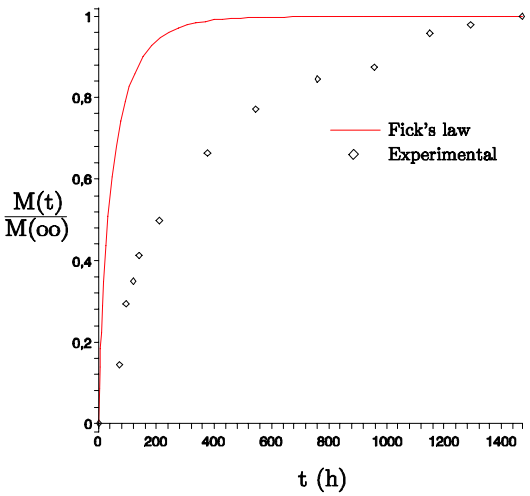

Figure 5-43: Moisture absorption for the $[0/90_4]$ laminates

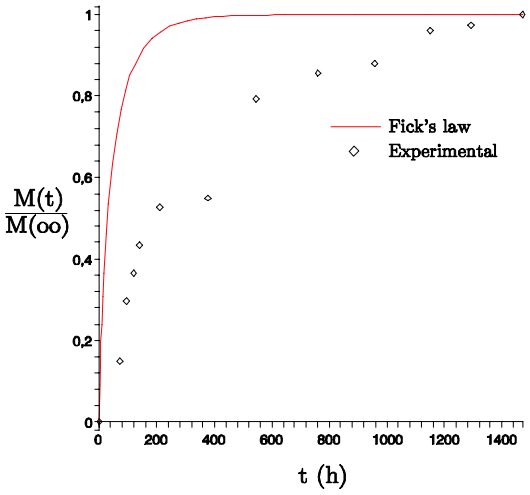

Figure 5-44: Moisture absorption for the $[90/0/90_3]$ laminates

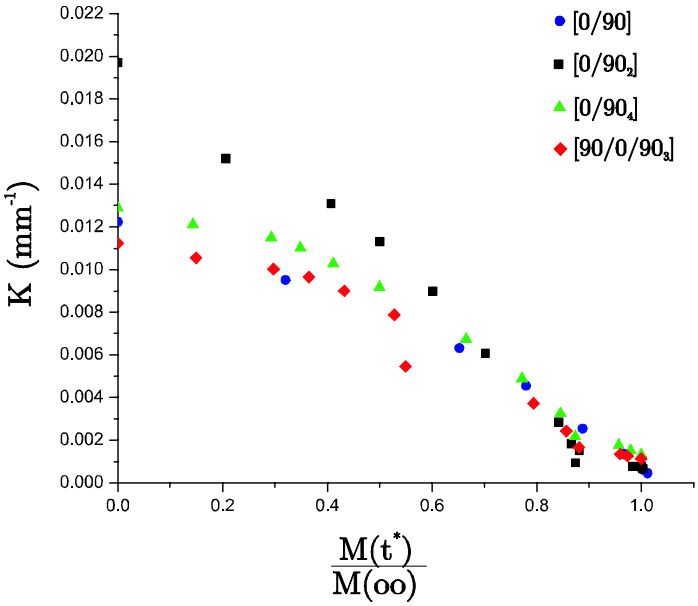

Figure 5-45: Curvature evolution with moisture

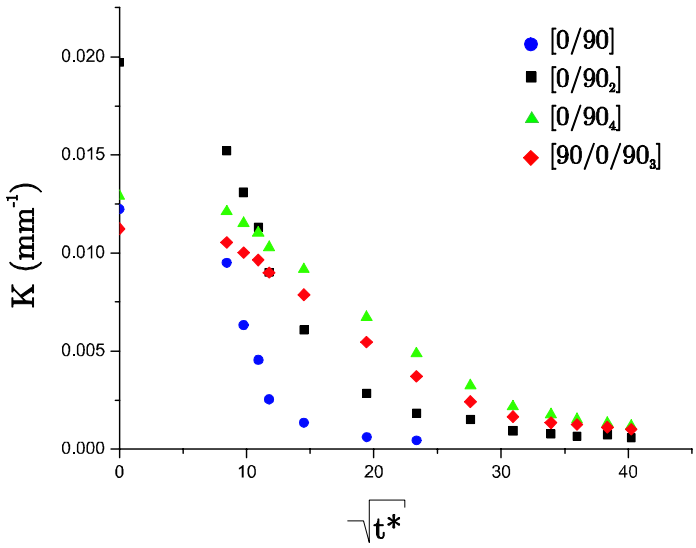

Figure 5-46: Curvature evolution with immersion time

Chapter 6

Analytical and Numerical Models

6.1 Open Hole Specimen subjected to Thermal load

In this section a numerical experiment using ABAQUS Standard [36] finite element technology is conducted to verify the behaviour of a plate subjected to a thermal load, which in this case was chosen to be a load corresponding to the difference between cure and ambient temperatures. In this case the temperature difference is 160^oC. A question related to wether the results would be different if the hole was made before or after applying the thermal load is answered. Figure 6-3 shows the geometry of the specimen used. It is a composite structure with a stacking sequence of $[0/90]_S$. The material constants are mentioned in Table 3.7 of Chapter 3.

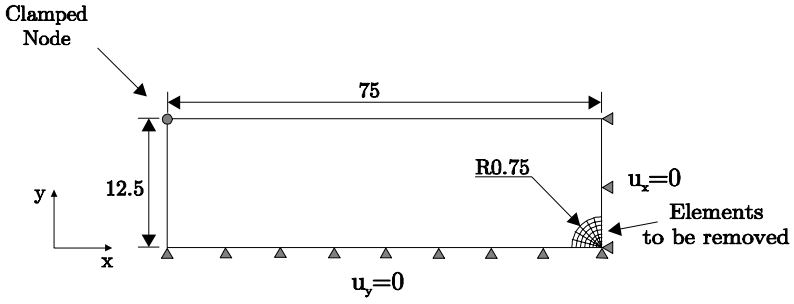

Figure 6-1: Geometry and boundary conditions used

The MODEL CHANGE function available in the ABAQUS Standard software was used to remove the elements corresponding to the hole's region after the thermal load was applied. Figures 6-2 and 6-3 show the results for the stress distribution with the hole made first and then using the MODEL CHANGE function, respectively.

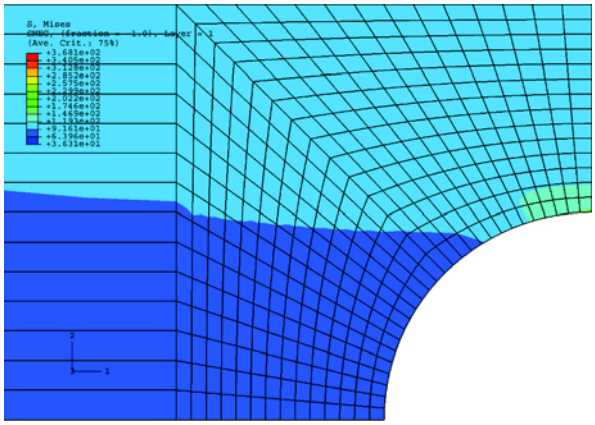

Figure 6-2: Stress distribution with hole

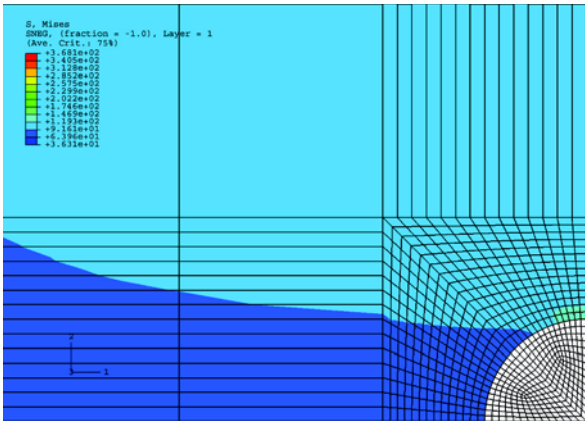

Figure 6-3: Stress distribution with removed elements

The stress distribution along the hole boundary for both cases is plotted in Figure 6-4. It is numerically indifferent to have the hole made before or after the thermal load is applied.

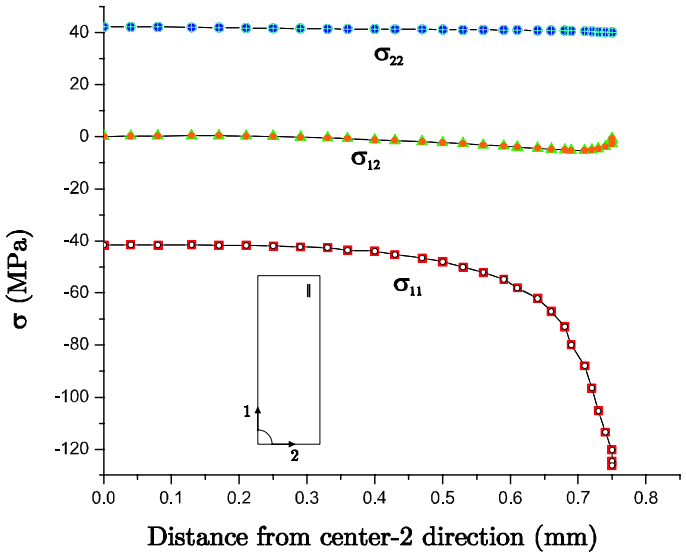

Figure 6-4: Stress distribution along the hole boundary

6.2 Prediction of curvatures of unsymmetrical laminates

Using the material properties obtained, the curvature after curing of the laminates of Table 3.14 is predicted. Figures 6-6 to 6-8 show the out of plane displacements for each case. Comparison is made between the experimentally obtained values and the finite element method and the classical laminate theory. The experimental values were obtained by manual measurement along the sides of the specimens. Then an average value was determined.

The curvature of a laminate (Figure 6-9) may be determined using equations (6.1) and (6.2).

$$R = \frac{\sin\left(\arctan\left(\frac{d}{h}\right)\right)\sqrt{d^2+h^2}}{\sin\left(\pi - 2\arctan\left(\frac{d}{h}\right)\right)} \tag{6.1}$$

$$\kappa = \frac{1}{R} \tag{6.2}$$

Table 6.1 shows the results of the calculated curvatures from experimental data and from classical laminate theory.

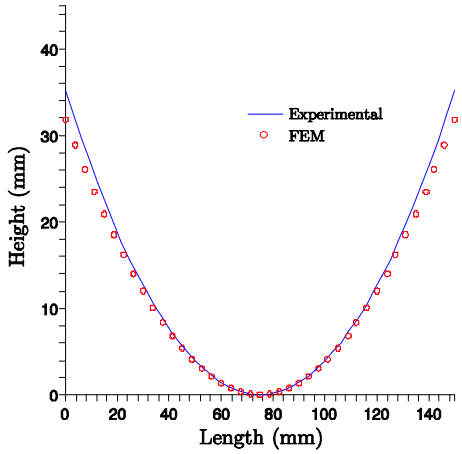

Figure 6-5: Out of plane displacements of the [0/90] laminate

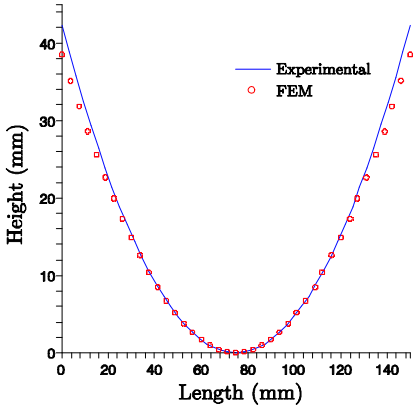

Figure 6-6: Out of plane displacements of the $[0/90_2]$ laminate

It may be concluded that the finite element predictions of the laminates curvatures agree quite well with the experimental data. The classical laminate theory, which is valid for very small displacements, is not able to correctly predict the curvatures of the $[0/90_2]$, $[0/90_4]$ and $[90/0/90_3]$ laminates, presenting a difference of more than 20%.

6.3 Micromechanical modelling of residual stresses

Due to the difference in the coefficients of thermal expansion of the constituents, residual curing stresses are generated at the micromechanical level, as mentioned

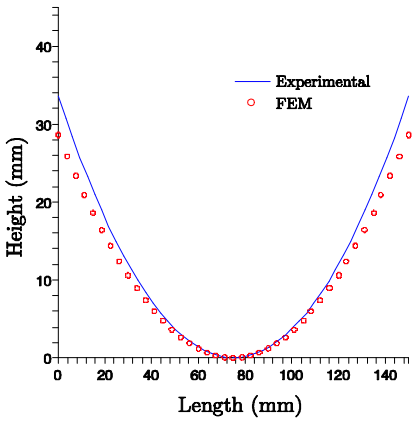

Figure 6-7: Out of plane displacements of the $[0/90_4]$ laminate

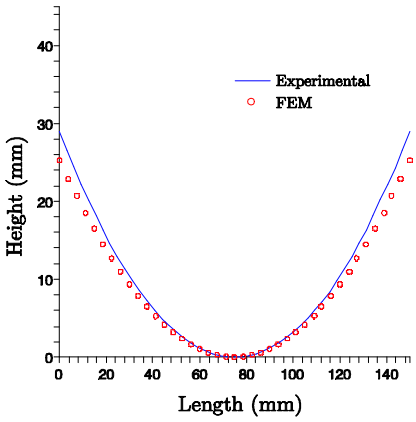

Figure 6-8: Out of plane displacements of the $[90/0/90_3]$ laminate

in Chapter 2. The residual stresses at the fiber/matrix level were determined, considering a thermal load of ΔT=150^{o}C, equal to the difference of the curing and ambient temperature. Also, the mechanical properties of the fibre and matrix calculated in Chapter 3 were used, except for the CTE of the fibre, which is considered to be orthotropic. The respective properties were obtained from a Hexcel product sheet. The influence of the fibre volume fraction V_f was studied, considering a square unit array and a hexagonal unit array. From a micromechanical perspective, the matrix is constrained in all three dimensions by the surrounding fibers. High stresses due to the curing process are created in the matrix. These high stresses may surpass the strength of the resin and create matrix

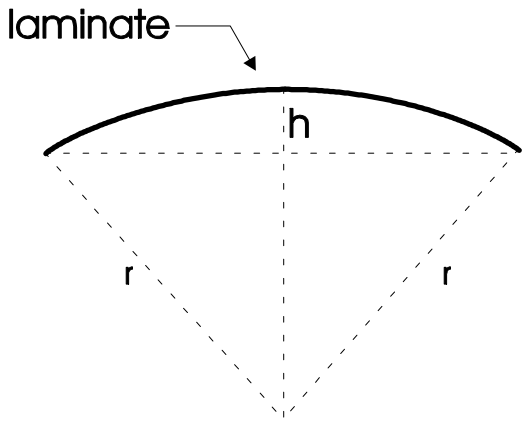

Figure 6-9: Laminate curvature calculation

Table 6.1: Comparison of curvatures (experimental and CLT)

Specimen	κ_{exp} (m^{-1})	κ_{clt} (m^{-1})	Difference (%)
[0/90]	12.24	12.90	-5.10
$[0/90_2]$	19.72	15.06	30.90
$[0/90_4]$	12.90	10.48	23.10
$[90/0/90_3]$	11.24	9.12	23.20

cracks. Two types of results were studied: the Von Mises equivalent stresses and the dilatational energy density U_v. These quantities are of special importance in the matrix, because plasticity related phenomenons or cracks may occur, if the respective critical values are surpassed. A complete analysis of micromechanical modelling of residual curing stresses may be found in reference [40]. The Von Mises failure criterion is associated wiht the elastic shear strain energy density and when it reaches a critical value, failure will occur. It assumes the material to be isotropic. The most usual formulation of the Von Mises criterion is the following:

$$\frac{\sigma_{VM}}{\sigma_{yd}} = \sqrt{\frac{(\sigma_1 - \sigma_2)^2 + (\sigma_2 - \sigma_3)^2 + (\sigma_1 - \sigma_2)^2}{6}} < 1 \qquad (6.3)$$

where the principal stresses are $\sigma_1 > \sigma_2 > \sigma_3$.

Another criterion to predict the formation of micro-holes in the matrix is the dilatational energy density criterion, which assumes the material to be linear

Table 6.2: Comparison of curvatures (experimental and FEM)

Specimen	κ_{exp} (m^{-1})	κ_{fem} (m^{-1})	Difference (%)
[0/90]	12.24	12.34	-0.80
$[0/90_2]$	19.72	15.64	26.10
$[0/90_4]$	12.90	11.50	12.20
$[90/0/90_3]$	11.24	9.62	16.9

elastic. It can be written:

$$\frac{U_V}{U_V^{cr}} = \frac{1-2\nu}{6E}\left(\sigma_1+\sigma_2+\sigma_3\right)^2 < 1 \tag{6.4}$$

where σ_1, σ_2 and σ_3 are the principal stresses, ν is the Poisson's ratio and E the Young's modulus [41].

6.3.1 Square array unit cells

Figure 6-10 shows a possible fibre arrangement in a unidirectional lamina. For this case only a quarter of the fibre needs to be analysed. Three cases were considered for different fibre volume fractions: 0.3, 0.6 and 0.785.

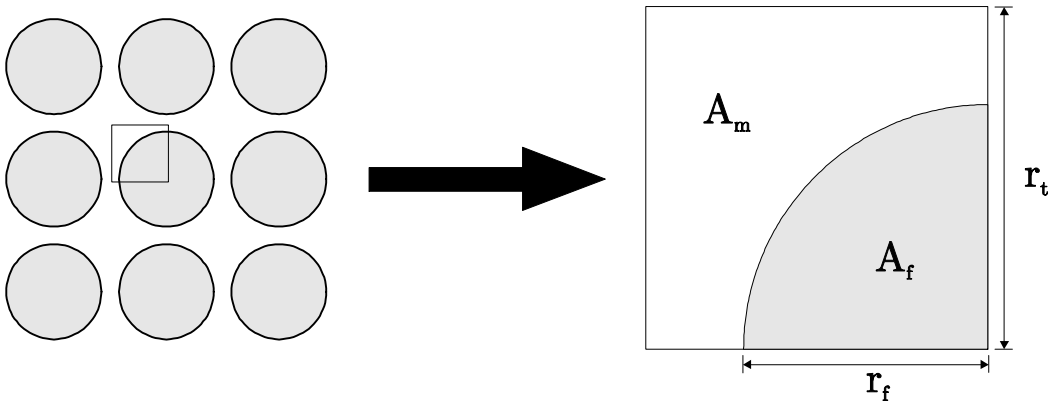

Figure 6-10: Square cell arrangement

The fibre volume fraction, V_f, (Equation 6.5) was controlled by varying the parameter r_t of Figure 6-10. The radius of the fibre, r_f, was constant and equal to 0.0025 mm.

$$V_f = \frac{A_f}{A_t} \tag{6.5}$$

$$A_f = \frac{\pi r_f^2}{4} \tag{6.6}$$

$$A_t = r_t^2 \tag{6.7}$$

The square unit cell has the following boundary conditions: the right side is constrained in the x-direction (u_x =0) and the bottom is constrained in the y-direction (u_y =0). The other two sides are free to move. Plane strain elements were used to generate the mesh.

σ_{VM}/σ_{yd} distribution

Taking σ_{yd} = 35 MPa to be the yielding stress for the composite resin, Figures 6-11 to 6-13 show the distribution of σ_{VM}/σ_{yd}.

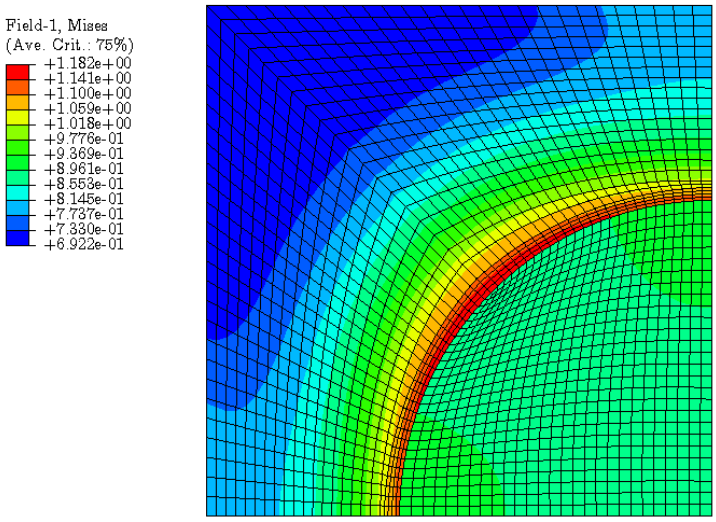

Figure 6-11: σ_{VM}/σ_{yd} (V_f = 30%)

Figure 6-14 shows the stress distributions in the matrix at the fibre border. For a fibre volume fraction of 30%, the maximum value of σ_{mises} is exactly at an angle of $\frac{\pi}{4}$ rad. When the fibre content was increased, two peaks of σ_{mises}

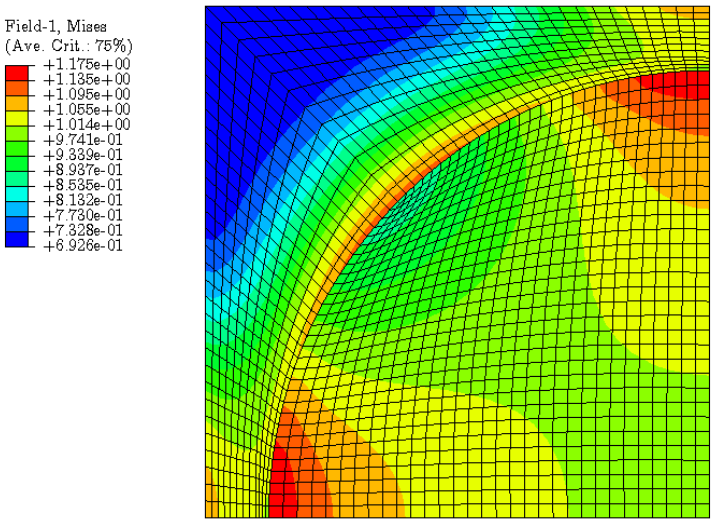

Figure 6-12: σ_{VM}/σ_{yd} ($V_f = 60\%$)

were encountered. These peaks tend to move to the edges of the fibre. At the maximum fibre content, $V_f = 78.5\%$, two stress peaks reaching approximately 1.09 were determined.

U_V/U_{cr} distribution

Figures 6-15 to 6-17 show the distribution of U_V/U_V^{cr}. The critical value of the dilatational energy density of a typical epoxy resin is 0.2 MPa.

Figure 6-18 shows the radial distribution of U_V/U_V^{cr} of the square unit cell at the fibre-matrix border. Again, the highest value occurs for $\theta = 45^o$. It may be seen that with an increase in the fibre volume fraction, the maximum value of U_V/U_V^{cr} decreases. For all cases, $U_V/U_V^{cr} < 1$ and according to this cell arrangement, micro-holes do not develop.

6.3.2 Hexagonal array unit cells

Figure 6-19 shows another possible fibre arrangement in a unidirectional lamina. Three cases were considered for different fibre volume fractions: 0.3, 0.6 and 0.9, which is closed to the maximum fibre volume allowed for this type of configuration.

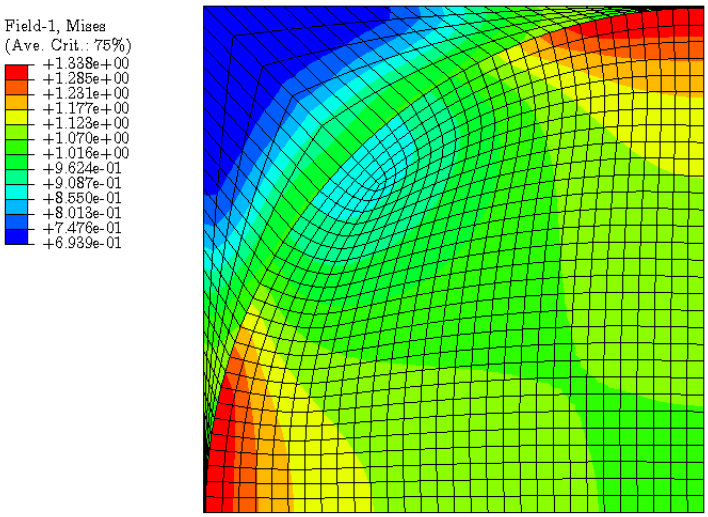

Figure 6-13: σ_{VM}/σ_{yd} ($V_f = 78.5\%$)

The fibre volume fraction, V_f, (Equations 6.12) was controlled by varying the parameter δ of Figure 6-19. The radius of the fibre, r_f, was constant and equal to 0.0025 mm.

$$r_t = r_f + \frac{\delta}{2} \tag{6.8}$$

$$h = 2r_f + \delta \tag{6.9}$$

$$h^2 = r_t^2 + l_2 \tag{6.10}$$

$$l = \sqrt{(2r_f + \delta)^2 - \left(r_f + \frac{\delta}{2}\right)^2} \tag{6.11}$$

$$V_f = \frac{\pi r_f^2}{2\left(r_f + \frac{\delta}{2}\right) l} \tag{6.12}$$

The hexagonal unit cell has the following boundary conditions: the right side is constrained in the x-direction (u_x =0) and the bottom is constrained in the y-direction (u_y =0). The other two sides are free to move. Plane strain elements

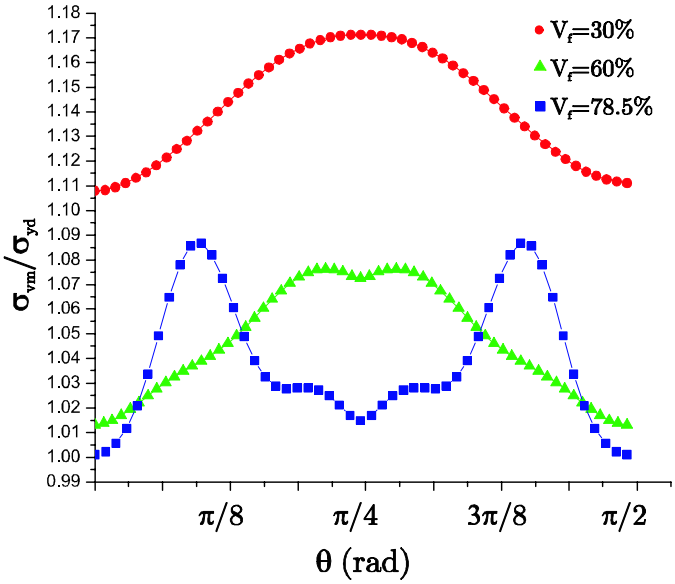

Figure 6-14: σ_{VM}/σ_{yd} distribution in the matrix

were used to generate the mesh.

σ_{VM}/σ_{yd} distribution

Figures 6-20 and 6-22 show the σ_{VM}/σ_{yd} distribution in the hexagonal uinit cell.

Figures 6-23 and 6-24 show the σ_{VM}/σ_{yd} distribution in the fibre-matrix interface for the bottom and top fibres, respectively, of the hexagonal unit cell. For fibre volumes of 30% and 60%, σ_{mises} around the fibre remained approximately constant, but at the maximum fibre content a rather pronounced peak of stress was reached, at a location corresponding to the point where the fibres nearly touched each other, as shown in Figure 6-22.

U_v/U_{cr} distribution

Figures 6-25 to 6-27 show the distribution of U/U_{cr} for fibre volume fractions of 30%, 60% and 90%.

Figures 6-28 and 6-29 show the U_v/U_{cr} distribution in the fibre-matrix interface for the bottom and top fibres, respectively, of the hexagonal unit cell.

It may be observed that for fibre volume fractions of 30% and 60% the ratio U_v/U_{cr} is smaller than unity and therefore, according to equation 6.4, the for-

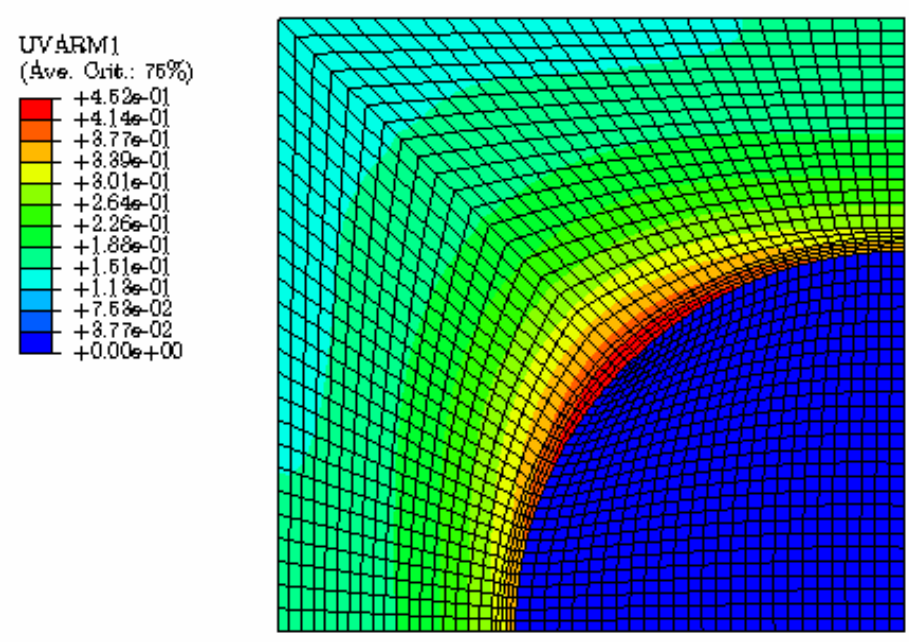

Figure 6-15: Energy based damage criterion ($V_f = 30\%$)

mation of micro-holes will not occur. For the maximum fibre volume fraction, $V_f = 90\%$, there is a rapid increase in U_v/U_{cr}. It happens exactly at the point where the fibres almost touch each other. In the top fibre there is also a second peak, for $\theta = 90^o$.

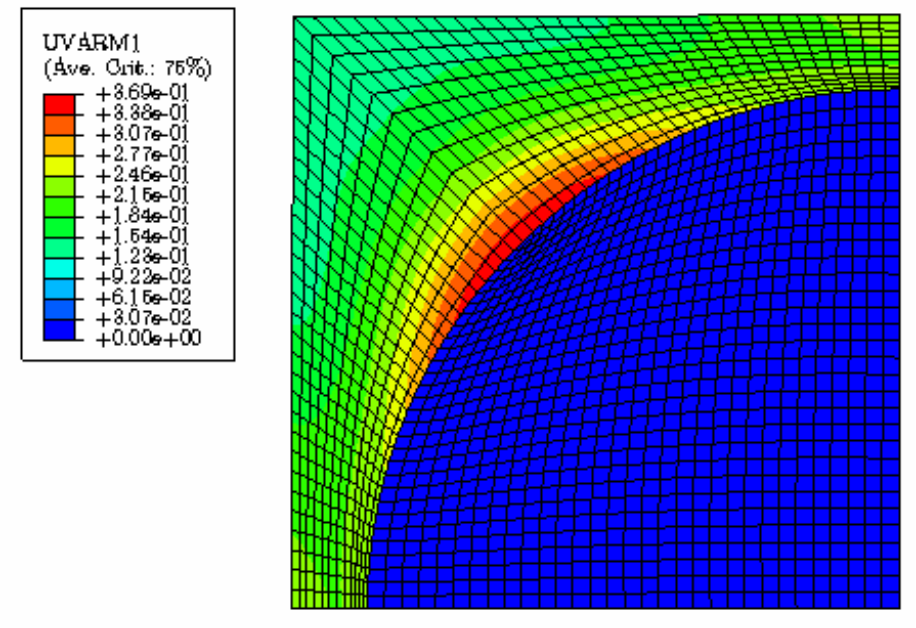

Figure 6-16: Energy based damage criterion ($V_f = 60\%$)

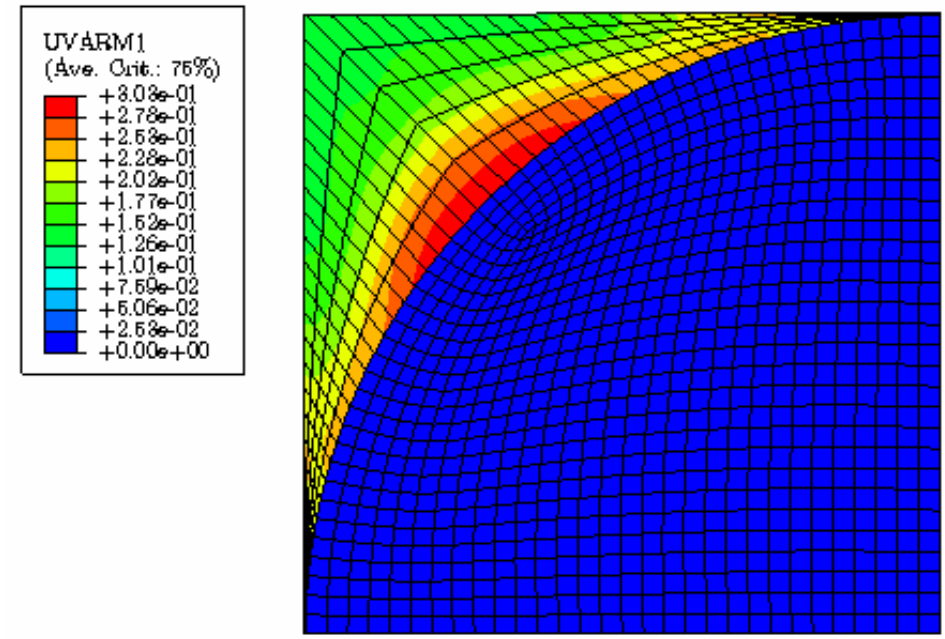

Figure 6-17: Energy based damage criterion ($V_f = 78.5\%$)

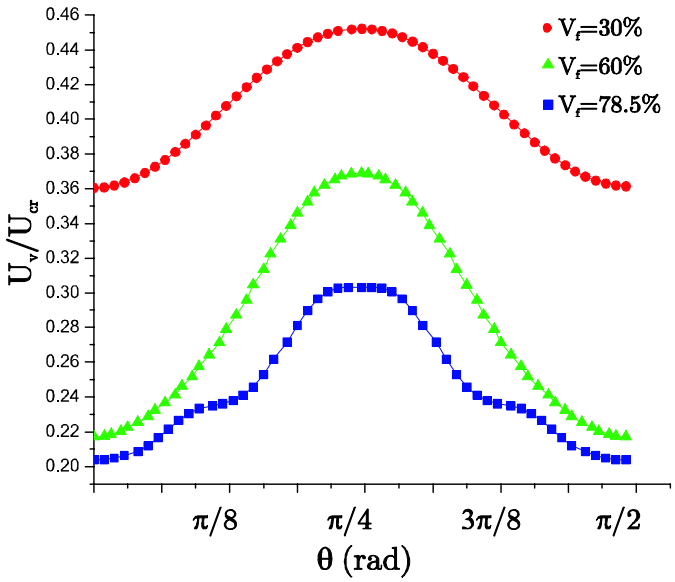

Figure 6-18: U_V/U_V^{cr} distribution of the square unit cell at the fibre-matrix border

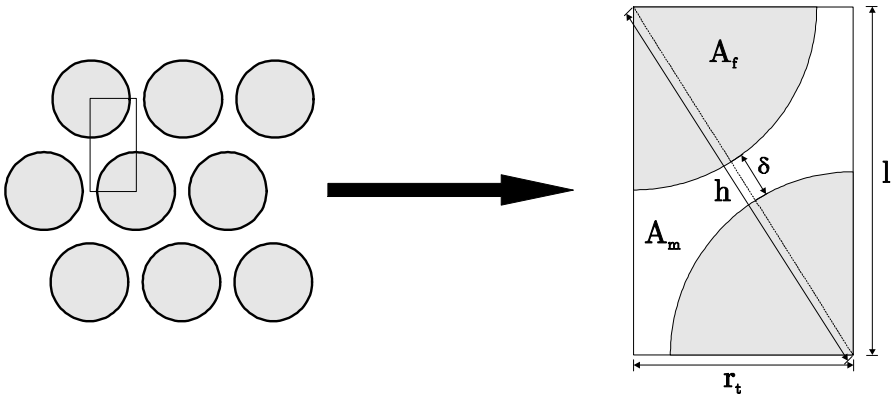

Figure 6-19: Hexagonal cell arrangement

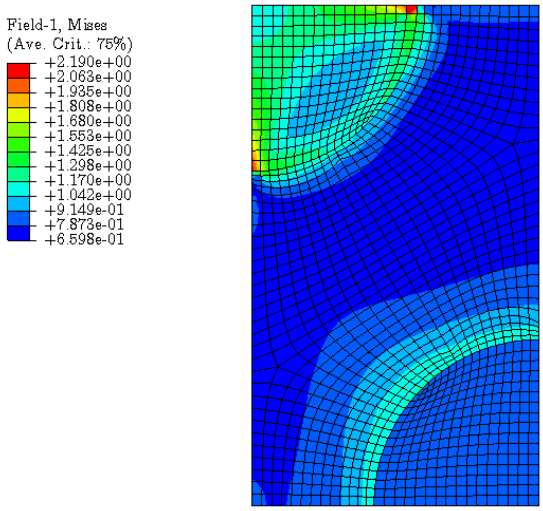

Figure 6-20: σ_{VM}/σ_{yd} ($V_f = 30\%$)

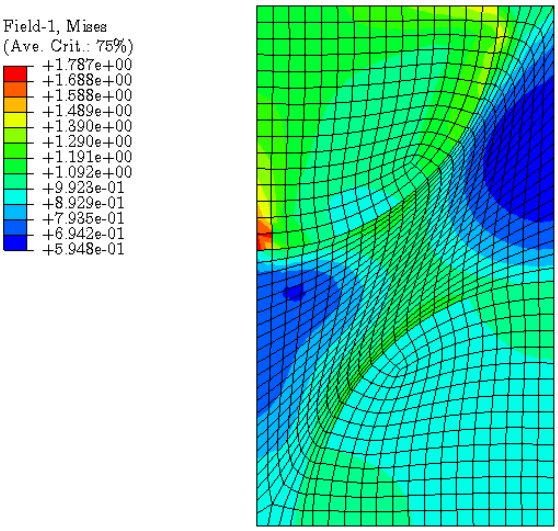

Figure 6-21: σ_{VM}/σ_{yd} distribution ($V_f = 60\%$)

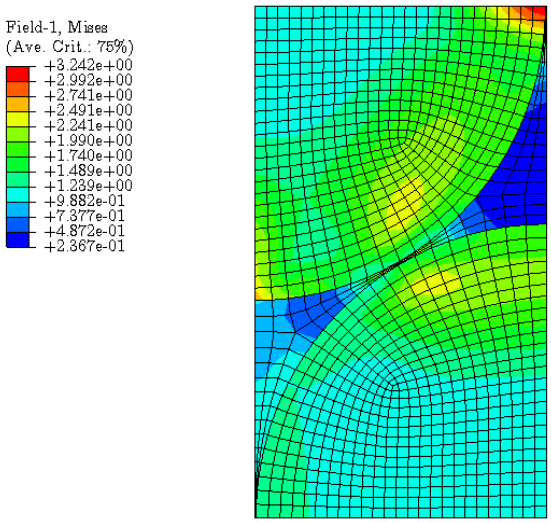

Figure 6-22: σ_{VM}/σ_{yd} distribution ($V_f = 90\%$)

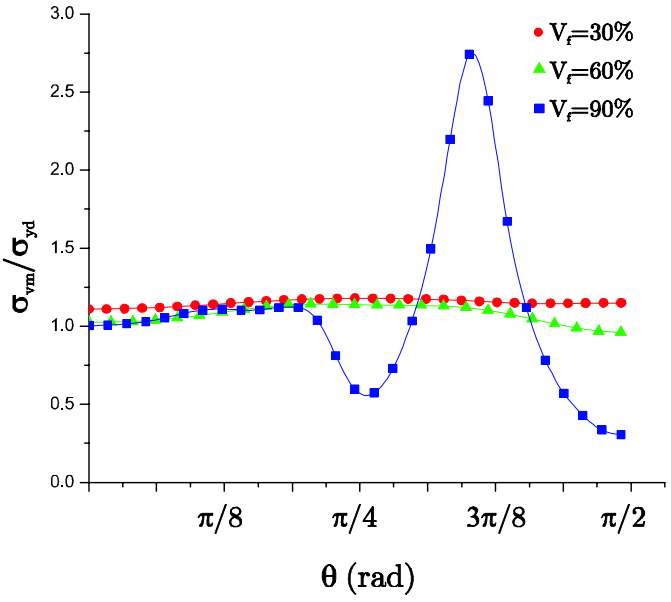

Figure 6-23: σ_{VM}/σ_{yd} distribution in the matrix for the bottom fibre

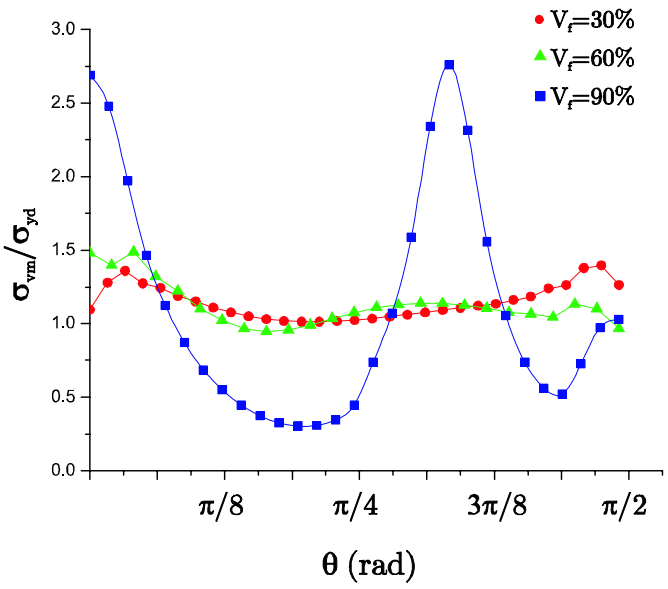

Figure 6-24: σ_{VM}/σ_{yd} distribution in the matrix for the top fibre

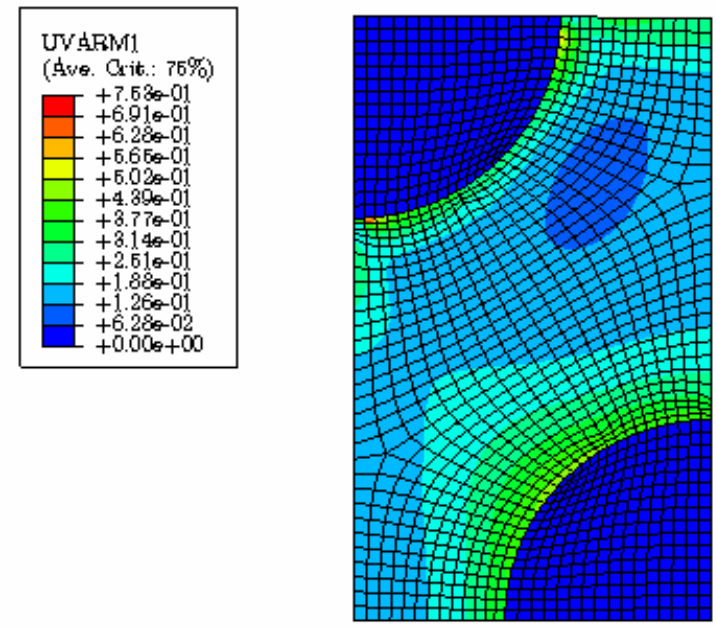

Figure 6-25: Energy based damage criterion ($V_f = 30\%$)

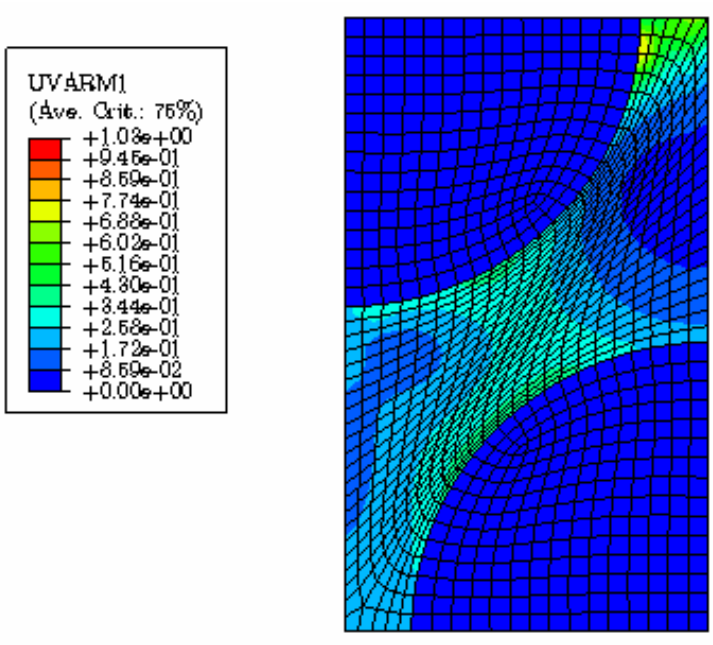

Figure 6-26: Energy based damage criterion ($V_f = 60\%$)

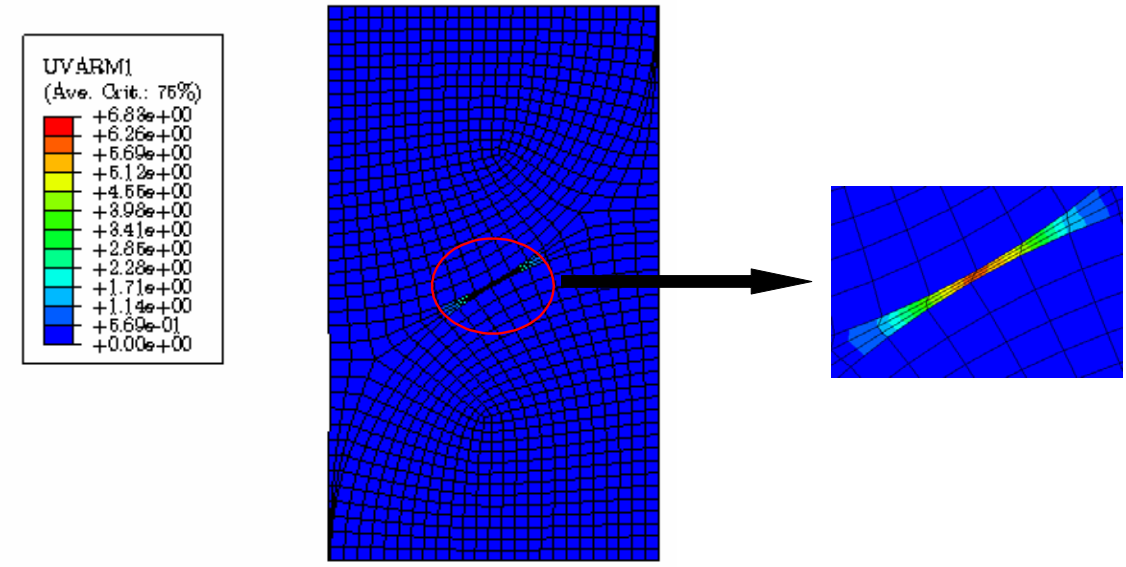

Figure 6-27: Energy based damage criterion ($V_f = 90\%$)

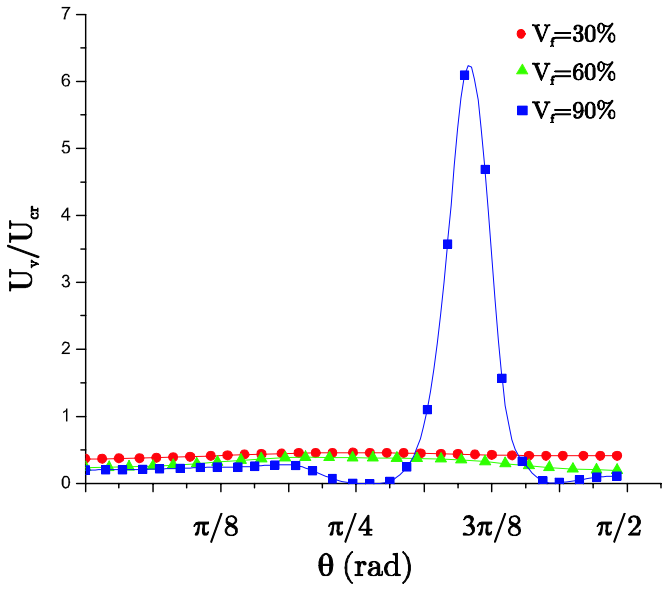

Figure 6-28: U_v/U_{cr} distribution in the matrix for the bottom fibre

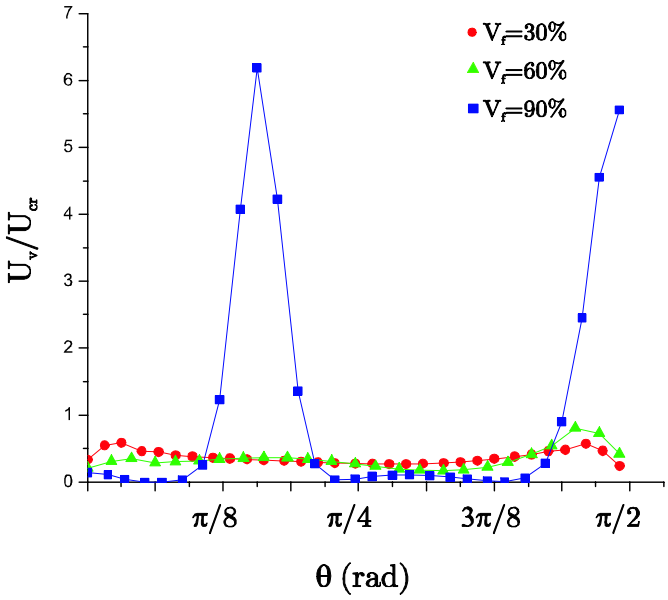

Figure 6-29: U_v/U_{cr} distribution in the matrix for the top fibre

Chapter 7

Conclusions

A brief introduction to composite materials was made in Chapter 1 and the need to study the influence of residual stresses was explained. A review of experimental procedures for residual stress determination was given in Chapter 2. Their principal advantages and disadvantages were discussed. Chapter 3 dealt with the detailed characterization of the material, including the determination of some basic micromechanical properties using the simple rule of mixtures. All manufacturing procedures and equipments were presented as well as detailed instrumentation guidelines. The coefficients of thermal expansion were determined. The determination of the stress-free temperature lead to an inconclusive result: the condensation phenomenon of the multi layered glass window of the temperature chamber influenced the pictures, making it hard to see the laminate when processing them. In chapter 4 the classical laminate theory was explained in detail. It was used to predict the curvatures of the unsymmetrical specimens after curing and to predict the residual stresses in the symmetrical specimen. A Maple programme which quickly accomplishes it was implemented. The hole drilling method is thoroughly described in Chapter 5. The drilling procedure itself was deeply investigated: micrographs of the drilled hole were made and verified for drilling induced damage. The drilling parameters chosen resulted in adequate hole surface quality, but cracks were spotted in the middle plies and therefore a certain amount of suspicion exists towards the determined residual

stresses. When comparing the residual stresses obtained through the hole drilling method with the values predicted by the classical laminate theory, it is apparent that the residual stresses are not constant through the thickness of the specimen. An apparent relaxation of the stresses seems to take place with time, but it was impossible to quantify it at the actual position of this work, because this phenomenon did not happen in all plies in a coherent manner. Also, the presence of the cracks may contribute to an apparent stress relaxation, because local material properties are diminished. The values of σ_2 corresponding to the 90^o plies were compared to the in-situ transversal strength of the plies. It was concluded that the residual stress level may reach about 37% of the in-situ transversal strength of the ply, but it is not thought to be the cause of the cracks. The moisture effect on unsymmetrical laminates was studied. In this work several laminates with stacking sequences of [0/90], $[0/90_2]$, $[0/90_4]$ and $[90/0/90_3]$ were immersed in water and their absorption behaviour and curvature were investigated. An almost perfect fit using Fick's equation was obtained for the [0/90] laminate, but for the remaining laminates the experimental data departed the linear Fickian behaviour. This subject will require furhter investigation. The curvature of the laminates decreased in an almost linear way with moisture increase. The increase in number of plies contributes to an increase in saturation time. In Chapter 6, a numerical experiment of a plate containing a hole was performed. The stress distribution along the hole boundary was determined and the results are the same if the elements are removed after or before the application of the thermal load. The finite element method was also used to predict the curvature of the cured unsymmetrical laminates. The experimental values agreed well with the finite element method predictions. On the other hand, the classical laminate theory was not able to predict the curvatures in a satisfactory manner. The determination of residual stresses at the micromechanical level, i.e. between fibres and matrix, using the properties determined in Chapter 3 was made. It was concluded that matrix cracks may develop, particularly at high fibre volume fractions. For future developments, it would be necessary to characterize the development of the

resin properties with time and temperature for a better modelling of micromechanical thermally induced residual stresses. Further experiments using the hole drilling method should be conducted using more increments per ply to explore the sensitivity of the method. It is important to mention the fact that some important progress has been accomplished, specially the walls of the hole due to the drilling process and the detailed material characterization. However, the presence of cracks in drilled specimens should be the subject of further investigation. For this purpose, several stacking sequences should be tested. Combining this with different composite materials should prove to be a challenging work. Without an excellent hole quality, the application of the hole drilling method in composite laminates will not advance. A programme which optimizes the determination of the calibration constants in function of hole geometry and laminate characteristics could be an interesting development, to facilitate the determination of the residual stresses. The relaxation of stresses is an interesting and complex subject but should consist in a potential objective for further exploration.

Bibliography

[1] Ori Ishai Isaac M. Daniel. *Engineering Mechanics of Composite Materials.* Oxford University Press, 1994.

[2] William F. Smith. *Principles of Materials Science and Engineering.* McGraw-Hill, Inc., 1996.

[3] Robert M. Jones. *Mechanics of Composite Materials.* Taylor Francis, Inc, 1999.

[4] H. Thomas Hahn Stephen W. Tsai. *Introduction to Composite Materials.* Technomic Publishing Company, 1980.

[5] Won J. Yu Paul Sunderland and Jan-Anders E. Manson. A technique for the measurement of process-induced internal stresses in polymers and polymer composites". *ICCM 10*, pages 125–132, 1995.

[6] ASTM International. Standard test method for determining residual stresses by the hole-drilling strain gage method (e 837-01). Technical report, November 2001.

[7] George S. Springer. *Environmental Effects on Composite Materials.* Technomic Publishing Company, Inc, 1981.

[8] M. Elahi Y.J. Weitsman. Effects of fluids on the deformation, strength and durability of polymeric composites- an overview. *Mechanics of Time-Dependent Materials*, pages 107–126, 2000.

[9] B. Fiedler et Al. The influence of thermal residual stresses on the transverse strength of cfrp using fem. *Composites: Part A*, 33:1323–1326.

[10] Göran Fernlund et Al. Residual stress, spring in and warpage in autoclaved composite parts. *ICCM 14*, pages 1–10, 2003.

[11] K.D. Potter M. Gigliotti, M.R. Wisnom. Development of curvature during the cure of AS4/8552 [0/90] unsymmetric composite plates. *Composites Science and Technology*, 63:187–197, 2003.

[12] Gong X.Lu et al. Residual stress distribution and its influence on the mechanical behaviour of composite laminates. *ICCM 12*, 1999.

[13] L.G.Stringer et Al. Curing stresses in thick polymer composite components; part II: Management of residual stresses.

[14] J.A. Nairn. Fracture mechanics of composites with residual stresses, traction-loaded cracks and imperfect interfaces. *Proc. 2nd ESIS TC4 Conference on Polymers and Composites, in press*, 1999.

[15] José Joaquim Lopes Morais. *Influência Do Meio Ambiente No Comportamento Ao Dano de Estruturas Em Materiais Compósitos.* PhD thesis, Universidade de Trás os Montes e Alto Douro, 1998.

[16] P.K. Predecki et al B. Benedikt, M. Kumosa. An analysis of residual thermal stresses in a unidirectional graphite/PMR-15 composite based on x-ray diffraction measurements. *Composites Science and Technology*, 61:1977–1994, 2001.

[17] Peter W. R. Beaumont Kevin D. Cowley. The measurement and prediction of residual stresses in carbon-fibre/polymer composites. *Composite Science and Technology*, 57:1445–1455, 1997.

[18] Pedro Camanho et Al. Failure models and criteria for FRP under in-plane or three-dimensional stress states including shear non-linearity. Technical report, NASA, 2005.

[19] A. Turnbull et Al. Residual stress in polymers: Evaluation of measurement techniques. *Journal of Materials Science*, 34:451–459, 1999.

[20] Maria Teresa Restivo Jorge Borges de Almeida, António Torres Marques. Utilização do método do furo para a determinação de tensões residuais em materiais poliméricos. In *3ž Congresso Luso-Moçambicano de Engenharia*, 2003.

[21] Jorge Borges de Almeida. Determination of residual stresses in CFRP laminates using the hole drilling method. Technical report, FEUP, June 2004.

[22] O. Sicot et al. Determination of residual stress in composite laminates using the incremental hole-drilling method". *Journal of Composite Materials*, 37:831–814, 2003.

[23] H. T. Hahn S. R. White. Process modeling of composite materials: Residual stress development during cure. part i. model formulation. *Journal of Composite Materials*, 26(16):2402–2422, 1992.

[24] ASTM. Standard test method for tensile properties of polymer matrix composite materials ASTM d 3039/d 3039m.00. Technical report, American Society for Testing and Materials (ASTM).

[25] ASTM. Standard test method for in-plane shear response of polymer matrix compos- ite materials by test of a ğ45o laminate, ASTM d 3518/3518m-94. Technical report, American Society for Testing and Materials (ASTM).

[26] Leif A. Carlsson R. Byron Pipes. *Experimental Characterization of Advanced Composite Materials*. Technomic Publishing Co. Inc., 1997.

[27] J.D.D. Melo D.W. Radford. Elastic characterization of PEEK/IM7 using coefficients of thermal expansion. *Composites: Part A*, 33:1505–1510, 2002.

[28] Murat H. Kural Donald L. Flaggs. Experimental determination of the in situ transverse lamina strength in graphite/epoxy laminates. *Journal of Composite Materials*, 16:103–114, 1982.

[29] Adrian Biran and Moshe Breiner. *Matlab 6 for Engineers*. Pearson Education, 2002.

[30] Waterloo Maple Inc. Canada. *Maple 9.5 Users Manual*, 2002.

[31] Componeering. *Esacomp 2.1 User's Manual*, 2000.

[32] W. Soete. Measurement and relaxation of residual stress. *Sheet Met Ind*, 26:1269–1281, 1949.

[33] B. R. Lake et Al. A method for measuring planar residual stresses in rectangular orthotropic materials. *Journal of Composite Materials*, 2:244–253, 1968.

[34] C. K. H. Dharan H. Ho-Cheng. Delamination during drilling in composite laminates. *American Society Mechanical Engineers*, 112:236–239, 1990.

[35] C. Würtz F. Klocke. The use of pcd tools for machining fibre reinforced materials. *European Conference Composite Materials 8*, pages 509–515, 2002.

[36] Karlsson Hibbitt and Sorensen. *Abaqus 6.4 User's Manuals*, 2003.

[37] Maria Odete Rodrigues Cadete. *A Linguagem Fortran 77*. Fundação Calouste Gulbenkian, 1997.

[38] O. Sicot X. L. Gong. Influence of experimental parameters on determination of residual stress using the incremental hole-drilling method. *Composites Science and Technology*, 64:171–180, 2004.

[39] Military handbook 17, polymer matrix composites. Technical report, U.S. Department of Defense, 1994.

[40] Mehdi S. Kiasat. *Curing Shrinkage and Residual Stresses in Viscoelastic Thermosetting Resins and Composites*. PhD thesis, Delft University of Technology, 2000.

[41] Daniel Trias Mansilla. *Analysis and Simulation of Transverse Random Fracture of Long Fibre Reinforced Composites.* PhD thesis, Universitat de Girona, 2005.

Appendix

In this appendix the Maple codes used in this work are listed.

Determination of the stress free temperature

PACKAGES

```
> restart:with(stats):with(ListTools):with(plots):with(plottools):with(linalg):with( StringTools ):
Warning, the assigned name Group now has a global binding
Warning, the name changecoords has been redefined
Warning, the assigned names arrow and transform now have a global binding
Warning, the protected names norm and trace have been redefined and unprotected
Warning, these names have been rebound: Group, Join, Reverse, Rotate, Split
```

INPUT PARAMETER

```
> n:=1:
```

GET FILES

```
> aux:=FileTools[ListDirectory]("ReadFiles2",'returnonly'="*.txt"):
> for i from 1 to n do  A[i]:=readdata(aux[i],2);  end do:
```

AVERAGE DETERMINATION AND CONVERSIONS

```
> avg:=add(A[i],i=1...n)/n:
> R := Transpose(avg):
> xvalues:=convert(R[1],list):
> yvalues:=convert(R[2],list):
```

CURVE FITTING

```
> eq_fit:=fit[leastsquare[[x,y], y=a*x+b, {a,b}]]([xvalues, yvalues]):
> eq_function:=unapply(rhs(eq_fit),x):
```

PLOTS

```
> p1:=pointplot(avg,symbol=box):
> p2:=plot(eq_function,0..220,labels=["Temperature (°C)","Height (mm)"],labeldirections=[horizontal,
  vertical],color=blue):
> display(p1,p2):
```

EQUATION SOLVER AND FINAL SOLUTION

```
> eq:=apply(eq_function,x):
> Stress_Free_Temperature :=solve(eq,x):
```

Determination of micromechanical properties

PACKAGES

```
> restart:with(LinearAlgebra):with(linalg):
Warning, the previous binding of the name GramSchmidt has been removed and it now has an assigned value

Warning, the protected names norm and trace have been redefined and unprotected
```

PLY MECHANICAL PROPERTIES

```
> #linear elastic prediction of fibre and matrix modulus based on laminate test results (for the
  laminate's modulus)and manufacturer information (for the matrix, resin contents)
> E[1]:=171.42*10^6:E[2]:=9.080*10^6:V[m]:=0.409:V[f]:=1-V[m]:
```

RULE OF MIXTURES

```
> Eq1:=E[f]*V[f]+E[m]*V[m]-E[1]:
> Eq2:=(V[f]/E[f])+(V[m]/E[m])-(1/E[2]):
> s:=solve({Eq1,Eq2},{E[m],E[f]}):
> assign(s):
> E[f],E[m]:
```

PLY THERMAL PROPERTIES

```
> alpha[m]:=69*10^(-6):nu[m]:=0.37:
> alpha[fl]:=-0.7*10^(-6):alpha[ft]:=10*10^(-6):nu[f]:=0.25:
> alpha[1]:=(E[m]*alpha[m]*V[m]+E[f]*alpha[fl]*V[f])/(E[m]*V[m]+E[f]*V[f]):
> alpha[2]:=alpha[m]*V[m]*(1+nu[m])+alpha[ft]*V[f]*(1+nu[f])-alpha[fl]:
> alpha[1]:=alpha[1]*10^6: #(units:10^-6/°C)
> alpha[2]:=alpha[2]*10^6: #(units:10^-6/°C)
```

Implementation of the classical laminate theory

```
> restart:with(LinearAlgebra):with(plots):with(linalg):
Warning, the name changecoords has been redefined
Warning, the name GramSchmidt has been rebound
Warning, the protected names norm and trace have been redefined and unprotected
```

INPUT LAMINATE DATA

NUMBER OF PLIES

```
> nc:=2:
```

PLY THICKNESS

```
> t:=0.134e-3:
```

PLIES ORIENTATIONS

```
> orient:=readdata("orient.txt",1):
> for i from 1 to nc do orientc[i]:=orient[i]*Pi/180;end do:
```

PLY PROPERTIES

```
> E1:=171.42*10^9:E2:=9.08*10^9:G12:=5.29*10^9:alpha1:=0.02e-6:alpha2:=50e-6:alpha3:=5*10^(-30):nu12:=0.32:nu21
  :=nu12*E2/E1:alphas:=Vector(3):alphas[1]:=alpha1:alphas[2]:=alpha2:alphas[3]:=alpha3:
```

THERMAL LOAD (ºC)

```
> DeltaT:=150:
```

TRANSFORMATION MATRICES

```
> for i from 1 to nc do m[i]:=cos(orientc[i]);n[i]:=sin(orientc[i]);
  TM[i]:=Matrix(3,3);TM[i][1,1]:=m[i]^2;TM[i][1,2]:=n[i]^2;TM[i][1,3]:=2*m[i]*n[i];TM[i][2,1]:=n[i]^2;TM[i][2,2
  ]:=m[i]^2;TM[i][2,3]:=(-2)*m[i]*n[i];TM[i][3,1]:=-m[i]*n[i];TM[i][3,2]:=m[i]*n[i];TM[i][3,3]:=m[i]^2-n[i]^2;T
  M[1];TM[2];end do:
```

TRANSFORMED REDUCED STIFFNESS MATRICES

```
> Q[1,1]:=E1/(1-nu12*nu21):Q[2,2]:=E2/(1-nu12*nu21):Q[1,2]:=nu21*E1/(1-nu12*nu21):Q[6,6]:=G12:
> for i from 1 to nc do QR[i]:=Matrix(3,3);
  QR[i][1,1]:=m[i]^4*Q[1,1]+n[i]^4*Q[2,2]+2*m[i]^2*n[i]^2*Q[1,2]+4*m[i]^2*n[i]^2*Q[6,6];
  QR[i][2,2]:=n[i]^4*Q[1,1]+m[i]^4*Q[2,2]+2*m[i]^2*n[i]^2*Q[1,2]+4*m[i]^2*n[i]^2*Q[6,6];
  QR[i][1,2]:=m[i]^2*n[i]^2*Q[1,1]+m[i]^2*n[i]^2*Q[2,2]+(m[i]^4+n[i]^4)*Q[1,2]-4*m[i]^2*n[i]^2*Q[6,6];
  QR[i][1,3]:=m[i]^3*n[i]*Q[1,1]-m[i]*n[i]^3*Q[2,2]+(m[i]*n[i]^3-m[i]^3*n[i])*Q[1,2]+2*(m[i]*n[i]^3-m[i]^3*n[i]
  )*Q[6,6];
  QR[i][2,3]:=m[i]*n[i]^3*Q[1,1]-m[i]^3*n[i]*Q[2,2]+(m[i]^3*n[i]-m[i]*n[i]^3)*Q[1,2]+2*(m[i]^3*n[i]-m[i]*n[i]^3
  )*Q[6,6];
  QR[i][3,3]:=m[i]^2*n[i]^2*Q[1,1]+m[i]^2*n[i]^2*Q[2,2]-2*m[i]^2*n[i]^2*Q[1,2]+(m[i]^2-n[i]^2)^2*Q[6,6];QR[i][2
  ,1]:=QR[i][1,2];QR[i][3,1]:=QR[i][1,3];QR[i][3,2]:=QR[i][2,3];end do:
```

FREE THERMAL STRAINS

```
> for i from 1 to nc do
  alphag[i]:=Vector(3);fstrainsg[i]:=Vector(3):alphag[i]:=MatrixVectorMultiply(MatrixInverse(TM[i]),alphas);fst
  rainsg[i]:=DeltaT*alphag[i];end do:
```

LAMINATE LOADS

```
> for i from 1 to nc do NHTg[i]:=Vector(3);NHTg[i]:=MatrixVectorMultiply(QR[i],t*fstrainsg[i]);end do:
> NHT:=Vector(3):                                                                    for j from 1 to
  3 do  total:=0:                                                                  for i from 1 to nc
  do              total:=total+NHTg[i][j];NHT[j]:=total:end do:end do:NHTg:=NHT:
```

LAMINATE MOMENTS

PLY COORDINATES

```
> for k from 1 to nc/2 do ht[k]:=(-1)*((nc/2)-k)*t:hb[k]:=(-1)*(ht[k]+t):z[k]:=(ht[k]+hb[k])/2;end do:
> for k from (nc/2)+1 to nc do ht[k]:=(-1)*((nc/2)-k)*t:hb[k]:=ht[k]-t; z[k]:=(ht[k]+hb[k])/2;end do:
> for i from 1 to nc do MHTg[i]:=Vector(3);MHTg[i]:=MatrixVectorMultiply(QR[i],z[i]*t*fstrainsg[i]);end do:
> MHT:=Vector(3):                                                                    for j from 1 to
  3 do  total:=0:                                                                  for i from 1 to nc
  do              total:=total+MHTg[i][j];MHT[j]:=total:end do:end do:MHTg:=MHT:
```

LAMINATE STIFFNESS MATRICES (A,B,D)

MATRIX A

```
> AL:=Matrix(3,3):BL:=Matrix(3,3):DL:=Matrix(3,3):                                  for i from
  1 to 3 do                                                                        for j from 1 to 3 do
  total:=0;                                                                      for k from 1 to nc do
  total:=total+QR[k][i,j]*(ht[k]-hb[k]);AL[i,j]:=total;end do;end do;end do:
```

MATRIX B

```
> for i from 1 to 3 do                                                                 for j from 1
  to 3 do total:=0;                                                                  for k from 1 to nc
  do total:=total+QR[k][i,j]*(ht[k]^2-hb[k]^2);BL[i,j]:=(1/2)*total;end do;end do;end do:
```

MATRIX D

```
> for i from 1 to 3 do                                                                 for j from 1
  to 3 do total:=0;                                                                  for k from 1 to nc
  do total:=total+QR[k][i,j]*(ht[k]^3-hb[k]^3);DL[i,j]:=(1/3)*total;end do;end do;end do:
```

LAMINATE COMPLIANCE MATRICES (a,b,c,d)

AUXILIARY MATRICES

```
> Aaux:=Matrix(3,3):Aaux:=MatrixInverse(AL):
> Baux:=Matrix(3,3):Baux:=(-1)*MatrixMatrixMultiply(Aaux,BL):
> Caux:=Matrix(3,3):Caux:=MatrixMatrixMultiply(BL,Aaux):
> Daux:=Matrix(3,3):Daux:=DL-MatrixMatrixMultiply(Caux,BL):
```

MATRIX a

```
> a:=Matrix(3,3):a:=Aaux-MatrixMatrixMultiply(MatrixMatrixMultiply(Baux,MatrixInverse(Daux)),Caux):
```

MATRIX b

```
> b:=Matrix(3,3):b:=MatrixMatrixMultiply(Baux,MatrixInverse(Daux)):
```

MATRIX c

```
> c:=Matrix(3,3):c:=(-1)*MatrixMatrixMultiply(MatrixInverse(Daux),Caux):
```

MATRIX d

```
> d:=Matrix(3,3):d:=MatrixInverse(Daux):
```

REFERENCE PLANE STRAINS

```
> refstrainsg:=Vector(3):refstrainsg:=MatrixVectorMultiply(a,NHT)+MatrixVectorMultiply(b,MHT):
```

LAMINATE CURVATURES

```
> klam:=Vector(3):klam:=MatrixVectorMultiply(c,NHT)+MatrixVectorMultiply(d,MHT):
```

NET STRAINS

```
> for i from 1 to nc do netstrainsg[i]:=refstrainsg+z[i]*klam;end do:
>
```

HYGROTHERMAL STRAINS

```
> for i from 1 to nc do htstrainsg[i]:=netstrainsg[i]-fstrainsg[i];end do:
```

RESIDUAL STRESSES

GLOBAL COORDINATES

```
> for i from 1 to nc do rstressg[i]:=MatrixVectorMultiply(QR[i],htstrainsg[i]);end do:
```

PLY COORDINATES

```
> for i from 1 to nc do rstressl[i]:=MatrixVectorMultiply(TM[i],rstressg[i]);end do:
```

NET STRAINS (TOP, BOTTOM, MIDPLANE)

```
> for i from 1 to nc do layerstrtopg[i]:=VectorAdd(refstrainsg,klam,1,ht[i]);end do:
>
> for i from 1 to nc do layerstrbotg[i]:=VectorAdd(refstrainsg,klam,1,hb[i]);end do:
> for i from 1 to nc do layerstrmidg[i]:=VectorAdd(refstrainsg,klam,1,z[i]);end do:
```

HYGROTHERMAL STRAINS (TOP, BOTTOM, MIDPLANE)

```
> for i from 1 to nc do htstrainstopg[i]:=layerstrtopg[i]-fstrainsg[i];end do:
> for i from 1 to nc do htstrainsbotg[i]:=layerstrbotg[i]-fstrainsg[i];end do:
> for i from 1 to nc do htstrainsmidg[i]:=layerstrmidg[i]-fstrainsg[i];end do:
```

RESIDUAL STRESSES (TOP, BOTTOM, MIDPLANE)

GLOBAL COORDINATES

```
> for i from 1 to nc do rstresstopg[i]:=MatrixVectorMultiply(QR[i],htstrainstopg[i]);end do:
> for i from 1 to nc do rstressbotg[i]:=MatrixVectorMultiply(QR[i],htstrainsbotg[i]);end do:
> for i from 1 to nc do rstressmidg[i]:=MatrixVectorMultiply(QR[i],htstrainsmidg[i]);end do:
```

PLY COORDINATES

```
> for i from 1 to nc do rstresstopl[i]:=MatrixVectorMultiply(TM[i],rstresstopg[i]);
  rstressbotl[i]:=MatrixVectorMultiply(TM[i],rstressbotg[i]);rstressmidl[i]:=MatrixVectorMultiply(TM[i],rstress
  midg[i]);end do:
>
```